



Michigan Technological University
Create the Future Digital Commons @ Michigan Tech

Dissertations, Master's Theses and Master's
Reports - Open

Dissertations, Master's Theses and Master's
Reports

2010

Multi-node TOA-DOA cooperative LOS-NLOS localization : enabling high accuracy and reliability

Zhonghai Wang
Michigan Technological University

Follow this and additional works at: <https://digitalcommons.mtu.edu/etds>



Part of the [Electrical and Computer Engineering Commons](#)

Copyright 2010 Zhonghai Wang

Recommended Citation

Wang, Zhonghai, "Multi-node TOA-DOA cooperative LOS-NLOS localization : enabling high accuracy and reliability", Dissertation, Michigan Technological University, 2010.
<https://doi.org/10.37099/mtu.dc.etds/56>

Follow this and additional works at: <https://digitalcommons.mtu.edu/etds>



Part of the [Electrical and Computer Engineering Commons](#)

Multi-Node TOA-DOA Cooperative LOS-NLOS Localization:

Enabling High Accuracy and Reliability

By

ZHONGHAI WANG

A DISSERTATION

Submitted in partial fulfillment of the requirements

for the degree of

DOCTOR OF PHILOSOPHY

(Electrical Engineering)

MICHIGAN TECHNOLOGICAL UNIVERSITY

2010

Copyright © Zhonghai Wang 2010

This dissertation, "Multi-Node TOA-DOA Cooperative LOS-NLOS Localization: Enabling High Accuracy and Reliability", is hereby approved in partial fulfillment of the requirements for the degree of DOCTOR OF PHILOSOPHY in the field of Electrical Engineering.

DEPARTMENT:
Electrical and Computer Engineering

Signatures:

Dissertation Advisor _____
Dr. Seyed A. (Reza) Zekavat

Committee _____
Dr. Daniel R. Fuhrmann

Dr. Chunxiao (Tricia) Chigan

Dr. Ossama O. Abdelkhalik

Department Chair _____
Dr. Daniel R. Fuhrmann

Date _____

CONTENTS

List of Figures	x
List of Tables.....	xiv
Acknowledgments	xv
Abstract.....	xvii
1. Introduction	1
1.1 Overview	2
1.1.1 Parameter Measurement.....	3
1.1.2 LOS Localization.....	11
1.1.3 LOS and NLOS Identification.....	15
1.1.4 NLOS Mitigation	16
1.1.5 NLOS Localization	17
1.2 Organization of This Dissertation	19
1.3 Research Contributions and Publications	21
2. LOS Target Node Localization Based on Semi-distributed Multi-node TOA-DOA Fusion	25
2.1 Introduction.....	25
2.2 Semi-distributed Multi-node TOA-DOA Fusion Localization Scheme	28

2.2.1 MANET Structure	28
2.2.2 Localization Scheme	28
2.2.3 Position Update Rate	31
2.3 Multi-node TOA-DOA Fusion	32
2.3.1 Non-Reference BNs Localization Fusion	32
2.3.2 TNs Localization Fusion	35
2.3.3 System Computational Complexity	39
2.4 Sub-optimal Reference-node Selection.....	40
2.5 Simulations and Discussions	42
2.6 Conclusions	50
2.7 Angle Calculation Ambiguity Removing	51
3. Localization Performance of the Semi-distributed Multi-node TOA-DOA Fusion	55
3.1 Introduction	55
3.2 CEP of the Semi-distributed Multi-node TOA-DOA Fusion.....	56
3.3 CEP of GPS-aided TOA Fusion and GPS-aided DOA Fusion	59
3.3.1 The Impact of GPS Positioning Error on the Final TOA (DOA) Estimation...	60
3.3.2 GPS-aided TOA (DOA) Fusion Localization error	64
3.3.3 Initialization of the Iteration Process.....	69
3.3.4. CEP of GPS-aided TOA (DOA) Fusion.....	70

3.4 Simulations and Discussions	72
3.5 Conclusions.....	81
3.6 Covariance Calculation	82
3.7 Point PDF Derivation	83
4. Localization with Kalman Filter in LOS Scenario	87
4.1 Introduction.....	87
4.2 Localization with the Integration of KF and Multi-node TOA-DOA Fusion and EKF	89
4.2.1 Localization Based on Fusion plus Kalman Filter.....	90
4.2.2 Localization Based on Extended Kalman Filter	93
4.3 Localization Accuracy, Stability and Complexity	95
4.3.1 Localization Accuracy and Filter Stability	95
4.3.2 Computational Complexity	98
4.4 Simulation and Discussion	100
4.5 Conclusions.....	105
5. Single Base Node LOS and NLOS Separation	107
5.1 Introduction.....	107
5.2 Received Signal Model.....	109
5.3 Phase Difference Variance	112

5.4 Data Reliability and LOS and NLOS Separation	117
5.5 Simulation and Discussion	119
5.6 Conclusions	124
6. Localization in NLOS Scenario	127
6.1 Introduction	128
6.2 System Model and Problem Definition.....	129
6.3 Localization in NLOS Scenario.....	132
6.3.1 Shared Reflectors Localization	133
6.3.2 Targe Node Localization	136
6.3.3 NLOS Identification	140
6.3.4 Shared Reflectors Determination	146
6.4 Simulations.....	151
6.5 Conclusions	157
7. Conclusions and Open Problems	159
7.1 Conclusions	160
7.2 Open Problems	164
7.2.1 Base Node Set Selection in the Fusion Process	164
7.2.2 Tradeoff between Multi-node TOA-DOA Fusion and TOA-only Fusion	166
7.2.3 Localization via Intermediate Target Node	166

7.2.4 Monitoring and Avoiding the Divergence of EKF	168
7.2.5 Finding LOS BN when Multiple NLOS BNs and One LOS BN Localize a TN Simultaneously	168
7.2.6 Discriminate Single Bounce and Multiple Bounces NLOS Channels.....	169
7.2.7 Extension of the Multi-node TOA-DOA Fusion from Two-Dimensional to Three-Dimensional.....	170
Appendix A. Republish Permission	173
References	177

List of Figures

Figure 1.1: Radar system.....	4
Figure 1.2: WLPS system.....	4
Figure 1.3: GPS system, satellites 1-4 are in one orbit, 5 and 6 are in the other two orbits.	5
Figure 1.4: TOA fusion localization.	12
Figure 1.5: TDOA fusion localization.....	12
Figure 1.6: DOA fusion localization.	13
Figure 1.7: Joint TOA-DOA localization.	13
Figure 1.8: Organization of the dissertation.	22
Figure 2.1: The clustered MANET structure.....	29
Figure 2.2: Positioning flow chart.	29
Figure 2.3: TOA-only localization method.	43
Figure 2.4: Efficiency of the sub-optimal reference-node selection method.	45
Figure 2.5: Average positioning MSE evaluation of the proposed semi-distributed localization technique and the TOA-only technique (here, α^o means the angle	

error standard deviation is α degree).....	46
Figure 2.6: Position update rate comparison between the proposed semi-distributed scheme and the centralized scheme.....	49
Figure 3.1: The structure of the MANET that applies GPS-aided TOA (DOA) fusion....	60
Figure 3.2: Transformation of GPS positioning error to range estimation error.	63
Figure 3.3: probability of TNs being localized vs. MANET radius, with 5 BNs.	74
Figure 3.4: point CEP with 5 BNs, $R_{max} = 80\sigma_R$, $\sigma_\theta = 2^\circ$ and the ratio $Z = 0.5$	74
Figure 3.5: Average CEP vs. BNs number with $R_{max} = 80\sigma_R$, $\sigma_\theta = 2^\circ$ and $Z=0.5$	76
Figure 3.6: Average CEP comparison vs. MANET radius with 5 BNs, $\sigma_\theta = 2^\circ$ and $Z=0.5$	76
Figure 3.7: Average CEP comparison vs. DOA estimation error with 5 BNs, $R_{max} = 80\sigma_R$, $\sigma_\theta = 2^\circ$ and $Z=0.5$	77
Figure 3.8: Average CEP comparison vs. Z with 5 BNs, $R_{max} = 80\sigma_R$ and $\sigma_\theta = 2^\circ$	77
Figure 4.1: Ad-hoc net work configuration.	89
Figure 4.2: Localization techniques. (a) Fusion plus KF. (b) EKF.	90
Figure 4.3: Localization error with 4 BNs, (a) $d = 250\sigma_\rho$, $e = 240\sigma_\rho$; (b) $d =$ $250\sigma_\rho$, $e = 250$	102

Figure 4.4: Comparison of localization error CDF with 1, 2 and 4 BNs.	103
Figure 4.5: Comparison of APCRLB with 2 and 4 BNs.	104
Figure 4.6: Computational complexity comparison.....	105
Figure 5.1: Synchronized two-receiver system.	109
Figure 5.2: Signals' phase difference at antennas 1 and 2.	111
Figure 5.3: Received signal phase at Receiver 1.	113
Figure 5.4: DOA estimation error vs. power ratio K	120
Figure 5.5: Verification of $f(\Delta\varphi_1)$ with different K	122
Figure 5.6: Verification of phase difference variance ($\sigma_{\Delta\varphi}^2$).	123
Figure 5.7: LOS and NLOS separation performance.....	124
Figure 6.1: NLOS localization system model.....	130
Figure 6.2: TN localization categorization.	131
Figure 6.3: Reflector and TN localization.	134
Figure 6.4: NLOS identification and shared reflector determination.	141
Figure 6.5: Miss-detection and false alarm for NLOS identification and shared reflectors	

determination with $d = 100\sigma_R$, $\sigma_\theta = 1^\circ$ and $\sigma_\theta = 2^\circ$	153
Figure 6.6: Target node localization error CDF, $d = 50\sigma_R$, (a) $\sigma_\theta = 1^\circ$, (b) $\sigma_\theta = 2^\circ$	155
Figure 6.7: Target node localization error CDF, $d = 100\sigma_R$, (a) $\sigma_\theta = 1^\circ$, (b) $\sigma_\theta = 2^\circ$..	156
Figure 7.1: Base node selection in the fusion process.	165
Figure 7.2: Localization through an intermediate TN.	167
Figure 7.3: Determine the LOS BN in multiple NLOS BN's plus one LOS BN.	169
Figure 7.4: The impact of multiple bounces NLOS on NLOS TN localization.	171

List of Tables

Table 2.1: Number of multiplications in each localization step	40
Table 2.2: Possible angle calculation ambiguity in all scenarios	53
Table 4.1: Number of multiplications in fusion plus KF.	99
Table 4.2: Number of multiplications in EKF.	100

Acknowledgments

This document reflects my research achievement under the guidance of my advisor, Dr. Seyed A. (Reza) Zekavat, throughout my Ph.D. studies at Michigan Tech. Dr. Zekavat opened the strategic field of research high performance localization to me. My research accomplishments were not possible without Dr. Zekavat's continuous support. His positive work attitude and professional insight helped me to not only publish many articles in the prestigious international conference and journals, but also receive hands on experience by contributing in Dr. Zekavat's Wireless Lab, where I also benefited from his perspicacity in advanced technologies, and collaborating with many young researchers and engineers.

I am also fortunate to have Dr. Daniel R. Fuhrmann, Dr. Chunxiao Chigan, and Dr. Ossama O. Abdelkhalik to serve as my advisory committee members. Their constructive and invaluable comments have significantly improved the quality of the dissertation.

Throughout the four and a half years' Ph.D. studies, my wife, my parents, my elder brother, younger sister and my third aunt have been a source of love, support, and encouragement.

During my stay at the snowy and beautiful upper-peninsula, I am happy that I met and spent time with my friends and lab mates, XiuKui Li, Laibin Cong, Chao Li, Hui Tong, Wenjie Xu, Shu Ting Goh, Xiaofeng Yang, Jie Tang, Changyu Sun, Mohsen Pourkhaataoun, Jafar Pourrostam, Irfan Ahmad and Imran Aslam. I would like to thank

them for their kind support in my personal and professional life.

Finally, I would like to thank all those who supported me during my studies at Michigan Tech.

Abstract

This dissertation investigates high performance cooperative localization in wireless environments based on multi-node time-of-arrival (TOA) and direction-of-arrival (DOA) estimations in line-of-sight (LOS) and non-LOS (NLOS) scenarios. Here, two categories of nodes are assumed: base nodes (BNs) and target nodes (TNs). BNs are equipped with antenna arrays and capable of estimating TOA (range) and DOA (angle). TNs are equipped with Omni-directional antennas and communicate with BNs to allow BNs to localize TNs; thus, the proposed localization is maintained by BNs and TNs cooperation.

First, a LOS localization method is proposed, which is based on semi-distributed multi-node TOA-DOA fusion. The proposed technique is applicable to mobile ad-hoc networks (MANETs). We assume LOS is available between BNs and TNs. One BN is selected as the reference BN, and other nodes are localized in the coordinates of the reference BN. Each BN can localize TNs located in its coverage area independently. In addition, a TN might be localized by multiple BNs. High performance localization is attainable via multi-node TOA-DOA fusion. The complexity of the semi-distributed multi-node TOA-DOA fusion is low because the total computational load is distributed across all BNs.

To evaluate the localization accuracy of the proposed method, we compare the proposed method with global positioning system (GPS) aided TOA (DOA) fusion, which are applicable to MANETs. The comparison criterion is the localization circular error probability (CEP). The results confirm that the proposed method is suitable for moderate scale MANETs, while GPS-aided TOA fusion is suitable for large scale MANETs.

Usually, TOA and DOA of TNs are periodically estimated by BNs. Thus, Kalman filter (KF) is integrated with multi-node TOA-DOA fusion to further improve its performance. The integration of KF and multi-node TOA-DOA fusion is compared with extended-KF (EKF) when it is applied to multiple TOA-DOA estimations made by multiple BNs. The comparison depicts that it is stable (no divergence takes place) and its accuracy is slightly lower than that of the EKF, if the EKF converges. However, the EKF may diverge while the integration of KF and multi-node TOA-DOA fusion does not; thus, the reliability of the proposed method is higher. In addition, the computational complexity of the integration of KF and multi-node TOA-DOA fusion is much lower than that of EKF.

In wireless environments, LOS might be obstructed. This degrades the localization reliability. Antenna arrays installed at each BN is incorporated to allow each BN to identify NLOS scenarios independently. Here, a single BN measures the phase difference across two antenna elements using a synchronized bi-receiver system, and maps it into wireless channel's K-factor. The larger K is, the more likely the channel would be a LOS one. Next, the K-factor is incorporated to identify NLOS scenarios. The performance of this system is characterized in terms of probability of LOS and NLOS identification. The latency of the method is small.

Finally, a multi-node NLOS identification and localization method is proposed to improve localization reliability. In this case, multiple BNs engage in the process of NLOS identification, shared reflectors determination and localization, and NLOS TN localization. In NLOS scenarios, when there are three or more shared reflectors, those reflectors are localized via DOA fusion, and then a TN is localized via TOA fusion based on the localization of shared reflectors.

Chapter 1

Introduction

Localization systems have emerging civilian and military applications. Examples include but not limited to battlefield command and control [1], fire fighters tracking [2], emergency 911 (E911) [3], collision avoidance in multi-robot system [4] and road traffic control [5], resource allocation [6], routing [7, 8] in sensor networks, etc.

This dissertation investigates high performance cooperative (active) localization based on time-of-arrival (TOA) and direction-of-arrival (DOA) fusion. Here, we consider base nodes (BNs) that are equipped with antenna arrays are capable of localizing cooperating active target nodes (TNs) in their coverage area independently via TOA-DOA estimation.

In some applications, such as traffic alert, road safety, and command and control, single BN localization is critical. While in many scenarios, multiple BNs are available, e.g., collaboration and coordination, and they can collaborate to achieve better performance.

In the proposed system, each BN can localize cooperating nodes (BNs or TNs) via TOA and DOA estimation, TOA and DOA measurement accuracy is altered by multi-path effects in wireless environments. In addition, TOA estimation resolution is limited by the available bandwidth. Thus, assuming the availability of line-of-sight (LOS), each BN would be able to localize other nodes; however, the localization accuracy would not be very high. Accordingly, multi-node TOA-DOA fusion is proposed to improve the

localization accuracy. In addition, assuming the availability of multiple observations of TOA and DOA, filtering techniques, such as Kalman filter, are employed to improve the localization performance.

In wireless environments, LOS might be obstructed. In these scenarios, the measured TOA and DOA would be neither accurate nor reliable. Therefore, the proposed TOA-DOA localization technique may not perform, or may perform poorly. Accordingly, we study techniques that can be applied to antenna array of each BN to allow the BN to identify non-LOS (NLOS) scenarios independently and allow reliable localization. This is specifically important when only one BN is available to localize a certain TN.

When multiple BNs are available to localize a TN, they may collaborate to not only identify the lack of availability of LOS but also localize the NLOS TN by localizing the positions of reflectors. In other words, we propose to exploit the scattering environment and the availability of reflectors to maintain NLOS localization.

1.1 Overview

Many localization methods have been proposed in the literature. Parameters that are measured in different localization systems include TOA, DOA and received signal strength (RSS). In addition, localization techniques are in general very sensitive to the availability of LOS. Specifically, in wireless environments such as urban and indoor areas, the LOS path between the transmitter and receiver could be easily obstructed. Thus, it is critical that localization techniques are capable of identifying the availability of LOS, mitigating NLOS

measurements, and localizing in NLOS environments.

1.1.1 Parameter Measurement

Here, we briefly introduce measurement techniques of TOA, DOA and RSS that are critical to all localization techniques.

1.1.1.1 TOA Measurement

TOA measurement techniques are mainly divided into two categories: round-trip and single-trip methods. Radar and wireless local positioning system (WLPS) [9] apply the round-trip method. Radar transmits a burst of radio energy and receives the reflections from all objects (e.g., target nodes, TNs) and processes them to detect the desired targets and computes the TOA of the round trip via pulse detection. This is a passive ranging process, because the TN does not cooperate in the ranging process (see Figure 1.1).

In WLPS, two nodes are assumed: (1) a BN which is capable of localizing nodes in its coverage area via TOA and DOA measurements, and (2) a TN which cooperates with BN to allow BN to find its position independently. In WLPS, a BN is equipped with antenna arrays to allow DOA estimation. BN transmits a direct-sequence spread spectrum (DSSS) inquiry signal to the TN. When the TN receives the inquiry signal, it transmits a DSSS response with a fixed and known delay back to the BN. The summation of the round-trip TOA and the known delay in the TN is calculated at the BN to find the range of TN with respect to BN. Here, the TN cooperates in the process of TOA and DOA estimation; thus, WLPS is an active/cooperative localization system (see Figure 1.2).

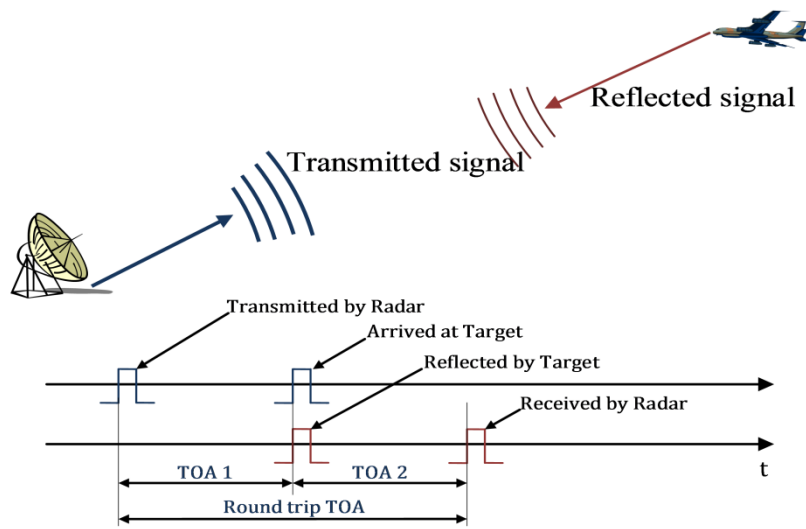


Figure 1.1: Radar system

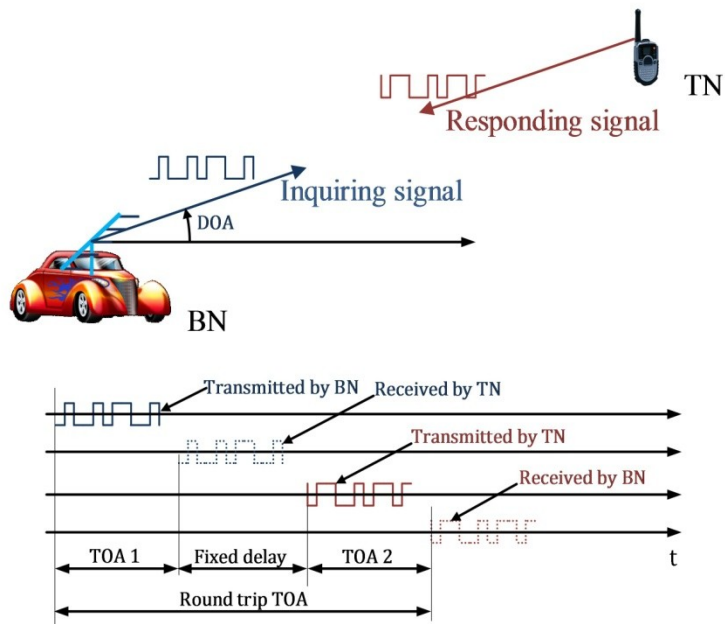


Figure 1.2: WLPS system.

GPS uses single-trip method to estimate the TOA of signals sent by satellites (BNs) to GPS receivers (TNs) for localization [10]. All GPS satellites are synchronized with the clock in the master control station (MCS) located at Schriever Air Force Base in Colorado. Each satellite broadcasts ranging codes and navigation data including its position and the time that the ranging code is transmitted. When a GPS receiver receives the signal from a satellite, single trip estimation method is applied to find the TOA of the ranging code, and compares it to a local clock to find the time delay from GPS satellite to GPS receiver. Then, the time delay is used for ranging. At least four LOS satellites are needed to maintain the localization scheme (see Figure 1.3).

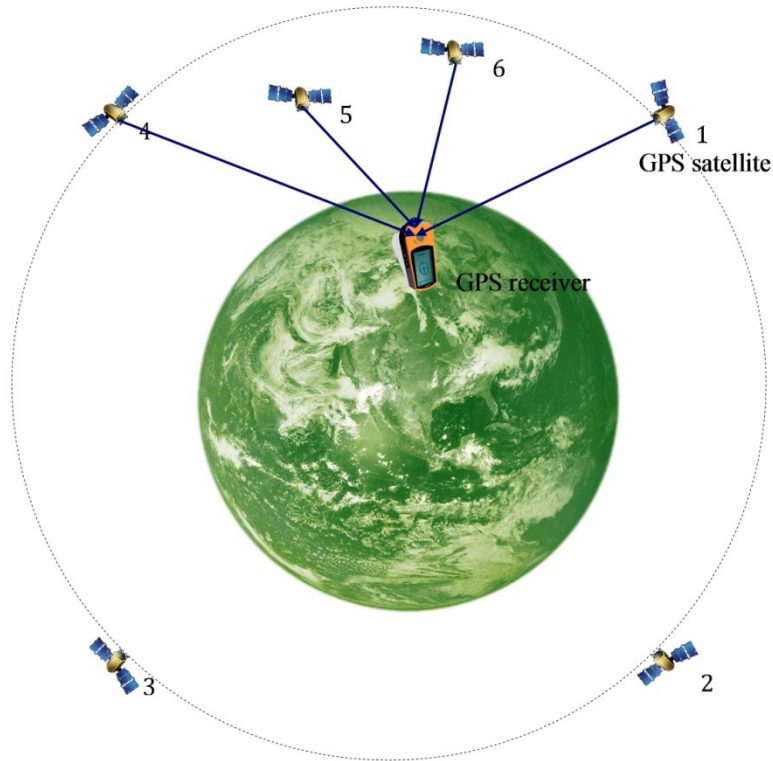


Figure 1.3: GPS system, satellites 1-4 are in one orbit, 5 and 6 are in the other two orbits.

A hybrid single trip TOA measurement technique is presented in [11]. Here, radio frequency (RF) and ultrasonic signals are used to measure the TOA of ultrasonic signal traveling between BN and TN. The received RF signal enables the TOA counter and the received ultrasonic signal ends the counter. In air, the ultrasonic speed (about 340 m/s) is much lower than that of RF signal's speed (about 3×10^8 m/s). The speed difference is applied to measure single trip TOA.

In general, the accuracy of range measurement (through TOA) based on RF signal is limited by the signal bandwidth [12], measurement technique, signal-to-noise ratio (SNR), and the number of reflections. Considering a single measurement (thus, no filtering is applied), and an estimation based on cross correlation that is used in GPS, or pulse detection that is applied to RADAR, and ignoring the impact of SNR, the TOA resolution (T_{res}), and range resolution (R_{res}) correspond to

$$T_{res} = \frac{1}{B_{eff}}, R_{res} = \frac{c}{B_{eff}}. \quad (1.1)$$

Where, B_{eff} is the effective bandwidth of the RF signal and c is the wave propagation speed. Because $c \approx 3 \times 10^8$ m/s, if high ranging accuracy is requested (e.g., 5 meters), then higher bandwidth should be used (the required bandwidth corresponding to 5 meters is 60 MHz). A low bandwidth signal always generates low ranging accuracy.

In hybrid RF – ultrasonic technique, the ranging accuracy is not sensitive to the RF signal bandwidth. Here, the ranging error (ΔR) is calculated by

$$\Delta R = V \cdot \Delta TOA. \quad (1.2)$$

In Equation (1.2), V is the ultrasonic speed in air ($V \approx 340 \text{ m/s}$). ΔTOA includes two parts, one is generated by RF signal and the other is generated by ultrasonic signal. If the RF signal bandwidth is 1MHz, the TOA measurement error generated by RF signal is about $1\mu s$. The corresponding ranging error is $340m/s \times 10^{-6}s = 0.34mm$. This error is small for ad-hoc network applications application and can be ignored.

1.1.1.2 DOA Measurement

Signal's DOA can be measured using directional antenna, antenna array or electronically steerable passive array radiator (ESPAR) antenna [13]. Because directional antenna is large and needs servomechanism, usually it is not used in ad-hoc networks. In ad-hoc networks, antenna array or ESPAR antenna is usually used to measure DOA, because their size is small, and they are cost effective. In a linear antenna array, delay-and-sum (DAS) [14], multiple signal classification (MUSIC) [15] and root-MUSIC [16] are usually applied to measure DOA.

In DAS, the signal received by each antenna element is assigned a complex weight to change its phase. The weight is determined by the assumed DOA of the signal, antenna array parameters (element distance, number of elements) and the signal carrier wavelength. Then the delayed signals are summed, and its output power is calculated. When the assumed DOA matches the true one, the output power of the weighted sum reaches its maximum value. Hence, when the maximum output power of the weighted

sum is observed, the corresponding assumed DOA is taken as the received signal DOA.

In MUSIC, the received signal of an antenna array is modeled by

$$X = A(\theta) \cdot S + W. \quad (1.3)$$

In (1.3), X is the received signal vector, A is the array of the antenna array response determined by the DOA (θ) of the signal, antenna array parameters and the signal carrier wavelength, and W is the received noise vector. The eigenvectors of the covariance matrix of X is calculated and the eigenvectors corresponding to the smallest eigenvalues are selected and used to construct a matrix E . Essentially, E represents the noise components. MUSIC exploits the orthogonality of noise and signal components: noise components are represented by E , and the signal components received from the angle θ are represented by $A(\theta)$. Thus, MUSIC estimates the DOA of received signal by finding the peaks of the MUSIC spectrum

$$P_{mu}(\theta) = \frac{1}{A^*(\theta) \cdot E \cdot E^* \cdot A(\theta)}. \quad (1.4)$$

While the root MUSIC directly finds the root of the polynomial

$$D(z) = \sum_{l=-M+1}^{M+1} a_l z^{-l}. \quad (1.5)$$

Where, M is the total number of antenna elements, $a_l = \sum_{m-n=l} B_{mn}$, B_{mn} is the element on the m^{th} row and n^{th} column of matrix B , $B = E \cdot E^*$, E is defined in (1.4), E^* is the transpose of E , and $z = \exp(-j2\pi d \sin\theta/\lambda)$. When the roots of the polynomial are

calculated, the corresponding DOA can be calculated for $z = \exp(-j2\pi d \sin\theta/\lambda)$. For details, see [16].

ESPAR antennas consist of a single active element surrounded by multiple parasitic elements loaded with variable reactance. By controlling the reactance of these parasitic elements, the ESPAR antenna beam-forming is implemented, and DOA is measured via electronic beam scanning [17].

DOA estimation accuracy is a function of the technique used, antenna array parameters, SNR, the channel structure (i.e., the availability of multiple paths), and the calibration of antenna array. It should be noted that in general, the receiver components connected to the antenna array do not operate fully equivalent. Thus, the phase and amplitude of signals received through each antenna element may vary from one to another. This effect can highly reduce the DOA estimation performance; hence, antenna array including receiver components should be calibrated prior to the DOA estimation [18].

1.1.1.3 Received Signal Strength Measurement

Assuming the availability of LOS, the received signal power (P_r) in a receiver at the measurement point can be calculated by

$$P_r = \frac{P_t G_{at} G_{ar} G_{re}}{(4\pi d/\lambda)^\mu}. \quad (1.6)$$

Where, P_t is the power transmitted by the transmitter, G_{at} is the transmit antenna gain, G_{ar} is the receiver antenna gain, G_{re} is the gain from receiving antenna output to the

measurement point in the receiver, d is the distance between transmitter and receiver, λ is the carrier wavelength, and μ (usually larger than 2) is the fading parameter determined by the channel.

When LOS is not available, the received signal power is not constant and may spatially and temporally vary. In this case, a shadowing effect random variable is added to the received signal power in Decibels. Usually, lognormal is considered as the probability density function (PDF) of this random variable. The model in (1.6) converted in Decibels often is called log-distance model. In addition to log-distance, other models have been introduced for the received signal strength that include Clutter path loss model [19], Ikegami path loss model [20].

Based on Equation (1.6), RSS is determined by the transmitting power, transmitting and receiving antennas' gain, the receiver structure, the distance between transmitter and receiver, the carrier wavelength and the channel fading parameter. A real Omni antenna beam pattern is not ideally Omni directional. Thus, the power in one direction might be higher than the other direction. In addition, the channels between multiple BNs and TN are not the same; hence, when the RSS is mapped into the distance [21], error may occur.

RSS can be measured in the intermediate frequency (IF) stage before the IF amplifier or in the baseband signal chain before the baseband amplifier in zero-IF systems. In a complex sampling system, when I and Q samples (sam_I and sam_Q) of the received signal are calculated, the power of the received signal can be obtained using

$$P = E(sam_I^2 + sam_Q^2)/R_{in}. \quad (1.7)$$

Where, $E(\cdot)$ is the expectation operator and R_{in} is the input load. Fading effects occur because of channel variations. Thus, the received signal amplitude is not constant. To achieve a better power measurement, in practice (assuming the signal is a mean ergodic process), a large number of samples are collected and sample mean is applied to calculate the expectation of Equation (1.7).

1.1.2 LOS Localization

Most of the available localization techniques are designed for LOS applications. Examples include TOA fusion [22, 23] including global positioning system (GPS) [10], time difference of arrival (TDOA) fusion [24, 25], DOA fusion [26, 27], joint TOA-DOA estimation [9], and range fusion based on received signal strength indication (RSSI) [21]. In these methods, the angles (distances) of a TN with respect to BN(s) are calculated based on DOA (TOA or received signal strength) measurements.

In TOA fusion and range fusion based on RSSI, the TN is localized at the crossing point of multiple (three or more) circles determined by the position of BNs and the distance between the TN and BNs (see Figure 1.4); in TDOA fusion, the TN is localized at the crossing point of multiple (three or more) hyperbolas determined by the position of BNs and the range difference between the TN and pairs of BNs (see Figure 1.5); in DOA fusion, the TN is localized on the crossing point of multiple (two or more) lines determined by the position of BNs and the angle of the TN with respect to BNs (see Figure 1.6); and, in joint

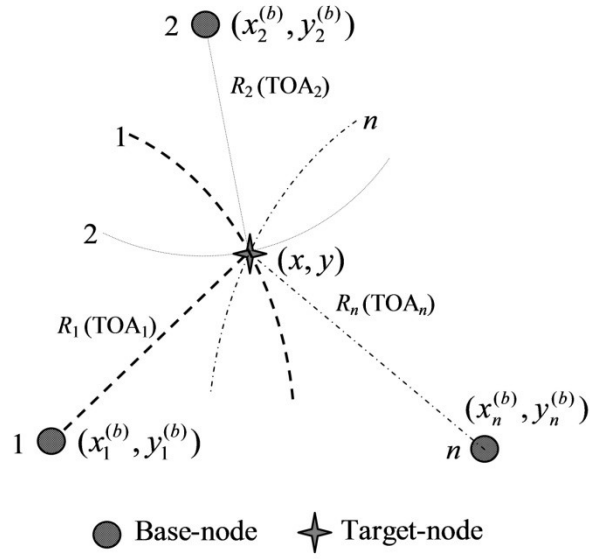


Figure 1.4: TOA fusion localization.

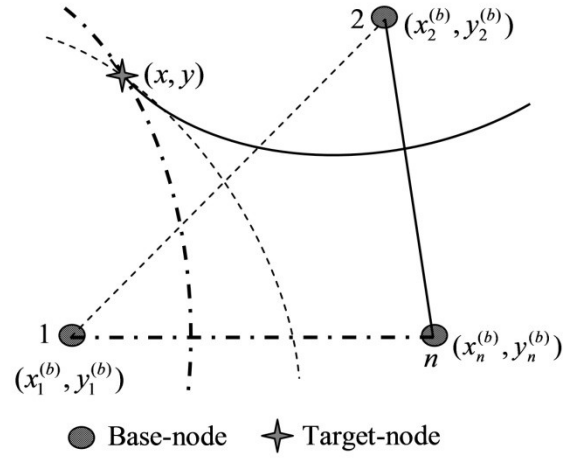


Figure 1.5: TDOA fusion localization.

TOA-DOA estimation, the TN is localized at the crossing point of the circle determined by the position of BN and the distance between BN and TN and the line determined by the position of BN and the angle of TN with respect to the BN (see Figure 1.7).

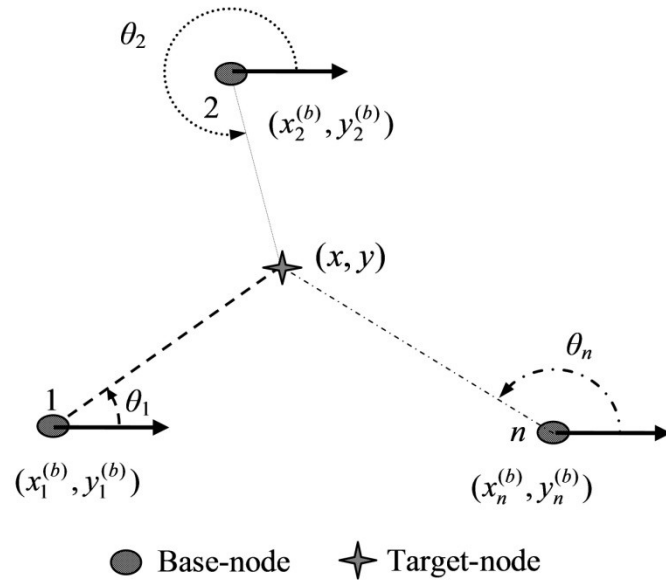


Figure 1.6: DOA fusion localization.

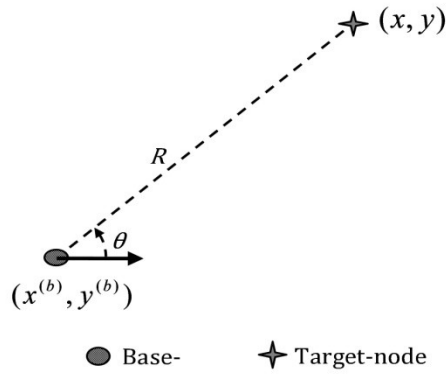


Figure 1.7: Joint TOA-DOA localization.

Except joint TOA-DOA estimation, the main limitations of these localization techniques include:

- (1) BNs position should be known or computed via other localization method, e.g.,

the position of BNs (i.e., GPS satellites) in GPS is calculated via tracking the orbit of satellites using base stations installed on the earth.

(2) Two or more BNs are needed to perform localization. In DOA fusion, at least two BNs are needed; in TDOA fusion, range fusion based on RSSI and TOA fusion based on round-trip (e.g., wireless local positioning system (WLPS) [9]) or hybrid single-trip TOA measurement [11], at least three BNs are needed; and, in TOA fusion based on single trip TOA measurement (e.g., GPS), at least three BNs for 2-dimensional and four BNs for 3-dimensional application are needed.

(3) Geometric dilution of precision (GDOP): The TN cannot be localized or the localization accuracy would be poor when the TN and BNs are on the same line in DOA fusion [28] or when BNs are close to each other in TOA fusion [10], TDOA fusion, and range fusion based on the received signal strength indication (RSSI).

The shortcoming of the localization method based on TOA-DOA estimation is that its localization accuracy decreases as the distance between BN and TN increases.

In this dissertation, a LOS localization method based on multi-node TOA-DOA fusion is proposed. It overcomes the above shortcomings related to the available LOS localization method. In this method, each BN has the capability of estimating other nodes' TOA and DOA. The localization approach is similar to the WLPS as discussed in Figure 1.2. One BN is selected as the reference BN and other nodes (including BNs and TNs) are localized in the coordinate of the reference BN. Because each BN can localize other BNs'

positions, the position of BN is not necessary. When there is only one BN localizing a TN, the TN can still be localized with a reasonable accuracy under any geometrical distribution of BNs and TN as long as a LOS between BN and TN is available. When multiple BNs are engaged in localizing one TN, higher localization accuracy is expected.

It should be noted that even when one BN is capable of localizing one TN and LOS is not available, LOS-NLOS identification techniques should be used by that BN to realize that the localization is not reliable. Thus, we investigate single node LOS-NLOS identification techniques. In addition, when multiple BNs are available to localize a TN, they may collaborate to not only identify the lack of availability of LOS but also localize the NLOS TN under certain conditions. The approach for this collaboration will also be studied.

1.1.3 LOS and NLOS Identification

In real applications, LOS channel between BNs and between BNs and TN may not be available. NLOS reduces or completely removes the reliability in localization [29]. Hence, if the NLOS BN can be identified, we can apply suitable method to deal with NLOS impact. For example, when there are enough LOS BNs, the data attained by NLOS BNs is discarded and the data achieved by LOS BNs is used in the localization process to obtain a reliable TN position estimation [30, 31].

Accordingly, LOS and NLOS separation is necessary in node localization and many NLOS identification techniques have been proposed. These techniques include the

separation method based on the root-mean-squared delay spread (RDS) [32] and the method based on the statistics of the measured range [29], etc.

In the method based on the RDS, the received ultra wideband (UWB) signal's TOA and RSS are first calculated, and then the RDS is calculated and used to separate LOS and NLOS [32]. Because UWB signal is needed in this method, it is not applicable to wideband or narrowband systems. In addition, UWB signals are only applicable to short range scenarios. The method based on the statistics of the measured range, tests the normality of the measured range. If the signal is coming from the LOS channel, the measured range should have normal or almost normal distribution; while if the signal is coming from NLOS channel, the measured range would not be normal [29]. This method involves some latency as the full statistics of the estimated range should be attained.

In this dissertation, two LOS and NLOS separation techniques are proposed, which have small or no latency and are applicable to wideband and narrowband systems. The first one is based on the variance of the phase difference of signals received by a synchronized bi-receiver system, which can separate LOS and NLOS when only one BN is available; and, the second one is designed to separate LOS and NLOS between multiple BNs and one TN (two or more BNs have LOS with the TN, or one or no BN has LOS with the TN), which is based on the geometrical relationship across BNs, TN and reflectors.

1.1.4 NLOS Mitigation

The severe impact of NLOS on localization performance motivates researchers to find

methods to deal with NLOS – mitigating NLOS impact on traditional LOS localization methods or designing new methods that directly use NLOS measurements in the localization process. The NLOS localization methods would be reviewed in the next subsection. The available NLOS mitigation techniques can be divided into two categories:

(1) Identifying NLOS BNs, discarding the data collected by these BNs in the localization process and using the data obtained by LOS BNs to localize TN [30, 31, 33].

(2) Identifying NLOS BNs and calibrating the data acquired via these NLOS BNs using the statistics obtained in NLOS channel models [34, 35] and then applying the data collected by LOS BNs and the calibrated data attained by NLOS BNs to implement the localization [35, 36, 37].

The first category of methods needs enough number of LOS BNs (at least two BNs for DOA fusion, and three BNs for TOA fusion). While in some scenarios, the number of LOS BNs may be smaller than the necessary number due to obstructions. Thus, these kinds of methods would not perform. The second category needs the statistics of the NLOS measurement. While in many applications, this information is not available or not accurate. Thus, the performance of the second category would be poor.

1.1.5 NLOS Localization

Typical NLOS localization examples include signature mapping [38], leveraging across multiple lines of possible mobile device location (LPMD) [39] and the crossing point of multiple lines [40]. In signature mapping, both BNs and TNs are Omni directional nodes.

While in the other two NLOS localization methods, BNs are equipped with antenna arrays and have the capability of estimating TOA and DOA of TN. In [39], TN is an Omni directional node. But in [40], TN is equipped with antenna arrays. These methods and their limitations follow.

In signature mapping [38], an RSS map (data base) of the environment is prepared. In this map, a set of RSS (reference signature) from multiple BNs is measured at each reference point m (x_m, y_m), m is the reference point index and $1 \leq m \leq M$, M is the total number of reference points. A TN listens to BNs beacon and achieves a received signature. The reference points with distances (the Manhattan distances or Euclidean distances between received signature and reference signatures) that are smaller than a threshold is selected; and then the TN is localized at the centroid of these selected reference points.

It is clear that in this technique the availability of LOS between BNs and TN is not required. But an RSS map of the application environment should be created prior to the implementation of Localization. When a priori information of the environment is not available, the RSS map would not be available, and this method would not perform. These maps can be generated using software such as “site planner” [41].

In the method based on leveraging LPMD, the reflectors are assumed to be either parallel or perpendicular to each other. This assumption is reasonable in most indoor environment and downtown area. But it is not reasonable in an area with irregular distribution of buildings such as in building complexes. In the method based on the crossing points of multiple lines determined by multiple NLOS TOA-DOA estimations, both BNs and TNs

are equipped with antenna arrays. Antenna arrays are expensive and consume much more power than an Omni directional receiver. In many applications, where cost and power consumption are critical, the method based on the crossing point of multiple lines [40] would not be a good option.

In this dissertation, we propose a NLOS localization method based on multiple BNs TOA-DOA estimations. In this method, the TN is an Omni directional node, and multiple (three or more) reflectors are shared by the TN and sets of BNs. First, the shared reflectors is determined and localized via DOA fusion; then, the distance between shared reflectors and the TN is calculated; and, finally, the TN is localized via TOA fusion based on the shared reflectors localization.

1.2 Organization of This Dissertation

We first propose a semi-distributed multi-node TOA-DOA fusion localization method. This is a cooperative method, i.e., TNs cooperate with BNs in order to allow them to find their position via TOA and DOA estimation. In this method, every BN equipped with antenna arrays is capable of estimating other nodes TOA and DOA, and therefore can independently localize other nodes in its local coordinate. When a TN is localized by multiple BNs and these BNs can localize each other (or their positions are known), the position of the TN calculated by these BNs can be transformed into a reference coordinate (one BN's local coordinate or the coordinate that these BNs are located in) and fused to obtain a better position estimation. This semi-distributed fusion scheme is

proposed in Chapter 2. Here, the term “semi-distributed” means a part of nodes in the system are in charge of the data processing of localization.

To evaluate the localization accuracy of the proposed method, in Chapter 3, we theoretically derive its localization circular error probability (CEP), and compare it with that of two other localization methods, GPS-aided TOA fusion and GPS-aided DOA fusion. The comparison shows that the proposed semi-distributed multi-node TOA-DOA fusion localization technique is suitable for moderate scale (i.e., coverage area) MANETs, while GPS-aided TOA fusion is suitable for large scale MANETs.

In Chapter 4, to further improve the localization performance of the multi-node TOA-DOA fusion localization method, we apply KF to the fusion result. Here, we assume that each BN attains TN position periodically. Therefore, multiple DOA and TOA, and accordingly a number of TN positions are acquired by each BN. The performance of the integration of KF and multi-node TOA-DOA fusion is compared to the extended KF (EKF). The comparison shows that the integration of KF and multi-node TOA-DOA fusion is stable and its performance is slightly lower than that of the EKF when EKF converges. But when the EKF diverges, the performance of the integration of KF and multi-node TOA-DOA fusion is much better than that of the EKF. IN addition, the computational complexity of the proposed method is much lower than that of the EKF.

To identify LOS and NLOS channels between BN and TN, and to improve the localization reliability, in Chapter 5, we propose a LOS-NLOS identification technique to discriminate LOS and NLOS channels. This technique allows each BN to independently

identify LOS and NLOS. Thus, in this technique, the availability of multiple BNs is not required. This technique is specifically important when there is only one BN that is capable of localizing a specific TN. The method is based on the statistics of the phase difference of the received signals by a synchronized bi-receiver system. In other words, here, we exploit the availability of multiple antennas at the BN receiver to identify NLOS situations. The proposed technique has a very small latency.

When multiple BNs are available to localize a specific TN, we present a technique that is capable of LOS and NLOS discrimination, *and* NLOS localization. The technique can also localize the position of reflectors in the environment. In other words, the proposed technique can be used for reflecting environment identification. Here, indeed the geometrical status of BNs and TN and the reflectors are exploited to maintain NLOS identification and localization. This separation technique is presented in Chapter 6. Here, the reflectors shared by TN and the sets of BNs are localized via DOA fusion, and then the distance between TN and these shared reflectors are calculated and the TN is localized via TOA fusion based on the shared reflectors localization.

Chapter 7 concludes this dissertation and discusses some open problems.

The basic structure of this dissertation is illustrated in Figure 1.8.

1.3 Research Contributions and Publications

This dissertation discusses the techniques of implementing node localization in LOS and

Chapter 1: Introduction		
Chapter 2: LOS Target node localization based on semi-distributed multi-node TOA-DOA fusion	Chapter 5: Single BN LOS and NLOS separation	Chapter 6: Localization in NLOS scenario
Chapter 3: Localization performance of the semi-distributed multi- node TOA-DOA fusion		
Chapter 4: Localization with Kalman filter in LOS scenario		
Chapter 7: Conclusions and open problems		

Figure 1.8: Organization of the dissertation.

NLOS scenarios. The following publications were created as part of the research presented in this dissertation.

- 1) [Book Chapter] S. A. Zekavat and Z. Wang, “Node Localization in Ad-hoc Networks”, submitted for publishing in “*Handbook of Research on Mobility and Computing: Evolving Technologies and Ubiquitous Impacts*” Maria Manuela Cruz-Cunha & Fernando Moreira (Editor).
- 2) W. Xu, Z. Wang and S. A. Zekavat, “LOS-NLOS Identification via Phase Difference Statistics across Two Antennas,” submitted to *IEEE Transactions on Wireless Communications*.
- 3) Z. Wang, and S. A. Zekavat, “Omni-Directional Mobile NLOS Identification and

- Localization via Multiple Cooperative Nodes”, submitted to *IEEE Transactions on Mobile Computing*.
- 4) Z. Wang, and S. A. Zekavat, “A Novel Semi-distributed Localization via Multi-node TOA-DOA Fusion”, *IEEE Transactions on Vehicular Technology*, vol. 58, issue 7, pp. 3426-3435, Sep. 2009.
 - 5) Z. Wang and S. A. Zekavat, “Comparison of Semi-Distributed Multi-Node TOA-DOA Fusion Localization and GPS-Aided TOA (DOA) Fusion Localization for MANETs,” *EURASIP Journal on Advances in Signal Processing*, vol. 2008, Article ID 439523, 16 pages, 2008. doi: 10.1155/2008/439523.
 - 6) Z. Wang and S. A. Zekavat, “A New TOA-DOA Node Localization for Mobile Ad-hoc Networks”, accepted in *IEEE ICT 2010*.
 - 7) Z. Wang, W. Xu, and S. A. Zekavat, “A New Multi-Antenna Based LOS - NLOS Separation Technique,” *IEEE DSP/SPE 2009*.
 - 8) Z. Wang, C. Li, and S. A. Zekavat, “A Novel Smart Antenna Calibration Technique,” *Virginia Tech Annual Wireless Symposium*, 2008.
 - 9) Z. Wang, and S. A. Zekavat “A Novel Semi-distributed Cooperative Localization Technique for MANET: Achieving High Performance,” *WCNC 2008*.
 - 10) S. A. Zekavat, A. Kolbus, X. Yang, Z. Wang, J. Pourrostam, and, M. Pourkhaatoon, “A Novel Implementation of DOA Estimation for Node Localization on Software

Defined Radios: Achieving High Performance with Low Complexity,” *ICSPC* 2007.

- 11) Z. Wang, and S. A. Zekavat, “MANET Localization via Multi-node TOA-DOA Optimal Fusion,” *MILCOM* 2006.

Chapter 2

LOS Target Node Localization Based on Semi-distributed Multi-node TOA-DOA Fusion¹

This chapter presents a semi-distributed multi-node TOA-DOA fusion localization technique. The fusion is implemented in the local coordinate of one of the BNs (reference-BN), and it improves the positioning performance with respect to the reference BN. In this chapter, the fusion weights and positioning error are derived theoretically, and the efficiency of a sub-optimal reference-BN selection method, the positioning error, and the position update rate are evaluated via simulations.

2.1 Introduction

In many TOA and DOA based localization techniques, it is assumed that BNs are fixed or their position is known (e.g., positioning in cellular network systems [42]). However, in many applications, such as MANET, BNs are mobile and localization techniques based on mobile BNs are required (e.g., TOA only method [43] and GPS-aided RSSI method [44]). Most systems use TOA [33, 43], DOA [45, 46], TDOA [47, 48] and RSSI [49, 50] to perform localization. A merger of these techniques might be incorporated to achieve better localization performance. Examples include but not limited to joint TOA-DOA

¹ © [2009] IEEE. Reprinted, with permission, from [IEEE Transactions on Vehicular Technology, A Novel Semi-distributed Localization via Multi-node TOA-DOA Fusion, Z. Wang, and S. A. Zekavat]. See Appendix A for full permission.

estimation [9, 51], DOA-RSSI [52], GPS-aided TOA [53], GPS-aided DOA [54], and GPS-aided RSSI [55]. These systems have emerging applications in multi-robot collaboration and coordination, sensor networks, road safety, security and defense.

This chapter presents a semi-distributed localization technique based on multi-node TOA-DOA fusion. A MANET composed of mobile BNs and TNs is assumed. TNs are equipped with Omni-directional antennas communicating with BNs to support TOA-DOA fusion. BNs are equipped with antenna arrays and capable of estimating received signal's TOA and DOA. In the system each BN can independently localize other nodes, i.e., find TOA and DOA of other nodes in its coverage area. An example of these systems is wireless local positioning systems [9]. In this kind of systems, usually BNs are expensive and TNs are very cheap. Thus, in real applications (e.g., battle field command and control) the number of TNs is designed much higher than that of BNs.

The positioning performance of the *single node joint TOA-DOA estimation positioning system* is highly dependent on the TOA and DOA estimation performance that is usually a function of the technique and many other parameters including the channel structure and the distance between BN and TN. In many scenarios, the localization performance achieved by single node positioning system is not adequate. Thus, fusion is applied across multiple BNs that localize a TN simultaneously to improve the positioning performance. We call this technique semi-distributed *multi-node TOA-DOA fusion*. Semi-distributed is opposed to the centralized fusion, in which all processes are accomplished by one node.

In the proposed technique, one BN is selected as the reference-node. All BNs are localized in the reference-node's local coordinate system. Non-reference BNs are localized via TOA-DOA fusion across non-reference BNs and the reference-node. TNs are localized via TOA-DOA fusion across all BNs. The fusion computational load is distributed across all BNs. Available BNs and TNs form clusters. Each cluster contains one BN and multiple TNs. The BN within each cluster is in charge of localization data fusion of TNs located in its coverage area.

We theoretically derive the fusion weights for non-reference BNs and TNs localization, propose a sub-optimal reference-node selection method, and calculate TNs localization mean square error (MSE). Simulations are conducted to evaluate the efficiency of the sub-optimal reference-node selection method, the localization error and the position update rate. The proposed technique is capable of positioning in GPS-denied environments, it possesses higher accuracy than single node localization, and it has higher position update rate than the centralized scheme.

While many localization systems have been proposed in the literature, few of them address the localization independently via mobiles considering any combination of TOA and/or DOA estimation without using other systems (e.g., GPS) in the GPS-denied environments. An example is the TOA-only technique proposed in [43]. Here, all nodes are localized in a local coordinate system which is determined by three BNs. These three BNs first localize themselves, then, they localize all TNs in the local coordinate system. In this chapter, we compare the performance of the proposed method to that of the TOA

only method proposed in [43].

In this chapter, we first introduce the MANET structure and the semi-distributed multi-node TOA-DOA fusion localization scheme; secondly, the fusion method is theoretically derived; then, we introduce the sub-optimal reference node selection scheme; and finally, simulations are conducted to evaluate the performance of the proposed method.

2.2 Semi-distributed Multi-node TOA-DOA Fusion Localization Scheme

2.2.1 MANET Structure

The proposed MANET is shown Figure 2.1, which is composed of BNs and TNs. We assume: (1) There are N BNs and M TNs uniformly distributed in the MANET; (2) BNs localize other nodes by TOA-DOA joint estimation; (3) Only LOS scenario is considered; (4) TOA and DOA estimation errors are independent zero mean Gaussian random variables, TOA error variance is σ_{TOA}^2 (the corresponding range error variance is $\sigma_R^2 = c^2 \sigma_{TOA}^2$, c is the speed of light), and DOA error variance is σ_θ^2 ; (5) DOA is measured anticlockwise with respect to the x-axis (e.g., east); and, (6) BNs' direction is aligned using a compass.

2.2.2 Localization Scheme

The proposed scheme includes three stages shown in the flow chart of Figure 2.2.

- (i) *Sub-optimal reference-node selection and node clustering*: BN i , $i \in \{1, \dots, N\}$,

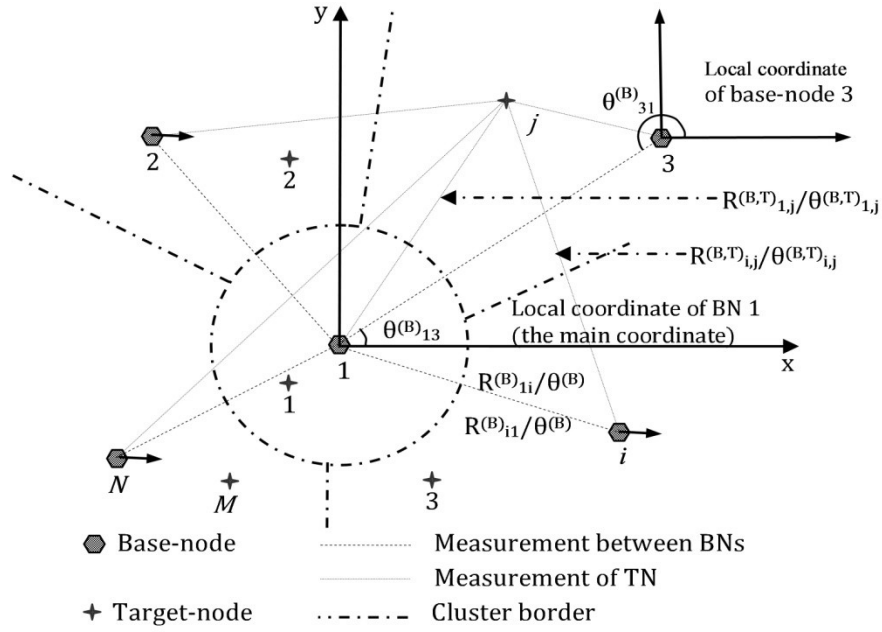


Figure 2.1: The clustered MANET structure.

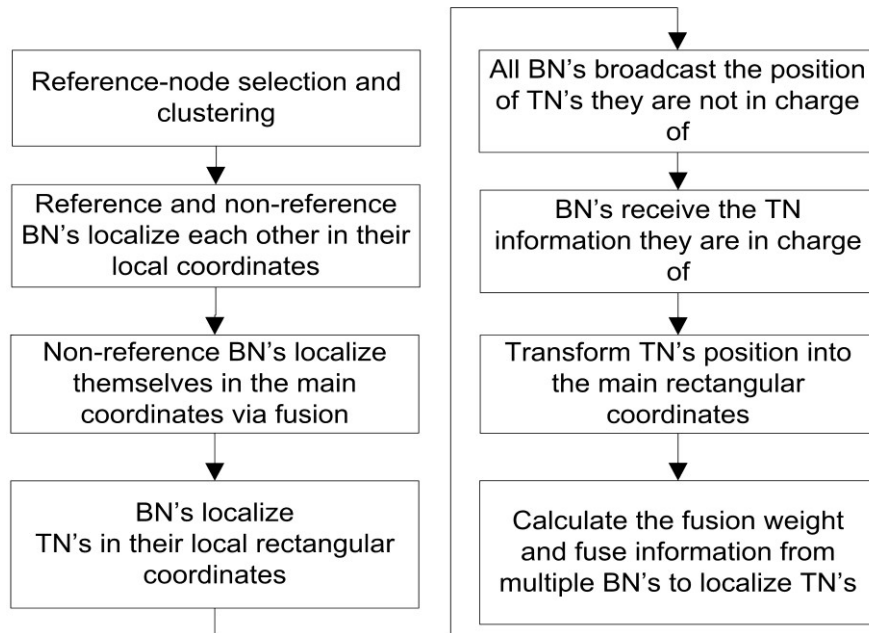


Figure 2.2: Positioning flow chart.

estimates the distance between itself and all TNs, $R_{i,j}^{(B,T)}$, $\forall j, j \in \{1, \dots, M\}$ (the superscript “ B, T ” indicates TNs information with respect to BN, and the subscript “ ij ”

indicates the TN j ’s information in the BN i ’s local coordinate); the BN v is selected as the reference-node using the following objective function (see Section 2.4 for details)

$$v_{sub-optimal} = \arg \min_i \sum_{j=1}^M R_{i,j}^{(B,T)^2}. \quad (2.1)$$

It should be noted that in this chapter all coordinates are local and they are defined for BNs. In other words, the location of each TN can be calculated in the local coordinate of any given BN. Now, one of these BNs is selected as the reference-node and its coordinate is called the main coordinate (see Figure 2.1). The proposed fusion is applied to the positions of all nodes measured in the main coordinate. In the following discussion, we assume BN 1 is selected as the reference-node.

To achieve higher position update rate, we divide the MANET into Q ($Q \leq N$) clusters. The clustering objective is to minimize the fusion time. Here, we assume a cluster includes one BN and a number of TNs. The BN in each cluster is in charge of localization data fusion for all nodes located within that cluster. In practice, the number of TNs within each cluster varies. However, assuming uniform distribution of nodes, in a long run, the average computation load (number of TNs) across all clusters would be equivalent.

(ii) *Non-reference BN position estimation*: The reference-node and each non-reference BN pair localize each other. Then, we have one pair of estimated positions:

non-reference BNs position in the main coordinate (i.e., with respect to the reference-node), and the reference-node's position in non-reference BNs local coordinate. The non-reference BN fuses the two estimated observables via weighted sum to make a better estimation of its position in the main coordinate. Finally, non-reference BNs broadcast their position to make each BN aware of their location in the main coordinate.

(iii) *TNs position estimation*: This stage consists of four steps: a) Every BN localizes TNs in its local coordinate; b) Each BN broadcasts the position of TNs that are not in its cluster to other BNs; c) Only the BN that is in the same cluster as the desired TN uses the broadcasted TN position information; d) That BN transforms TNs position to the main rectangular coordinate and fuses them to localize the TN.

2.2.3 Position Update Rate

Position update rate is an important parameter in a localization system. For example, GPS update rate is limited to 10Hz [56]; thus, INS (Inertial Navigation System) is integrated with GPS to achieve higher update rate, e.g., to navigate unmanned vehicles [56]. The position update rate, $Rate_u$, is determined by data acquisition time, t_a , data transmission time, t_t , and data processing time, t_p , i.e., $1/Rate_u = t_a + t_t + t_p$.

The data acquisition process is the same for centralized and semi-distributed schemes; hence, the data acquisition time for the two methods is the same, i.e., $t_a^{(ce)} = t_a^{(s-d)}$. Here, the superscript “ce” indicates the centralized scheme, and the superscript “s-d” refers to the semi-distributed scheme. In the centralized scheme, all non-reference BNs transmit

TNs position to the reference-node and the reference-node processes all data. In this case, the data transmission time corresponds to $t_T^{(ce)} = t_{T1} \cdot \max_i u_i$, and the data processing time is $t_p^{(ce)} = M \cdot t_{p1}$. Here, t_{T1} is the data transmission time for one TN; u_i is the number of TNs localized by BN i ; and, t_{p1} is the data processing time for localizing one TN.

As mentioned, in the semi-distributed scheme, BNs broadcast the position of TNs that are not in their clusters. Thus, the data transmission time corresponds to $t_T^{(s-d)} = t_{T1} \cdot \max_i (u_i - h_i)$, $i \in \{1, \dots, N\}$, h_i is the number of TNs in the cluster containing BN i ; and, the data processing time is $t_p^{(s-d)} = t_{p1} \cdot \max_i h_i$.

Now, assume a small scale MANET, in which, all BNs localize all TNs (i.e., $u_i = u_j = M$, $\forall i, j \in \{1, \dots, N\}$). In this case, the data transmission time in the centralized scheme ($t_T^{(ce)} = M \cdot t_{T1}$) would be larger than that of the semi-distributed scheme ($t_T^{(s-d)} = t_{T1} (M - \min_i h_i)$). Considering uniform clustering (the same number of TNs in each cluster), h_i would be in the order of M/N . Hence, $t_p^{(s-d)} = (M/N) \cdot t_{p1} < t_p^{(ce)} = M \cdot t_{p1}$, and we achieve higher position update rate than the centralized scheme.

2.3 Multi-node TOA-DOA Fusion

2.3.1 Non-Reference BNs Localization Fusion

The reference-node (BN 1) and non-reference BN i localize each other, and achieve the

distance and angle pairs $(R_{li}^{(B)}, \theta_{li}^{(B)})$ and $(R_{il}^{(B)}, \theta_{il}^{(B)})$. The superscript (B) indicates BN, and the subscript li (or il) indicates the BN i 's (or l 's) information in the BN l 's (or i 's) coordinate. BN i is localized by fusing the two sets of data in the main polar coordinate via weighted sum. Assuming similar zero mean Gaussian noise at all BNs, we have $E(R_{li}^{(B)}) = R_{li}^{(B,t)}$, $E(R_{il}^{(B)}) = R_{il}^{(B,t)}$, $E(\theta_{li}^{(B)}) = \theta_{li}^{(B,t)}$ and $E(\theta_{il}^{(B)}) = \theta_{il}^{(B,t)}$. $E(\cdot)$ denotes the expectation operation and the superscript (t) indicates the true value. In addition, $R_{li}^{(B,t)} = R_{il}^{(B,t)}$, $\theta_{li}^{(B,t)} = \theta_{il}^{(B,t)} - \pi$, if $\theta_{li}^{(B,t)} < \pi$ and $\theta_{il}^{(B,t)} = \theta_{il}^{(B,t)} + \pi$, if $\theta_{li}^{(B,t)} \geq \pi$. The BN i 's position estimated via fusion, $(\hat{R}_{li}^{(B)}, \hat{\theta}_{li}^{(B)})$, corresponds to

$$\begin{aligned} \hat{R}_{li}^{(B)} &= a_{li} \cdot R_{li}^{(B)} + a_{il} \cdot R_{il}^{(B)}, \\ \hat{\theta}_{li}^{(B)} &= \begin{cases} b_{li} \cdot \theta_{li}^{(B)} + b_{il} \cdot (\theta_{il}^{(B)} - \pi), & \text{if } \theta_{li}^{(B)} < \pi \\ b_{li} \cdot \theta_{li}^{(B)} + b_{il} \cdot (\theta_{il}^{(B)} + \pi), & \text{if } \theta_{li}^{(B)} \geq \pi \end{cases}. \end{aligned} \quad (2.2)$$

Where, a_{li} , a_{il} , b_{li} and b_{il} are fusion weights. In (2.2), we face ambiguity generated by two reasons: (1) the angle estimation error $(\Delta\theta_{li}^{(B)})$ makes $\theta_{li}^{(B)} < \pi$ while $\theta_{li}^{(B,t)} \geq \pi$, or inversely $\theta_{li}^{(B)} \geq \pi$ while $\theta_{li}^{(B,t)} < \pi$; and, (2) the angle estimation error $(\Delta\theta_{il}^{(B)})$ makes $3\pi/2 < \theta_{il}^{(B)} < 2\pi$ while $0 < \theta_{il}^{(B,t)} < \pi/2$, or inversely $0 < \theta_{il}^{(B)} < \pi/2$ while $3\pi/2 < \theta_{il}^{(B,t)} < 2\pi$. This ambiguity is removed using the periodicity of angle (see Appendix 2.7). Because $E(\hat{R}_{li}^{(B)}) = E(R_{li}^{(B)})$, hence, $a_{li} + a_{il} = 1$. Similarly, $b_{li} + b_{il} = 1$. In (2.2), the fusion objective function is the minimization of the positioning MSE, which corresponds to

$$(a_{li}, a_{il}, b_{li}, b_{il}) = \arg \min_{s.t. a_{li} + a_{il} = 1, b_{li} + b_{il} = 1} E((\Delta r_{li}^{(B)})^2). \quad (2.3)$$

Here, $\Delta r_{li}^{(B)}$ is the positioning error of BN i with respect to BN 1. In the main rectangular coordinate, BN i 's true position, $(x_{li}^{(B,t)}, y_{li}^{(B,t)})$, corresponds to

$$\begin{aligned} x_{li}^{(B,t)} &= R_{li}^{(B,t)} \cos \theta_{li}^{(B,t)}, \\ y_{li}^{(B,t)} &= R_{li}^{(B,t)} \sin \theta_{li}^{(B,t)}. \end{aligned} \quad (2.4)$$

Moreover, the BN i 's position estimated via fusion, $(\hat{x}_{li}^{(B)}, \hat{y}_{li}^{(B)})$, corresponds to

$$\begin{aligned} \hat{x}_{li}^{(B)} &= \hat{R}_{li}^{(B)} \cos \hat{\theta}_{li}^{(B)}, \\ \hat{y}_{li}^{(B)} &= \hat{R}_{li}^{(B)} \sin \hat{\theta}_{li}^{(B)}. \end{aligned} \quad (2.5)$$

In (2.4), $x_{li}^{(B,t)} = \hat{x}_{li}^{(B)} + \Delta \hat{x}_{li}^{(B)}$, $y_{li}^{(B,t)} = \hat{y}_{li}^{(B)} + \Delta \hat{y}_{li}^{(B)}$, $R_{li}^{(B,t)} = \hat{R}_{li}^{(B)} + \Delta \hat{R}_{li}^{(B)}$ and $\theta_{li}^{(B,t)} = \hat{\theta}_{li}^{(B)} + \Delta \hat{\theta}_{li}^{(B)}$.

The fused positioning error of BN i on x-axis, $\Delta \hat{x}_{li}^{(B)}$, and y-axis, $\Delta \hat{y}_{li}^{(B)}$, are calculated via applying Taylor series to (2.4) about the point $(\hat{R}_{li}^{(B)}, \hat{\theta}_{li}^{(B)})$ and taking the first order terms.

$$\begin{aligned} \Delta \hat{x}_{li}^{(B)} &= \Delta \hat{R}_{li}^{(B)} \cos \hat{\theta}_{li}^{(B)} - \Delta \hat{\theta}_{li}^{(B)} \hat{R}_{li}^{(B)} \sin \hat{\theta}_{li}^{(B)}, \\ \Delta \hat{y}_{li}^{(B)} &= \Delta \hat{R}_{li}^{(B)} \sin \hat{\theta}_{li}^{(B)} + \Delta \hat{\theta}_{li}^{(B)} \hat{R}_{li}^{(B)} \cos \hat{\theta}_{li}^{(B)}. \end{aligned} \quad (2.6)$$

Rang and angle errors are independent zero mean Gaussian random variables; thus, the localization errors $\Delta \hat{x}_{li}^{(B)}$ and $\Delta \hat{y}_{li}^{(B)}$ are jointly zero mean Gaussian random variables.

Because $(\Delta r_{li}^{(B)})^2 = (\Delta \hat{x}_{li}^{(B)})^2 + (\Delta \hat{y}_{li}^{(B)})^2$, hence, $E((\Delta r_{li}^{(B)})^2) = \sigma_{\hat{R}_{li}^{(B)}}^2 + (\hat{R}_{li}^{(B)})^2 \sigma_{\hat{\theta}_{li}^{(B)}}^2$. Here,

$\sigma_{\hat{R}_{li}^{(B)}}^2 = E((\hat{R}_{li}^{(B)} - R_{li}^{(B,t)})^2)$ and $\sigma_{\hat{\theta}_{li}^{(B)}}^2 = E((\hat{\theta}_{li}^{(B)} - \theta_{li}^{(B,t)})^2)$. Applying Lagrange multipliers to

(2.3) leads to

$$\nabla[\sigma_{\hat{R}_{li}^{(B)}}^2 + (R_{li}^{(B, t)})^2 \sigma_{\hat{\theta}_{li}^{(B)}}^2 + \lambda_1(a_{li} + a_{2i} - 1) + \lambda_2(b_{li} + b_{2i} - 1)] = 0. \quad (2.7)$$

Here, $\nabla(\cdot)$ refers to differentiation with respect to a_{li} , a_{2i} , b_{li} and b_{2i} . Because BN 1 and BN i perform independently, using (2.2), we can show $\sigma_{\hat{R}_{li}^{(B)}}^2 = a_{li}^2 \sigma_{R_{li}^{(B)}}^2 + a_{2i}^2 \sigma_{R_{li}^{(B)}}^2$ and $\sigma_{\hat{\theta}_{li}^{(B)}}^2 = b_{li}^2 \sigma_{\theta_{li}^{(B)}}^2 + b_{2i}^2 \sigma_{\theta_{li}^{(B)}}^2$. Incorporating these equations into (2.6) and eliminating λ_1 and λ_2 , we achieve

$$\begin{bmatrix} \sigma_{R_{li}^{(B)}}^2 & -\sigma_{R_{li}^{(B)}}^2 & 0 & 0 \\ 1 & 1 & 0 & 0 \\ 0 & 0 & \sigma_{\theta_{li}^{(B)}}^2 & -\sigma_{\theta_{li}^{(B)}}^2 \\ 0 & 0 & 1 & 1 \end{bmatrix} \cdot \begin{bmatrix} a_{li} \\ a_{2i} \\ b_{li} \\ b_{2i} \end{bmatrix} = \begin{bmatrix} 0 \\ 1 \\ 0 \\ 1 \end{bmatrix}. \quad (2.8)$$

BNs have the same range and angle error variances, i.e., $\sigma_{R_{li}^{(B)}}^2 = \sigma_{R_{li}^{(B)}}^2 = \sigma_R^2$ and $\sigma_{\theta_{li}^{(B)}}^2 = \sigma_{\theta_{li}^{(B)}}^2 = \sigma_\theta^2$. Thus, (2.8) leads to $a_{li} = a_{2i} = b_{li} = b_{2i} = 0.5$. Incorporating these fusion weights into (2.2), we achieve the fused BN i 's position in the main polar coordinate. Moreover, using (2.5), we obtain BN i 's position in the main rectangular coordinate estimated via fusion. The corresponding positioning error variance, $(\sigma_{\hat{x}_{li}^{(B)}}^2, \sigma_{\hat{y}_{li}^{(B)}}^2)$, is

$$\begin{aligned} \sigma_{\hat{x}_{li}^{(B)}}^2 &= \left(\sigma_R^2 \cos^2 \theta_{li}^{(B, t)} + \sigma_\theta^2 (R_{li}^{(B, t)})^2 \sin^2 \theta_{li}^{(B, t)} \right) / 2, \\ \sigma_{\hat{y}_{li}^{(B)}}^2 &= \left(\sigma_R^2 \sin^2 \theta_{li}^{(B, t)} + \sigma_\theta^2 (R_{li}^{(B, t)})^2 \cos^2 \theta_{li}^{(B, t)} \right) / 2. \end{aligned} \quad (2.9)$$

2.3.2 TNs Localization Fusion

TN position is estimated *directly* (one-hop) by the reference-node, and, *indirectly* (two-

hop) through non-reference BNs. In this fusion, all positioning information of a TN is transformed to the main rectangular coordinate and then the projections on x and y axes are fused via weighted sum, respectively.

i) *Coordinate transformation*: In non-reference BNs localization, we have calculated non-reference BNs position in the main coordinate. Hence, TN position provided by any BN can be transformed into the main coordinate. The TN j 's position estimated by BN i is $(R_{i,j}^{(B,T)}, \theta_{i,j}^{(B,T)})$, the subscript " i,j " indicate TN j 's information in the BN i 's local coordinate. Moreover, in the BN i 's local rectangular coordinate, its position, $(x_{i,j}^{(B,T)}, y_{i,j}^{(B,T)})$, is

$$\begin{aligned} x_{i,j}^{(B,T)} &= R_{i,j}^{(B,T)} \cos \theta_{i,j}^{(B,T)}, \\ y_{i,j}^{(B,T)} &= R_{i,j}^{(B,T)} \sin \theta_{i,j}^{(B,T)}. \end{aligned} \quad (2.10)$$

The TN j 's localization error in the coordinate of BN i is calculated using the same method calculating the non-reference BN localization error.

$$\begin{aligned} \Delta x_{i,j}^{(B,T)} &= \Delta R_{i,j}^{(B,T)} \cos \theta_{i,j}^{(B,T)} - \Delta \theta_{i,j}^{(B,T)} R_{i,j}^{(B,T)} \sin \theta_{i,j}^{(B,T)}, \\ \Delta y_{i,j}^{(B,T)} &= \Delta R_{i,j}^{(B,T)} \sin \theta_{i,j}^{(B,T)} + \Delta \theta_{i,j}^{(B,T)} R_{i,j}^{(B,T)} \cos \theta_{i,j}^{(B,T)}. \end{aligned} \quad (2.11)$$

Rang and angle errors are independent zero mean Gaussian random variables; thus, the localization errors $\Delta x_{i,j}^{(B,T)}$ and $\Delta y_{i,j}^{(B,T)}$ are jointly zero mean Gaussian random variables.

The corresponding positioning variance, $(\sigma_{x_{i,j}^{(B,T)}}^2, \sigma_{y_{i,j}^{(B,T)}}^2)$, is

$$\begin{aligned}\sigma_{x_{i,j}^{(B,T)}}^2 &= \sigma_R^2 \cos^2 \theta_{i,j}^{(B,T,t)} + \sigma_\theta^2 (R_{i,j}^{(B,T,t)})^2 \sin^2 \theta_{i,j}^{(B,T,t)}, \\ \sigma_{y_{i,j}^{(B,T)}}^2 &= \sigma_R^2 \sin^2 \theta_{i,j}^{(B,T,t)} + \sigma_\theta^2 (R_{i,j}^{(B,T,t)})^2 \cos^2 \theta_{i,j}^{(B,T,t)}.\end{aligned}\quad (2.12)$$

When we transform TN j 's position into the main rectangular coordinate, we achieve

$$(x_{1i,j}^{(B,T)}, y_{1i,j}^{(B,T)})$$

$$\begin{aligned}x_{1i,j}^{(B,T)} &= \hat{x}_{1i}^{(B)} + x_{i,j}^{(B,T)}, \\ y_{1i,j}^{(B,T)} &= \hat{y}_{1i}^{(B)} + y_{i,j}^{(B,T)}.\end{aligned}\quad (2.13)$$

The corresponding positioning error $(\Delta x_{1i,j}^{(B,T)}, \Delta y_{1i,j}^{(B,T)})$ and its variance $(\sigma_{x_{1i,j}^{(B,T)}}^2, \sigma_{y_{1i,j}^{(B,T)}}^2)$ are

$$\begin{aligned}\Delta x_{1i,j}^{(B,T)} &= \Delta \hat{x}_{1i}^{(B)} + \Delta x_{i,j}^{(B,T)}, \quad \Delta y_{1i,j}^{(B,T)} = \Delta \hat{y}_{1i}^{(B)} + \Delta y_{i,j}^{(B,T)}; \\ \sigma_{x_{1i,j}^{(B,T)}}^2 &= \sigma_{\hat{x}_{1i}^{(B)}}^2 + \sigma_{x_{i,j}^{(B,T)}}^2, \quad \sigma_{y_{1i,j}^{(B,T)}}^2 = \sigma_{\hat{y}_{1i}^{(B)}}^2 + \sigma_{y_{i,j}^{(B,T)}}^2.\end{aligned}\quad (2.14)$$

The reference-node is located at the origin; hence, in (2.13), $\hat{x}_{11}^{(B)} = \hat{y}_{11}^{(B)} = 0$; and, in (2.14),

$$\sigma_{\hat{x}_{11}^{(B)}}^2 = \sigma_{\hat{y}_{11}^{(B)}}^2 = 0.$$

ii) *Fusion*: The weighted sum is applied to fuse multiple positioning information of TN provided by multiple BNs to estimate the TN position in the main rectangular coordinate.

The fused TN j 's position $(\hat{x}_{1,j}^{(T)}, \hat{y}_{1,j}^{(T)})$ and the positioning error $(\Delta \hat{x}_{1,j}^{(T)}, \Delta \hat{y}_{1,j}^{(T)})$ respectively correspond to

$$\begin{aligned}\hat{x}_{1,j}^{(T)} &= \sum_{i=1}^N p_{i,j} x_{1i,j}^{(B,T)}, \\ \hat{y}_{1,j}^{(T)} &= \sum_{i=1}^N q_{i,j} y_{1i,j}^{(B,T)};\end{aligned}\tag{2.15}$$

and,

$$\begin{aligned}\Delta \hat{x}_{1,j}^{(T)} &= \sum_{i=1}^N p_{i,j} \Delta x_{1i,j}^{(B,T)}, \\ \Delta \hat{y}_{1,j}^{(T)} &= \sum_{i=1}^N q_{i,j} \Delta y_{1i,j}^{(B,T)}.\end{aligned}\tag{2.16}$$

In (2.16), $\Delta x_{1i,j}^{(B,T)} = \Delta \hat{x}_{1i}^{(B)} + \Delta x_{i,j}^{(B,T)}$ and $\Delta y_{1i,j}^{(B,T)} = \Delta \hat{y}_{1i}^{(B)} + \Delta y_{i,j}^{(B,T)}$, $i=1,2,\dots$; in addition, $\Delta \hat{x}_{1i}^{(B)}$, $\Delta \hat{y}_{1i}^{(B)}$, $\Delta x_{i,j}^{(B,T)}$ and $\Delta y_{i,j}^{(B,T)}$ are linear combinations of independent zero mean Gaussian random variables (range and angle errors); thus, $\Delta \hat{x}_{1,j}^{(T)}$ and $\Delta \hat{y}_{1,j}^{(T)}$ are jointly zero mean Gaussian random variables, as well. The fusion weights $p_{i,j}$ and $q_{i,j}$ are calculated by minimizing the positioning MSE $\left(E(\Delta r_{1,j})^2\right)$

$$\begin{aligned}(p_{1,j}, \dots, \dots, \dots) &\arg \min E((\Delta r_{1,j})^2). \\ \text{s.t. } \sum_{i=1}^N p_{i,j} &= 1, \sum_{i=1}^N q_{i,j} = 1\end{aligned}\tag{2.17}$$

The constraints $\sum_{i=1}^N p_{i,j} = 1$ and $\sum_{i=1}^N q_{i,j} = 1$ are derived using the same approach as the constraints on (2.3). Incorporating $(\Delta r_{1,j})^2 = (\Delta \hat{x}_{1,j}^{(T)})^2 + (\Delta \hat{y}_{1,j}^{(T)})^2$ into (2.17) and using the same approach applied to (2.3) (see Equation (2.7)), the fusion weights $p_{i,j}$ and $q_{i,j}$ are calculated

$$\begin{aligned}
p_{i,j} &= (1 / \sigma_{x_{1i,j}}^{2(B,T)}) / \sum_{k=1}^N (1 / \sigma_{x_{1k,j}}^{2(B,T)}), \\
q_{i,j} &= (1 / \sigma_{y_{1i,j}}^{2(B,T)}) / \sum_{k=1}^N (1 / \sigma_{y_{1k,j}}^{2(B,T)}).
\end{aligned} \tag{2.18}$$

Incorporating (2.18) in (2.15), the fused TN j 's position is calculated, and the positioning MSE is

$$E\left((\Delta r_{1,j})^2\right) = 1 / \sum_{k=1}^N (1 / \sigma_{x_{1k,j}}^{2(B,T)}) + 1 / \sum_{k=1}^N (1 / \sigma_{y_{1k,j}}^{2(B,T)}). \tag{2.19}$$

2.3.3 System Computational Complexity

The system computational complexity (C_{NOM}) is defined as the number of multiplications in one estimation of all TNs' position. In the complexity calculation, we assume the values of sine and cosine functions are achieved via a lookup table. Moreover, seven multiplications are required for the inverse operation [57]. The number of multiplications in each localization step is listed in Table 2.1. Adding all multiplications listed in Table 2.1 leads to

$$C_{NOM} = 7MN^2 + (24M + 18)N - 18. \tag{2.20}$$

Considering evenly clustering, the computational complexity of the semi-distributed method (in the order of $M \cdot N$) would be much lower than that of the centralized scheme (in the order of MN^2).

Table 2.1: Number of multiplications in each localization step

Localization step	Number of multiplications
Reference-node selection	$N \cdot M$
Non-reference BNs localization	$4 (N-1)$
Non-reference BNs positioning variance calculation	$14 (N-1)$
Localizing TNs in BNs local coordinate	$2 N \cdot M$
TNs positioning variance calculation in BNs local coordinate	$12 N \cdot M$
Fusion weights calculation	$7 (N+1) \cdot N \cdot M$
TNs position estimation fusion	$2 N \cdot M$

2.4 Sub-optimal Reference-node Selection

As discussed in Section 2.2.2, the reference-node is carefully selected. The optimal selection algorithm follows: (a) let $i = 1$; (b) assume BN i , $i \in \{1, 2, \dots, N\}$, is the reference-node, localize non-reference BNs and form clusters in the MANET; (c) localize TNs via fusion and generate TNs positioning MSE for this selection, $E(\Delta r_{i,j}^2)$, $j = 1, \dots, M$, and $\Delta r_{i,j}$ is the TN j 's positioning error in the condition that BN i is the reference-node; (d) if $i < N$, replace i with $i+1$ and go to step (b); (e) select BN that minimizes the positioning MSE across all TNs as the optimal reference-node, $v_{optimal}$, i.e.,

$$v_{optimal} = \arg \min_i \sum_j E(\Delta r_{i,j}^2), i \in \{1, 2, \dots, N\}, j \in \{1, 2, \dots, M\}. \quad (2.21)$$

As discussed in the steps (b) to (d) of the optimal reference-node selection, in this method, all TNs need to be localized N times via data fusion. This leads to a high time and power consumption.

To reduce the time and power consumption, we propose a sub-optimal scheme.

Considering (2.14) and (2.19), we evaluate the upper bound of $\sum_j E(\Delta r_{i,j}^2)$

$$\begin{aligned} \sum_j E(\Delta r_{i,j}^2) &= \left(\sum_j 1 / \sum_{k=1}^N (1 / \sigma_{x_{ik,j}}^{2(B,T)}) + 1 / \sum_{k=1}^N (1 / \sigma_{y_{ik,j}}^{2(B,T)}) \right) \\ &< \sum_j \left(\min_k (\sigma_{x_{ik,j}}^{2(B,T)}) + \min_k (\sigma_{y_{ik,j}}^{2(B,T)}) \right) \\ &\leq \sum_j \left(\sigma_{x_{ii,j}}^{2(B,T)} + \sigma_{y_{ii,j}}^{2(B,T)} \right) \end{aligned} \quad (2.22)$$

In (22), the first inequality is well known and we ignore its proof. Here, $\sigma_{x_{ik,j}}^{2(B,T)}$ is the x -axis positioning error variance of TN j measured by the BN k , in the local coordinate of reference BN i . This is two-hop positioning that includes the positioning error of the TN with respect to the BN *and* that of the non-reference BN with respect to the reference BN.

Thus, $\sigma_{x_{ik,j}}^{2(B,T)} \leq \sigma_{x_{ii,j}}^{2(B,T)}$. Here, $\sigma_{x_{ii,j}}^{2(B,T)}$ is the x -axis positioning error variance of the TN j measured by the reference BN i that is single hop positioning. Similarly, $\sigma_{y_{ik,j}}^{2(B,T)} \leq \sigma_{y_{ii,j}}^{2(B,T)}$.

This proves the second inequality in (22).

The total positioning error variance of the TN j measured by the reference BN is $\sigma_{x_{ii,j}}^{2(B,T)} + \sigma_{y_{ii,j}}^{2(B,T)}$. Using (2.14) and (2.12), and considering BN i is the reference BN, using some simple mathematical manipulations, it is proved that

$$\sum_j \left(\sigma_{x_{ii,j}}^{2(B,T)} + \sigma_{y_{ii,j}}^{2(B,T)} \right) = \sum_j \left(\sigma_R^2 + \sigma_\theta^2 (R_{i,j}^{(B,T,t)})^2 \right). \text{ Here, } \sigma_R^2 \text{ and } \sigma_\theta^2 \text{ are constants; hence,}$$

$\arg \min_i \sum_j \left(\sigma_R^2 + \sigma_\theta^2 \left(R_{i,j}^{(B,T,t)} \right)^2 \right) = \arg \min_i \sum_j \left(R_{i,j}^{(B,T,t)} \right)^2$. Comparing this equation with (2.21),

we observe that in the proposed sub-optimal method, $\Delta r_{i,j}$ in the optimal method of (2.21) has been replaced by $R_{i,j}^{(B,T,t)}$, i.e.,

$$v_{sub-optimal} = \arg \min_i \sum_j \left(R_{i,j}^{(B,T,t)} \right)^2. \quad (2.23)$$

Thus, in the proposed sub-optimal approach, the BN that has the minimum total squared distance from all TNs is selected as the reference BN. Thus, in the proposed sub-optimal method, the non-reference BN positioning error is not minimized. In real applications, $R_{i,j}^{(B,T,t)}$ (true value) in (23) is replaced by $R_{i,j}^{(B,T)}$ (estimated value), and we achieve (2.1). Here, the distance of BNs to TNs ($R_{i,j}^{(B,T)}$) is measured once, while the summation across its square value is calculated N (the number of BNs) times; hence, considerable time and power are saved.

2.5 Simulations and Discussions

Simulations are conducted to evaluate the efficiency of the sub-optimal reference-node selection scheme, the positioning error and the position update rate of the proposed localization method. We also compare the positioning error of the proposed technique with the TOA-only technique proposed in [43]. In TOA-only technique, all nodes are localized in a local coordinate system which is determined by three BNs: one BN is located at the coordinate origin (BN A), the second one is located on the x-axis and its x-coordinate is

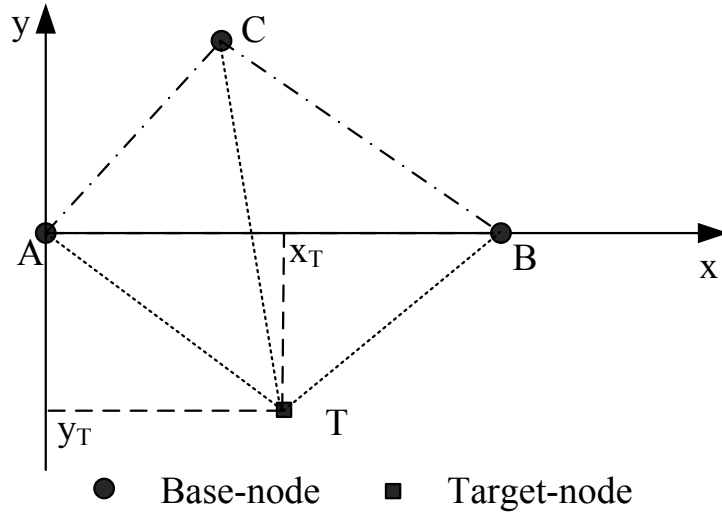


Figure 2.3: TOA-only localization method.

assumed larger than zero (BN B), and the third one's y-coordinate is assumed larger than zero (BN C). Figure 2.3 represents the TOA-only scenario.

The TOA-only estimation technique has been summarized as follow: (1) the three BNs use TOA estimation to find the angle $\angle CAB$; (2) the angle $\angle CAB$ is used to setup the local coordinate system; (3) the BNs use the TOA estimation to find the angle $\angle CAT$ and $\angle BAT$ (T is the target position); and, (4) they use $\angle CAB$, $\angle CAT$, and $\angle BAT$ and the range between BN A and TN T to find the target position.

The proposed localization method and the TOA-only method presented in [43] are comparable: a local coordinate system is first determined via localizing BNs, and then TNs are localized in the local coordinate system. In other words, the two localization systems perform independently. Hence, we compare the positioning error of the proposed

localization method and the TOA-only method via simulations.

Here, we assume: (1) All BNs in the MANET are involved in TNs localization; (2) The impact of nodes mobility is ignored; (3) The MANET coverage radius is normalized to σ_R ; (4) nodes distribution in the proposed localization technique and the TOA-only localization technique is the same; (5) Processor performs 450 million multiplications per second; (6) DOA estimation needs 7000 multiplications [58], and TOA estimation and data detection have the same complexity; (7) TOA, DOA estimation and data detection are implemented at BNs, TOA estimation and data detection are implemented at TNs; and, (8) The communication data rate is 2Mbps and TOA-DOA occupies 40bits.

The efficiency of the sub-optimal reference-node selection is evaluated in terms of average positioning MSE increment percentage defined as:

$$\left(\sum_j E[(\Delta r_{i,j}^{(T)})^2]_{sub-optimal} - \sum_j E[(\Delta r_{i,j}^{(T)})^2]_{optimal} \right) / \sum_j E[(\Delta r_{i,j}^{(T)})^2]_{optimal} \times 100\%.$$

Figure 2.4 depicts that the average positioning MSE increment decreases with number of TNs, i.e., the performance of the sub-optimal method tends to that of the optimal one as the number of TNs increases. If the number of TNs is not large enough and they are not distributed uniformly the optimal and the sub-optimal methods may lead to different selection of reference BNs which reduces the localization performance. The probability, by which the reference-nodes selected using the two methods are different, decreases as the nodes distribution tends to uniform distribution. In a MANET including more than two BNs and five TNs, the average positioning MSE increment is less than 1.6%.

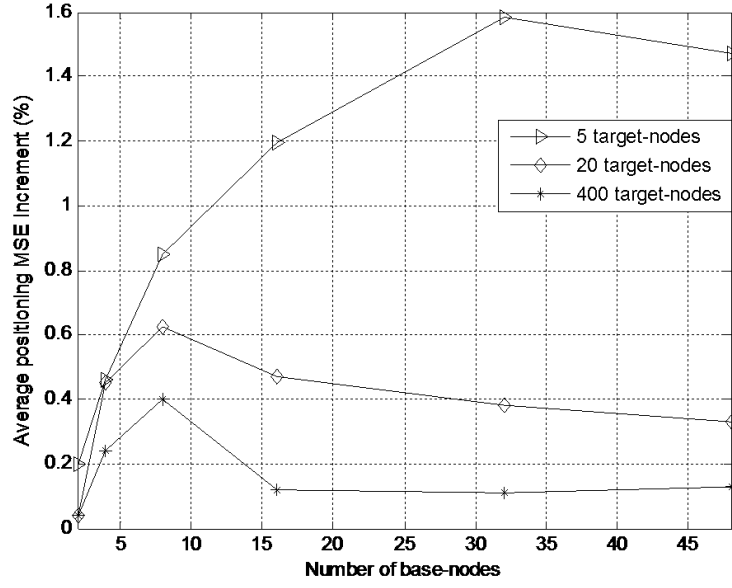


Figure 2.4: Efficiency of the sub-optimal reference-node selection method.

The positioning performance of the proposed method and the TOA-only method is evaluated in terms of the average positioning MSE normalized to the range error variance (σ_R^2). In Figure 2.5, x-axis is the MANET coverage radius normalized to σ_R , y-axis is the average positioning MSE normalized to σ_R^2 , the curve that is marked by circle represents the performance of TOA-only localization method and other curves represent the proposed TOA-DOA method. Figure 2.5 depicts that: (i) the average positioning MSE of the proposed localization method decreases as the number of BNs increases, and the positioning error decreasing rate decreases as the number of BNs increases; for example, with $80\sigma_R$ MANET radius, 3° angle error standard deviation, the average positioning MSE is $9.6\sigma_R^2$ (with one BN), $4.1\sigma_R^2$ (with three BNs), and $2.4\sigma_R^2$ (with five BNs); (ii) the average positioning MSE

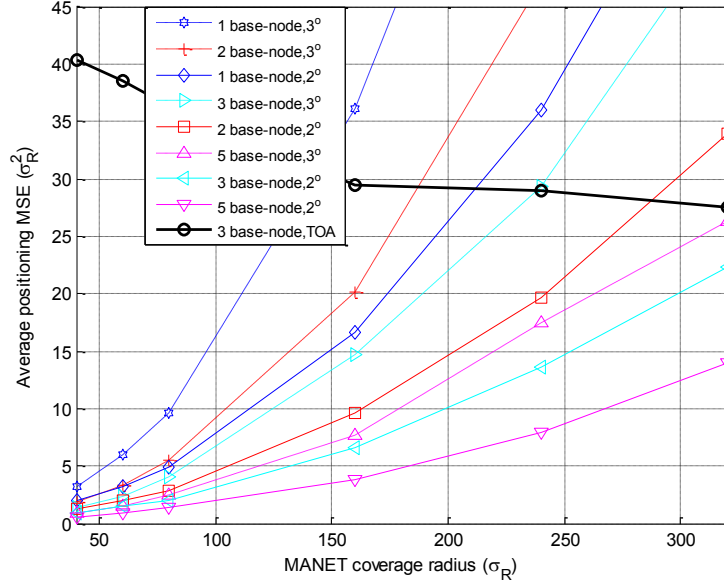


Figure 2.5: Average positioning MSE evaluation of the proposed semi-distributed localization technique and the TOA-only technique (here, α° means the angle error standard deviation is α degree).

of the proposed localization method increases to more than 20 times as the MANET radius increases from $40\sigma_R$ to $320\sigma_R$; while the average positioning MSE of the TOA-only method decreases to 68% as the MANET radius increases from $40\sigma_R$ to $320\sigma_R$; and, (iii) the average positioning MSE of the proposed localization method increases to 1.5 to 2.4 times as the DOA error standard deviation increases from 2° to 3° .

Thus, the proposed technique performance would be considerably superior to the TOA-only estimation technique, if the DOA-estimation error is low and the MANET coverage area is small enough (for a given DOA estimation error). As the DOA estimation error

increases or the MANET coverage area increases, the TOA-only estimation technique would perform better. On the other hand, the simulations depict that in the TOA-only method, the positioning error could increase if the BNs are closely located: in the TOA-only technique, TOA estimation is used to measure the angle $\angle CAB$ in Figure 2.3. For a given TOA estimation error, closely located BNs lead to higher error in the estimation of $\angle CAB$, this ultimately degrades the TN localization performance. Thus, there are limitations in the TOA-only estimation as well.

In addition, comparing to the TOA-only method (in which at least three BNs are required), the proposed localization technique is able to localize TN with less number of BNs (1 or more). However, the complexity of each BN in the proposed TOA-DOA technique is higher compared to the TOA-only estimation: DOA estimation needs multiple-antennas.

Based on the above discussion, one future direction of our research can be formed: we might be able to modify the proposed TOA-DOA technique and maintain a tradeoff between our technique and the TOA-only technique based on some variables. Those variables include: DOA estimation error, MANET coverage area and the BNs relative positions.

The proposed localization technique does not depend on GPS; hence, it is applicable to GPS-denied environments. Its localization error is bounded by the single BN positioning error. In other words, any extra BN helps decrease the localization error. The TOA-only

method presented in [43] is also applicable in GPS-denied environments. However, in the TOA-only localization technique only three BNs contribute in the TN localization process. Hence, the localization performance cannot be enhanced by adding extra BNs to the system (unless we use the available BNs and select those that possess a better distribution).

In the proposed TOA-DOA method, the positioning performance increases with a lower rate as the number of BNs increases. However, computational complexity increases with a higher rate as the number of BNs increases. Hence, if we increase the number of BNs beyond a specific number, we may highly increase the complexity, while its impact on the performance enhancement would be minimal. For instance, given $M = 200$ TNs, $80\sigma_R$ MANET radius, 2° angle error standard deviation, and the maximum complexity of 12000, we should maintain the number of BNs equal to 5 to achieve the MSE of $1.43\sigma_R^2$. Moreover, if nodes are not uniformly distributed, some BNs may not localize some TNs. This reduces the performance of the proposed method.

Figure 2.6 compares the position update rate of the proposed semi-distributed scheme and the centralized scheme. It depicts that: a) if the number of TNs increases to n times (n is a positive number), then the position update rate of the two methods would decrease to $1/n$ times; b) the position update rate of the two method decreases as the number of BNs increases, and the position update rate of the centralized method decreases much faster than the semi-distributed method; d) the position update rate of the semi-distributed method is always higher than that of the centralized scheme; and, e) if the MANET

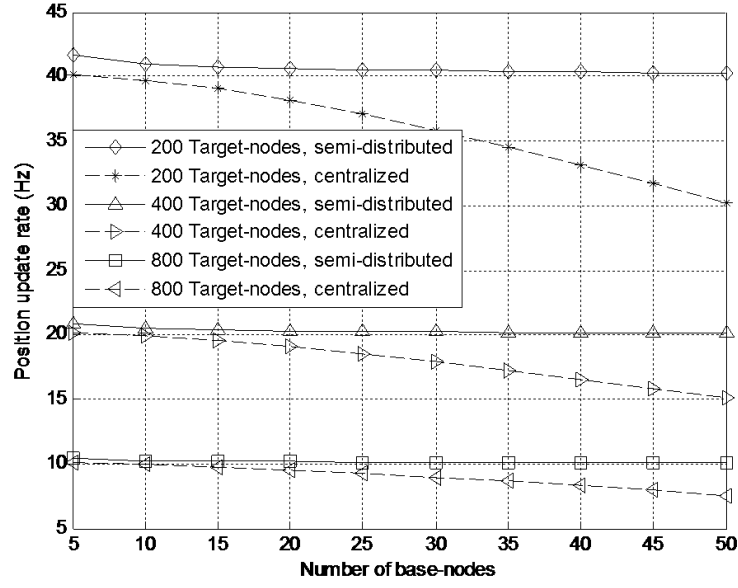


Figure 2.6: Position update rate comparison between the proposed semi-distributed scheme and the centralized scheme.

includes less than 50 BNs and 400 TNs, the proposed semi-distributed scheme position update rate would be larger (more than 20 Hz) than that of GPS (limited to 10Hz).

Taylor series are used to calculate nodes' positioning error and the fusion weight, which holds if errors are small; hence, this method is not suitable for those scenarios with large TOA and DOA estimation errors. For example, if LOS is not available or the number of reflections in the channel is high, the estimated DOA would not be reliable. Hence, in general, BNs should be capable of discriminating signals received through LOS and NLOS in order to evaluate the reliability of localization and fusion. This LOS and NLOS separation problem is addressed in Chapter 5. Moreover, if nodes are not uniformly distributed, some BNs may not localize some TNs. This reduces the performance of the

proposed method.

In the proposed TOA-DOA localization technique, all nodes are localized in the local coordinate of the reference-node. If nodes' positions in a global coordinate system are required, GPS or other global localization system should be applied to determine the reference-node position.

2.6 Conclusions

In this chapter, we proposed a novel semi-distributed localization technique based on multi-node TOA-DOA fusion. Here, based-nodes are capable of localizing TNs independently. The proposed method can be applied to MANETs in the GPS-available and GPS-denied environments. A sub-optimal reference-node selection scheme was proposed. The fusion weights and TNs positioning MSE were theoretically derived. Simulations confirm that: (1) the sub-optimal reference-node selection method is efficient: compared to the optimal method less than 1.6% extra localization error is introduced; (2) multi-node TOA-DOA fusion leads to higher positioning accuracy with higher number of BNs.

Typically, the localization error using five BNs is reduced to 50% to 70% compared to the three BN scenario; (3) the positioning error of the proposed method increases to more than 20 times as the MANET radius increases from $40\sigma_R$ to $320\sigma_R$, the proposed method is suitable for moderate scale MANET; (4) the TOA-only method positioning error would not change considerably if the MANET radius is larger than some value (e.g., $160\sigma_R$), hence, the TOA-only method is suitable for large scale MANET; (5) the positioning error

of the proposed method increases to 1.5 to 2.4 times as the angle error standard deviation increases from 2° to 3° ; and, (6) the position update rate of the proposed method would be larger than 20Hz assuming less than 50 BNs and 400 TNs are available within the MANET.

2.7 Angle Calculation Ambiguity Removing

DOA estimation error of smart antenna array is determined by many parameters that include: (1) the number of array elements; (2) DOA estimation method; (3) signal-to-noise ratio (SNR); (4) the number of observations (snapshots); and, (5) the correlation coefficient of snapshots [59]. Considering a ten-element uniform linear antenna array, 5dB SNR, 400 snapshots, and less than 0.5 snapshots' correlation coefficient, applying root MUSIC DOA estimation method, the root mean square of DOA estimation error would be less than 1° [59]. Assume DOA estimation error is zero mean Gaussian random variables, the probability that the absolute value of DOA estimation error is larger than $\pi/4$ would be ignorable, and we can take $|\Delta\theta_{li}^{(B)}| < \pi/4$ and $|\Delta\theta_{il}^{(B)}| < \pi/4$. This scenario limits node's true and estimated position either in the same quadrant or in the neighboring quadrants that makes the ambiguity analysis easier.

In (2.2), we explained two sources of ambiguity. If source 2 that is the error in $\theta_{il}^{(B)}$ (i.e., $\Delta\theta_{il}^{(B)}$) does not generate ambiguity, i.e., $3\pi/2 < \theta_{il}^{(B)} < 2\pi$ and $3\pi/2 < \theta_{il}^{(B,t)} < 2\pi$, then the following four scenarios may happen: (a) the error in $\theta_{li}^{(B)}$ (i.e., $\Delta\theta_{li}^{(B)}$) makes

$\pi \leq \theta_{li}^{(B)} < 3\pi/2$ while $\pi/2 < \theta_{li}^{(B,t)} < \pi$; (b) $\Delta\theta_{li}^{(B)}$ makes $\pi/2 < \theta_{li}^{(B)} < \pi$ while $\pi \leq \theta_{li}^{(B,t)} < 3\pi/2$; (c) $\Delta\theta_{li}^{(B)}$ makes $3\pi/2 < \theta_{li}^{(B)} < 2\pi$ while $0 < \theta_{li}^{(B,t)} < \pi/2$; and, (d) $\Delta\theta_{li}^{(B)}$ makes $0 < \theta_{li}^{(B)} < \pi/2$ while $3\pi/2 < \theta_{li}^{(B,t)} < 2\pi$.

In the scenario (a), $\theta_{li}^{(B, t)} = \theta_{li}^{(B, t)} - \pi$ and $\pi \leq \theta_{li}^{(B)} < 3\pi/2$. Using (2.2) and the calculated fusion weights b_{li} and b_{2i} , we calculate the fused angle $\hat{\theta}_{li}^{(B)}$

$$\begin{aligned}\hat{\theta}_{li}^{(B)} &= [\theta_{li}^{(B)} + (\theta_{li}^{(B)} + \pi)]/2 \\ &= [\theta_{li}^{(B, t)} + \Delta\theta_{li}^{(B)} + (\theta_{li}^{(B, t)} + \Delta\theta_{li}^{(B)} + \pi)]/2 \\ &= [\theta_{li}^{(B, t)} + \Delta\theta_{li}^{(B)} + (\theta_{li}^{(B, t)} + \pi + \Delta\theta_{li}^{(B)} + \pi)]/2 \\ &= \theta_{li}^{(B, t)} + (\Delta\theta_{li}^{(B)} + \Delta\theta_{li}^{(B)})/2 + \pi.\end{aligned}\tag{2.24}$$

Similarly, we calculate the fused angle in scenarios (b), (c) and (d)

$$\hat{\theta}_{li}^{(B)} = \begin{cases} \theta_{li}^{(B, t)} + (\Delta\theta_{li}^{(B)} + \Delta\theta_{li}^{(B)})/2 - \pi, & \text{scenario (b);} \\ \theta_{li}^{(B, t)} + (\Delta\theta_{li}^{(B)} + \Delta\theta_{li}^{(B)})/2 + 2\pi, & \text{scenario (c);} \\ \theta_{li}^{(B, t)} + (\Delta\theta_{li}^{(B)} + \Delta\theta_{li}^{(B)})/2 - 2\pi, & \text{scenario (d).} \end{cases}\tag{2.25}$$

Sine and cosine functions are periodic with the period of 2π ; hence, scenarios (c) and (d) do not introduce error in the BN i 's position calculation [see (2.5)]. But in scenarios (a) and (b), errors would be introduced. Using the same analysis method, we calculate the fused angle in the other scenarios. Table 2.2 summarizes all scenarios. It is observed that finally only four scenarios lead to ambiguity. Table 2.2 also shows that how correction can be applied. The ultimate angle fusion equation corresponds to

$$\hat{\theta}_{li}^{(B)} = \begin{cases} [\theta_{li}^{(B)} + (\theta_{l1}^{(B)} - \pi)]/2, & \text{if } 0 \leq \theta_{li}^{(B)} \leq \pi/2; \\ [\theta_{li}^{(B)} + (\theta_{l1}^{(B)} - \pi)]/2 + \pi, & \text{if } \pi/2 < \theta_{li}^{(B)} < \pi \text{ and } 0 < \theta_{l1}^{(B)} < \pi/2; \\ [\theta_{li}^{(B)} + (\theta_{l1}^{(B)} - \pi)]/2, & \text{if } \pi/2 < \theta_{li}^{(B)} < \pi \text{ and } 3\pi/2 < \theta_{l1}^{(B)} < 2\pi; \\ [\theta_{li}^{(B)} + (\theta_{l1}^{(B)} + \pi)]/2 - \pi, & \text{if } \pi \leq \theta_{li}^{(B)} < 3\pi/2 \text{ and } 3\pi/2 < \theta_{l1}^{(B)} < 2\pi; \\ [\theta_{li}^{(B)} + (\theta_{l1}^{(B)} + \pi)]/2, & \text{if } \pi \leq \theta_{li}^{(B)} < 3\pi/2 \text{ and } 0 < \theta_{l1}^{(B)} < \pi/2; \\ [\theta_{li}^{(B)} + (\theta_{l1}^{(B)} + \pi)]/2, & \text{if } 3\pi/2 \leq \theta_{li}^{(B)} < 2\pi. \end{cases} \quad (2.26)$$

Table 2.2: Possible angle calculation ambiguity in all scenarios

BN i	BN 1	Error of	Correction	$\theta_{li}^{(B)}$	$\theta_{l1}^{(B)}$
2→3 ²	4→4	π	$-\pi$	$\pi \leq \theta_{li}^{(B)} < 3\pi/2$	$3\pi/2 < \theta_{l1}^{(B)} < 2\pi$
3→2	1→1	$-\pi$	π	$\pi/2 < \theta_{li}^{(B)} < \pi$	$0 < \theta_{l1}^{(B)} < \pi/2$
1→4	3→3	0	0	$3\pi/2 < \theta_{li}^{(B)} < 2\pi$	$\pi \leq \theta_{l1}^{(B)} < 3\pi/2$
4→1	2→2	0	0	$0 < \theta_{li}^{(B)} < \pi/2$	$\pi/2 < \theta_{l1}^{(B)} < \pi$
2→3	4→1 ³	0	0	$\pi \leq \theta_{li}^{(B)} < 3\pi/2$	$0 < \theta_{l1}^{(B)} < \pi/2$
3→2	1→4	0	0	$\pi/2 < \theta_{li}^{(B)} < \pi$	$3\pi/2 < \theta_{l1}^{(B)} < 2\pi$
2→2	4→1	$-\pi$	π	$\pi/2 < \theta_{li}^{(B)} < \pi$	$0 < \theta_{l1}^{(B)} < \pi/2$
3→3	1→4	π	$-\pi$	$\pi \leq \theta_{li}^{(B)} < 3\pi/2$	$3\pi/2 < \theta_{l1}^{(B)} < 2\pi$

² BN i 's true position is in BN 1's second quadrant, but the estimated position is in BN 1's third quadrant.

³ BN 1's true position is in BN i 's fourth quadrant, but the estimated position is in BN i 's first quadrant.

Chapter 3

Localization Performance of the Semi-distributed Multi-node TOA-DOA Fusion

This chapter evaluates the performance of the proposed semi-distributed multi-node TOA-DOA fusion localization technique and compares it with the other two localization methods, GPS-aided TOA fusion and GPS-aided DOA fusion, in terms of localization CEP. The localization CEP of the three techniques is derived theoretically, verified via simulations and compared. The comparison confirms that in moderate scale MANETs, the semi-distributed multi-node TOA-DOA fusion localization technique achieves the best performance; while in large scale MANETs, GPS-aided TOA fusion leads to the best performance.

3.1 Introduction

Different localization performance evaluation standards have been introduced. These standards include cumulative localization error distribution [60], mean and standard deviation of the positioning error [61], normalized mean square of the positioning error [62], and geometrical dilution of precision (GDOP) [10, 28, 63]. GDOP only provides the positioning performance of a system considering single category of measurement (TOA or DOA) and assuming the measurement errors are independent and identically-distributed. Normalized mean square, mean and standard deviation of the positioning

error can be applied to any positioning system, but it only provides one statistics of the positioning performance. Cumulative localization error distribution, also known as CEP [64], incorporates the cumulative density function (CDF) of the positioning error. Hence, it includes more information on the statistics of the positioning error. In addition, it can be applied to any positioning system in any scenario.

Accordingly, we evaluate the performance of the semi-distributed multi-node TOA-DOA fusion localization technique in terms of localization CEP in the condition of all TNs being localized and compare it to that of GPS-aided TOA fusion (the performance of TOA fusion and TDOA fusion is the same [65]) and GPS-aided DOA fusion. In the condition that not all TNs are localized, we use the probability of TNs being localized as standard to compare the three localization methods.

In this chapter, we first derive the localization CEP of the semi-distributed multi-node TOA-DOA fusion; then, we study the impact of GPS positioning error on TOA (DOA) estimation and derive the localization CEP of these two methods; and finally, simulations are conducted to verify the theoretical derivation and compare the three localization methods.

3.2 CEP of the Semi-distributed Multi-node TOA-DOA Fusion

CEP of the TN position estimation by the semi-distributed multi-node TOA-DOA fusion with any given BNs and TN geometrical distribution corresponds to

$$\begin{aligned}
CEP_{point} &= P_{point}(\Delta r_j \leq \beta \sigma_R) \\
&= \int_0^{\beta \sigma_R} f_{point, \Delta r_j}(\Delta r_j) d\Delta r_j.
\end{aligned} \tag{3.1}$$

Here, β is a non-negative number that normalizes the positioning error with respect to σ_R . Δr_j is the TN j 's position estimation circular error with given BNs and TN j 's geometrical distribution (the relative position of BNs and TN j). It is the same with the localization error, $\Delta r_{1,j}$, defined in (2.15), if BN 1 is selected as the reference-node. Because in this chapter, we do not consider reference-node selection, we simply note the localization error as Δr_j . In addition, $f_{point, \Delta r_j}(\Delta r_j)$ is the circular error PDF with the given nodes geometrical distribution. In MANETs, all nodes are moving; hence, nodes' geometrical distribution is continuously changing. We can achieve infinite possible geometrical distribution as there are infinite *points* in an area. In (3.1), we use the subscript “point” to represent a possible node geometrical distribution in MANETs. The circular error PDF changes with the variations in the BNs and TN geometrical distribution. Now, in order to find the CEP, the PDF of Δr_j [$f_{point, \Delta r_j}(\Delta r_j)$] should be first determined. Recall that $\Delta r_j = \sqrt{\Delta \hat{x}_j^{(T)^2} + \Delta \hat{y}_j^{(T)^2}}$, $(\Delta x_j^{(T)}, \Delta y_j^{(T)})$ is the localization error of TN j via multi-node TOA-DOA fusion, it is the same as the fused localization error $(\Delta x_{1,j}^{(T)}, \Delta y_{1,j}^{(T)})$ defined in (2.14) if the BN 1 is selected as the reference node. Because we do not consider reference-node selection in this chapter, we simply note it as $(\Delta x_j^{(T)}, \Delta y_j^{(T)})$. Hence, if we find the joint PDF of $\Delta \hat{x}_j^{(T)}$ and $\Delta \hat{y}_j^{(T)}$, i.e.,

$f_{\Delta\hat{x}_j^{(T)}, \Delta\hat{y}_j^{(T)}}(\Delta\hat{x}_j^{(T)}, \Delta\hat{y}_j^{(T)})$, the PDF of Δr_j would be able to simply calculated. The covariance matrix of $\Delta\hat{x}_j^{(T)}$ and $\Delta\hat{y}_j^{(T)}$ corresponds to

$$\begin{aligned}\Lambda &= \begin{bmatrix} \Lambda_{11} & \Lambda_{12} \\ \Lambda_{21} & \Lambda_{22} \end{bmatrix} \\ &= \begin{bmatrix} \sigma_{\hat{x}_j^{(T)}}^2 & \rho\sigma_{\hat{x}_j^{(T)}}^2\sigma_{\hat{y}_j^{(T)}}^2 \\ \rho\sigma_{\hat{x}_j^{(T)}}^2\sigma_{\hat{y}_j^{(T)}}^2 & \sigma_{\hat{y}_j^{(T)}}^2 \end{bmatrix}.\end{aligned}\quad (3.2)$$

Considering (2.13), the fused TN j 's positioning error variances $(\sigma_{\hat{x}_j^{(T)}}^2, \sigma_{\hat{y}_j^{(T)}}^2)$ can be calculated using

$$\begin{aligned}\sigma_{\hat{x}_j^{(T)}}^2 &= \sum_{i=1}^n p_{i,j}^2 \cdot \sigma_{x_{i,j}}^2, \\ \sigma_{\hat{y}_j^{(T)}}^2 &= \sum_{i=1}^n q_{i,j}^2 \cdot \sigma_{y_{i,j}}^2.\end{aligned}\quad (3.3)$$

The covariance of $\Delta\hat{x}_j^{(T)}$ and $\Delta\hat{y}_j^{(T)}$ are calculated in Section 3.6. In addition, in Chapter 2, we have shown that $\Delta\hat{x}_j^{(T)}$ and $\Delta\hat{y}_j^{(T)}$ are jointly Gaussian. Hence, the joint PDF of $\Delta\hat{x}_j^{(T)}$ and $\Delta\hat{y}_j^{(T)}$ corresponds to [66, 2.1-150]

$$f_{\Delta\hat{x}_j^{(T)}, \Delta\hat{y}_j^{(T)}}(\Delta\hat{x}_j^{(T)}, \Delta\hat{y}_j^{(T)}) = \frac{1}{2\pi|\Lambda|^{0.5}} \exp\left(-\frac{1}{2}[\Delta\hat{x}_j^{(T)} \ \Delta\hat{y}_j^{(T)}]\Lambda^{-1}[\Delta\hat{x}_j^{(T)} \ \Delta\hat{y}_j^{(T)}]^T\right). \quad (3.4)$$

Where, $|\cdot|$ refers to the matrix determinant calculation. Recall that

$\Delta r_j = \sqrt{\Delta \hat{x}_j^{(T)^2} + \Delta \hat{y}_j^{(T)^2}}$, the CDF of Δr_j would correspond to (3.40) in Section 3.7.

According to the details presented in Section 3.7, the point PDF of Δr_j corresponds to

$$f_{po\text{int}, \Delta r_j}(\Delta r_j) = \frac{\Delta r_j}{|\Lambda|^{0.5}} \exp\left(\frac{\Lambda_{11} + \Lambda_{22}}{-4|\Lambda|} \Delta r_j^2\right) \cdot I_0\left(\frac{\Delta r_j^2 \sqrt{(\Lambda_{22} - \Lambda_{11})^2 + \Lambda_{12}^2}}{4|\Lambda|}\right). \quad (3.5)$$

Incorporating (3.5) into (3.1), we can calculate the point CEP of the TN position estimation for any given BNs and TN geometrical distribution, which corresponds to

$$CEP_{po\text{int}} = \int_0^{\beta\sigma_R} \frac{\Delta r_j}{|\Lambda|^{0.5}} \exp\left(\frac{\Lambda_{11} + \Lambda_{22}}{-4|\Lambda|} \Delta r_j^2\right) \cdot I_0\left(\frac{\Delta r_j^2 \sqrt{(\Lambda_{22} - \Lambda_{11})^2 + \Lambda_{12}^2}}{4|\Lambda|}\right) d\Delta r_j. \quad (3.6)$$

There is no theoretical solution for the integration of (3.6); hence, we evaluate it numerically and compare the numerical result with the simulation result. The average CEP is achieved by averaging the point CEP in (3.6) over all possible BNs and TN geometrical distribution (i.e., all possible point CEP's) in the MANET.

3.3 CEP of GPS-aided TOA Fusion and GPS-aided DOA Fusion

Here, first we derive the relationship of the total range (angle) estimation error and the range (angle) errors generated due to two factors: BNs range (angle) estimations and GPS positioning errors (Section 3.3.1). In the next step, we derive the relationship of the BNs total range (angle) estimation errors and the TN positioning errors projected on x and y axes (Section 3.3.2). Finally, using the relationship derived in Section 3.3.2, we derive

the positioning CEP for GPS-aided TOA (DOA) fusion in Section 3.3.4.

3.3.1 The Impact of GPS Positioning Error on the Final TOA (DOA) Estimation

Figure 3.1 shows the structure of the MANET that applies GPS-aided TOA (DOA) fusion to localize TN. Here, we assume TOA/range (DOA/angle) estimation errors are independent zero mean Gaussian random variables. In these two localization methods, the position of BN i $[(x_i^{(B,t)}, y_i^{(B,t)})]$, $i=1,2,\dots$ and N is the number of BNs in the MANET] is estimated using GPS receiver

$$\begin{aligned} x_i^{(B,t)} &= x_{G,i}^{(B)} + \Delta x_{G,i}^{(B)}, \\ y_i^{(B,t)} &= y_{G,i}^{(B)} + \Delta y_{G,i}^{(B)}. \end{aligned} \quad (3.7)$$

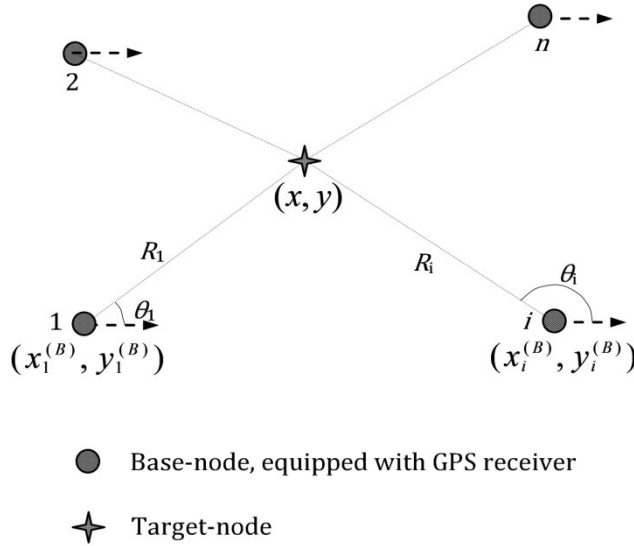


Figure 3.1: The structure of the MANET that applies GPS-aided TOA (DOA) fusion.

In (3.7), $(x_{G,i}^{(B)}, y_{G,i}^{(B)})$ is BN i 's position estimated by GPS receiver, and it is known; and, $(\Delta x_{G,i}^{(B)}, \Delta y_{G,i}^{(B)})$ is the positioning error. The range and angle from the TN with assumed known position (x, y) to BN i are respectively represented by

$$\begin{aligned} R_i &= f_{G,i}(x_i^{(B,t)}, y_i^{(B,t)}) \\ &= \sqrt{(x_i^{(B,t)} - x)^2 + (y_i^{(B,t)} - y)^2} \\ &= \sqrt{(x_{G,i}^{(B)} + \Delta x_{G,i}^{(B)} - x)^2 + (y_{G,i}^{(B)} + \Delta y_{G,i}^{(B)} - y)^2}. \end{aligned} \quad (3.8)$$

and,

$$\begin{aligned} \theta_i &= g_{G,i}(x_i^{(B,t)}, y_i^{(B,t)}) \\ &= \tan^{-1} \left(\frac{y_i^{(B,t)} - y}{x_i^{(B,t)} - x} \right) \\ &= \tan^{-1} \left(\frac{y_{G,i}^{(B)} + \Delta y_{G,i}^{(B)} - y}{x_{G,i}^{(B)} + \Delta x_{G,i}^{(B)} - x} \right). \end{aligned} \quad (3.9)$$

Here, the subscript G, i indicates that the data is achieved via GPS receiver for the BN i .

$$\text{Let } R_{Gi0} = \sqrt{(x_{G,i}^{(B)} - x)^2 + (y_{G,i}^{(B)} - y)^2}, \quad a_{Gxi} = \frac{\partial f_{G,i}(x_{G,i}^{(B)}, y_{G,i}^{(B)})}{\partial x_{G,i}^{(B)}}, \quad a_{Gyi} = \frac{\partial f_{G,i}(x_{G,i}^{(B)}, y_{G,i}^{(B)})}{\partial y_{G,i}^{(B)}},$$

$$b_{Gxi} = \frac{\partial g_{G,i}(x_{G,i}^{(B)}, y_{G,i}^{(B)})}{\partial x_{G,i}^{(B)}} \text{ and } b_{Gyi} = \frac{\partial g_{G,i}(x_{G,i}^{(B)}, y_{G,i}^{(B)})}{\partial y_{G,i}^{(B)}}. \text{ Applying Taylor series to expand (3.8)}$$

and (3.9) and only taking the first order terms, the range estimation error $(\Delta R_{G,i})$ and angle estimation error $(\Delta \theta_{G,i})$ generated by the GPS positioning error are derived

$$\begin{aligned} \Delta R_{G,i} &= f_{G,i}(x_i^{(B)}, y_i^{(B)}) - f_{G,i}(x_{G,i}^{(B)}, y_{G,i}^{(B)}) \\ &= a_{Gxi} \cdot \Delta x_{G,i}^{(B)} + a_{Gyi} \cdot \Delta y_{G,i}^{(B)}; \end{aligned} \quad (3.10)$$

and,

$$\begin{aligned}\Delta\theta_{G,i} &= g_{G,i}(x_i^{(B)}, y_i^{(B)}) - g_{G,i}(x_{G,i}^{(B)}, y_{G,i}^{(B)}) \\ &= b_{Gxi} \cdot \Delta x_{G,i}^{(B)} + b_{Gyi} \cdot \Delta y_{G,i}^{(B)}.\end{aligned}\quad (3.11)$$

Based on [10], $\Delta x_{G,i}^{(B)}$ and $\Delta y_{G,i}^{(B)}$ are jointly zero mean Gaussian random variables with the same variances σ_G^2 ; in addition, GPS receivers perform independently; hence, $\Delta R_{G,i}(\Delta\theta_{G,i}), i=1,2,\dots$, are independent zero mean Gaussian random variables. The variances of $\Delta R_{G,i}$ and $\Delta\theta_{G,i}$ correspond to

$$\begin{aligned}\sigma_{R_{G,i}}^2 &= E[(a_{Gxi} \cdot \Delta x_{G,i}^{(B)} + a_{Gyi} \cdot \Delta y_{G,i}^{(B)})^2] \\ &= \sigma_G^2,\end{aligned}\quad (3.12)$$

and,

$$\begin{aligned}\sigma_{\theta_{G,i}}^2 &= E[(b_{Gxi} \cdot \Delta x_{G,i}^{(B)} + b_{Gyi} \cdot \Delta y_{G,i}^{(B)})^2] \\ &= \sigma_G^2 / R_{Gi0}^2.\end{aligned}\quad (3.13)$$

Here, a_{Gxi} and a_{Gyi} are the direction cosines of the unit vector pointing from TN to the BN i 's position estimated by GPS with respect to x and y axis, respectively (see Figure 3.2). Because BNs and GPS receivers perform independently, in GPS-aided TOA fusion, two independent sources of errors can be defined: BNs range estimation error (ΔR_i) and the range estimation error ($\Delta R_{G,i}$) generated by the GPS positioning error.

Now, when the GPS positioning error is very small with respect to the distance between

BN i and TN, the line connecting the calculated position of the BN to the TN and the line connecting the true position of the BN and TN (see Figure 3.2) would approximately overlap. In this case, the range error generated by the GPS positioning error ($\Delta R_{G,i}$) can be projected on the line connecting TN and the true position of the BN as well. In addition, the BN range estimation error (ΔR_i) is in the direction from TN to BN.

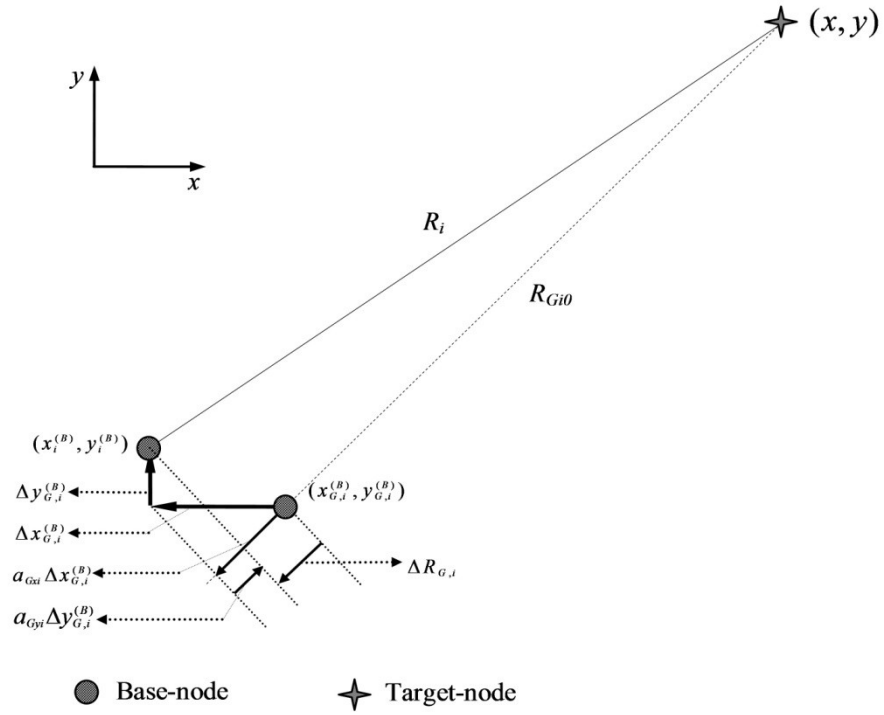


Figure 3.2: Transformation of GPS positioning error to range estimation error.

These two errors can be linearly combined to achieve the total range estimation error $\Delta R'_i$. Base on the same discussion, we can calculate the total angle estimation error $\Delta \theta'_i$. The total range and angle estimation errors correspond to

$$\begin{aligned}\Delta R_i' &= \Delta R_i + \Delta R_{G,i}, \\ \Delta \theta_i' &= \Delta \theta_i + \Delta \theta_{G,i}.\end{aligned}\tag{3.14}$$

The estimation errors (ΔR_i and $\Delta \theta_i$) and the errors generated by GPS positioning error ($\Delta R_{G,i}$ and $\Delta \theta_{G,i}$) are independent zero mean Gaussian random variables. Hence, the total range estimation error $\Delta R_i'$ and the total angle estimation error $\Delta \theta_i'$ are zero mean Gaussian random variables, as well.

The corresponding range and angle error variance are

$$\begin{aligned}\sigma_{R_i'}^2 &= \sigma_R^2 + \sigma_{R_{G,i}}^2, \\ \sigma_{\theta_i'}^2 &= \sigma_\theta^2 + \sigma_{\theta_{G,i}}^2.\end{aligned}\tag{3.15}$$

Here, σ_R^2 (σ_θ^2) is the BN range (angle) estimation error variance. Based on equations (3.12), (3.13) and (3.15), we achieve that $\sigma_{R_i'}^2 = \sigma_{R_j'}^2 = \sigma_R^2$ for any i and j , but $\sigma_{\theta_i'}^2 \neq \sigma_{\theta_j'}^2$, if $i \neq j$.

3.3.2 GPS-aided TOA (DOA) Fusion Localization error

In this subsection, we first introduce the iterative algorithm that addresses TOA (DOA) fusion equations, and then derive the relationship of the total range (angle) estimation errors, i.e., $\Delta R_i'$ ($\Delta \theta_i'$) in Equation (3.14), and the TN positioning errors projected on x and y axes.

Consider (x, y) as the unknown true position of the TN, then the TN range (R_i) and angle

(θ_i) with respect to BN i are expressed as

$$\begin{aligned} R_i &= f_i(x, y) \\ &= \sqrt{(x_i^{(B,t)} - x)^2 + (y_i^{(B,t)} - y)^2}, \end{aligned} \quad (3.16)$$

and,

$$\begin{aligned} \theta_i &= g_i(x, y) \\ &= \tan^{-1}\{(y_i^{(B,t)} - y) / (x_i^{(B,t)} - x)\}. \end{aligned} \quad (3.17)$$

Here, $(x_i^{(B,t)}, y_i^{(B,t)})$ is BN i 's true position that is known, and $i \in \{1, 2, \dots, N\}$, N is the number of BNs. In TOA fusion, $N \geq 3$; and, in DOA fusion, $N \geq 2$. Please note that (3.17) has the same structure as (3.9), however, (3.9) is used to transform GPS positioning error to angle estimation error (the TN position (x, y) is assumed known), while (3.17) is used to transform the total angle estimation error to positioning error (BN i 's true position $(x_i^{(B,t)}, y_i^{(B,t)})$ is assumed known). Equations (3.16) and (3.17) are nonlinear equations; hence, we apply iterative algorithm to calculate x and y in (3.16) and (3.17) using TN range (angle) with respect to multiple BNs [10]. The algorithm replaces (x, y) in (3.16) and (3.17) with an initial guess of TN position and calculates the associated position error. Then it updates the initial guess and repeats the process till the error satisfies the accuracy requirement. The algorithm details follow.

Let (x_T, y_T) denote the approximate TN position in TOA fusion. In the first step, we guess the approximate position (see Section 3.3.3 below for generating the initial guess).

Then, the TN position is expressed as

$$\begin{aligned} x &= x_T + \Delta x_T, \\ y &= y_T + \Delta y_T. \end{aligned} \quad (3.18)$$

Here, $(\Delta x_T, \Delta y_T)$ denotes the offset of the approximate TN position from the true position. Using the approximate position (x_T, y_T) , the approximate range (R_i'') is calculated

$$\begin{aligned} R_i'' &= f_i(x_T, y_T) \\ &= \sqrt{(x_i^{(B,t)} - x_T)^2 + (y_i^{(B,t)} - y_T)^2}. \end{aligned} \quad (3.19)$$

Incorporating (3.18) in (3.16), we achieve

$$\begin{aligned} R_i &= f_i(x_T + \Delta x_T, y_T + \Delta y_T) \\ &= \sqrt{[x_i^{(B,t)} - (x_T + \Delta x_T)]^2 + [y_i^{(B,t)} - (y_T + \Delta y_T)]^2}. \end{aligned} \quad (3.20)$$

Expanding (3.20) using Taylor series about the approximate position and ignoring higher order terms leads to

$$\begin{aligned} R_i &= f_i(x_T + \Delta x_T, y_T + \Delta y_T) \\ &= f_i(x_T, y_T) + \frac{\partial f_i(x_T, y_T)}{\partial x_T} \Delta x_T + \frac{\partial f_i(x_T, y_T)}{\partial y_T} \Delta y_T. \end{aligned} \quad (3.21)$$

Let $h_{xi} = \frac{\partial f_i(x_T, y_T)}{\partial x_T}$, $h_{yi} = \frac{\partial f_i(x_T, y_T)}{\partial y_T}$. Now, rearranging (3.21), we obtain the

approximated range error

$$\begin{aligned}\Delta R_i'' &= R_i - R_i'' \\ &= h_{xi} \cdot \Delta x_T + h_{yi} \cdot \Delta y_T.\end{aligned}\quad (3.22)$$

Two unknown values Δx_T and Δy_T in (3.22) can be calculated using range information obtained by multiple ($N \geq 3$) BNs: Let $\mathbf{R} = [R_1 \cdots R_n]^T$, $\mathbf{R}'' = [R_1'' \cdots R_n'']^T$,

$$\Delta \mathbf{R}'' = \mathbf{R} - \mathbf{R}'' = [\Delta R_1'' \cdots \Delta R_n''], \quad \mathbf{H} = \begin{bmatrix} h_{x1} & \cdots & h_{xn} \\ h_{y1} & \cdots & h_{yn} \end{bmatrix}^T, \quad \mathbf{X} = [x \ y]^T, \quad \mathbf{X}_T = [x_T \ y_T]^T \quad \text{and}$$

$\Delta \mathbf{X}_T = \mathbf{X} - \mathbf{X}_T = [\Delta x_T \ \Delta y_T]^T$, we have (see [67])

$$\Delta \mathbf{R}'' = \mathbf{H} \cdot \Delta \mathbf{X}_T. \quad (3.23)$$

The position offset (the positioning error) corresponds to

$$\Delta \mathbf{X}_T = (\mathbf{H}^T \mathbf{H})^{-1} \mathbf{H}^T \cdot \Delta \mathbf{R}''. \quad (3.24)$$

Note that (3.24) is calculated using the TN approximate position (x_T, y_T) . If the position offset does not satisfy the positioning accuracy requirement, we can iterate the above process with the updated approximation till the position offset satisfies the accuracy requirement. The approximation is updated by replacing \mathbf{X}_T with $\mathbf{X}_T + \Delta \mathbf{X}_T$, i.e.,

$$\mathbf{X}_T \leftarrow \mathbf{X}_T + \Delta \mathbf{X}_T. \quad (3.25)$$

When the position offset satisfies the accuracy requirement, we localize the TN at \mathbf{X}_T and achieve the position offset $(\Delta \mathbf{X}_T)$.

In GPS-aided TOA fusion, the approximate range error $(\Delta R_i'')$ defined in (3.22) can be

modeled as a linear combination of the total range estimation error ($\Delta R_i'$) defined in (3.14) and a complementary part ($\Delta R_{C,i}$) [10], i.e.,

$$\Delta R_i'' = \Delta R_i' + \Delta R_{C,i}. \quad (3.26)$$

Accordingly, the TN position offset ($\Delta x_T, \Delta y_T$) can be modeled as a linear combination of the position error ($\Delta x_T', \Delta y_T'$) generated by the total range estimation error ($\Delta R_i'$) and the position error ($\Delta x_{C,T}, \Delta y_{C,T}$) generated by the complementary range error ($\Delta R_{C,i}$).

$$\begin{aligned} \Delta x_T &= \Delta x_T' + \Delta x_{C,T}, \\ \Delta y_T &= \Delta y_T' + \Delta y_{C,T}. \end{aligned} \quad (3.27)$$

Let $\Delta \mathbf{R}' = [\Delta R_1' \ \cdots \ \Delta R_n']^T$, $\Delta \mathbf{R}_C = [\Delta R_{C,1} \ \cdots \ \Delta R_{C,n}]^T$, $\Delta \mathbf{X}_T' = [\Delta x_T' \ \Delta y_T']^T$ and $\Delta \mathbf{X}_{C,T} = [\Delta x_{C,T} \ \Delta y_{C,T}]^T$, in the matrix form, we have

$$\begin{aligned} \Delta \mathbf{R}'' &= \Delta \mathbf{R}' + \Delta \mathbf{R}_C, \\ \Delta \mathbf{X}_T &= \Delta \mathbf{X}_T' + \Delta \mathbf{X}_{C,T}. \end{aligned} \quad (3.28)$$

$\Delta \mathbf{X}_T'$ is generated by the total range estimation error ($\Delta \mathbf{R}'$), and it cannot be diminished in the iteration process. While $\Delta \mathbf{R}_C$ and $\Delta \mathbf{X}_{C,T}$ are generated by the arithmetic and diminished in the iteration process. At the end of the iteration, $\Delta \mathbf{X}_{C,T}$ and $\Delta \mathbf{R}_C$ are small and can be ignored. In other words, the final positioning error is a function of GPS precision and the BN range estimation accuracy. Incorporating (3.28) in (3.24) and ignoring $\Delta \mathbf{X}_{C,T}$ and $\Delta \mathbf{R}_C$, the positioning error in GPS-aided TOA fusion corresponds to

$$\Delta \mathbf{X}'_T = (\mathbf{H}^T \mathbf{H})^{-1} \mathbf{H}^T \cdot \Delta \mathbf{R}'. \quad (3.29)$$

In DOA fusion, using the same iteration method presented above, we can estimate the TN position with the TN angles with respect to two or more BNs. And the TN position estimation error corresponds to

$$\Delta \mathbf{X}'_D = (\mathbf{B}^T \mathbf{B})^{-1} \mathbf{B}^T \cdot \Delta \boldsymbol{\theta}'. \quad (3.30)$$

In (3.30), $\Delta \mathbf{X}'_D = \mathbf{X} - \mathbf{X}_D = [\Delta x'_D \ \Delta y'_D]^T$ is the TN position error generated by the total angle estimation error, $\mathbf{X}_D = [x_D \ y_D]^T$ is the estimated TN position via the iteration method, $\mathbf{B} = \begin{bmatrix} b_{x1} & \cdots & b_{xn} \\ b_{y1} & \cdots & b_{yn} \end{bmatrix}^T$, $b_{xi} = \frac{\partial g_i(x_D, y_D)}{\partial x_D}$, $b_{yi} = \frac{\partial g_i(x_D, y_D)}{\partial y_D}$ and $\Delta \boldsymbol{\theta}' = [\Delta \theta'_1 \ \cdots \ \Delta \theta'_n]^T$ is the total angle estimation error.

3.3.3 Initialization of the Iteration Process

The initial guess that leads to the convergence of the iteration process should support the following properties. For GPS-aided TOA fusion, first, the determinant of the matrix $\mathbf{H}^T \mathbf{H}$ [\mathbf{H} has been defined in (3.23)] should not be zero (i.e., $|\mathbf{H}^T \mathbf{H}| \neq 0$). If $|\mathbf{H}^T \mathbf{H}| = 0$, $(\mathbf{H}^T \mathbf{H})^{-1}$ would not exist, and we cannot continue the iteration to estimate the TN position. Hence, in each iteration step, we calculate $|\mathbf{H}^T \mathbf{H}|$, if the initial guess makes $|\mathbf{H}^T \mathbf{H}|$ equal zero or very small, we should ignore this initial guess and try a new initial guess to restart the iteration process.

Second, the approximate TN position circular error ($\sqrt{\Delta x_r^2 + \Delta y_r^2}$) should converge to a small value as the iteration process continues. In the iteration process, if the approximate TN position circular error in each step is not obviously smaller than that in the previous step, the iteration would diverse. Hence, in each iteration step, we calculate the ratio of the circular error of the new step to the previous one. If this ratio is considerably less than one, we keep the initial guess; else, we ignore that and try a new one.

Similarly, in GPS-aided DOA fusion, we monitor the determinant of $\mathbf{B}^T \mathbf{B}$ (i.e., $|\mathbf{B}^T \mathbf{B}|$) [\mathbf{B} was defined in (3.30)], and the TN position circular error (i.e., $\sqrt{\Delta x_d^2 + \Delta y_d^2}$) to guarantee the validity of the initial guess.

3.3.4. CEP of GPS-aided TOA (DOA) Fusion

In Section 3.3.1, we showed that $\Delta R_i'$, $i=1,2,\dots$, are zero mean Gaussian random variables with the same variance. In addition, BNs perform independently and GPS receivers perform independently; hence, $\Delta R_i'$, $i=1,2,\dots$, are independent and identically-distributed zero mean Gaussian random variables. Positioning errors $\Delta x_r'$ and $\Delta y_r'$ are linear combinations of $\Delta R_i'$, $i=1,2,\dots$; hence, $\Delta x_r'$ and $\Delta y_r'$ are jointly Gaussian random variables. Based on similar analysis, in GPS-aided DOA fusion, positioning errors $\Delta x_d'$ and $\Delta y_d'$ would also be jointly Gaussian random variables. Let

$$\mathbf{V} = \begin{bmatrix} V_{11} & V_{12} \\ V_{21} & V_{22} \end{bmatrix} = \text{cov}(\Delta \mathbf{X}_r') \text{ and } \mathbf{U} = \begin{bmatrix} U_{11} & U_{12} \\ U_{21} & U_{22} \end{bmatrix} = \text{cov}(\Delta \mathbf{X}_d'), \text{ and apply the same approach as}$$

that of Section 3.2, the point PDF in GPS-aided TOA (DOA) fusion is derived.

$$f_{point, \Delta r_T}(\Delta r_T) = \frac{\Delta r_T}{|\mathbf{V}|^{0.5}} \exp\left(\frac{V_{11} + V_{22}}{-4|\mathbf{V}|} \Delta r_T^2\right) \cdot I_0\left(\frac{\Delta r_T^2 \sqrt{(V_{22} - V_{11})^2 + V_{12}^2}}{4|\mathbf{V}|}\right), \quad (3.31)$$

and,

$$f_{point, \Delta r_D}(\Delta r_D) = \frac{\Delta r_D}{|\mathbf{U}|^{0.5}} \exp\left(\frac{U_{11} + U_{22}}{-4|\mathbf{U}|} \Delta r_D^2\right) \cdot I_0\left(\frac{\Delta r_D^2 \sqrt{(U_{22} - U_{11})^2 + U_{12}^2}}{4|\mathbf{U}|}\right). \quad (3.32)$$

Here, $\Delta r_T = \sqrt{\Delta x_T'^2 + \Delta y_T'^2}$ ($\Delta r_D = \sqrt{\Delta x_D'^2 + \Delta y_D'^2}$) is the GPS-aided TOA (DOA) fusion positioning circular error with a given nodes' geometrical distribution. Incorporating (3.31) and (3.32) into (3.1), the point CEP of GPS-aided TOA fusion and GPS-aided DOA fusion are derived.

$$CEP_{point, T} = \int_0^{\beta \sigma_R} \frac{\Delta r_T}{|\mathbf{V}|^{0.5}} \exp\left(\frac{V_{11} + V_{22}}{-4|\mathbf{V}|} \Delta r_T^2\right) \cdot I_0\left(\frac{\Delta r_T^2 \sqrt{(V_{22} - V_{11})^2 + V_{12}^2}}{4|\mathbf{V}|}\right) d\Delta r_T, \quad (3.33)$$

and,

$$CEP_{point, D} = \int_0^{\beta \sigma_\theta R_s} \frac{\Delta r_D}{|\mathbf{U}|^{0.5}} \exp\left(\frac{U_{11} + U_{22}}{-4|\mathbf{U}|} \Delta r_D^2\right) \cdot I_0\left(\frac{\Delta r_D^2 \sqrt{(U_{22} - U_{11})^2 + U_{12}^2}}{4|\mathbf{U}|}\right) d\Delta r_D. \quad (3.34)$$

In (3.34), we select $R_s = \sigma_R / \sigma_\theta$ for the convenience of comparing GPS-aided DOA fusion and the other two techniques. Averaging the point CEP achieved in (3.33) and (3.34) over all possible nodes' geometrical distribution in the MANET, we calculate the average CEP of the MANET.

3.4 Simulations and Discussions

In this part, (1) we compare the probability of TNs being localized in the three localization techniques with respect to the MANET coverage radius in the condition that the MANET coverage area radius is greater than half of the BN coverage radius; (2) verify the theoretically computed point CEP and compare the average localization CEP of the three localization methods in the condition that the MANET coverage radius is smaller or equal to half of the BN coverage radius. We consider the same nodes' geometrical distribution for the two comparisons. In addition, we compare the average localization CEP with respect to different parameters. These parameters include the number of BNs in the MANET, the MANET coverage radius, DOA estimation error standard deviation and the ratio of GPS positioning error variance on x (y) axis, σ_G^2 , to the BN range estimation error variance, σ_R^2 , that is $Z = \sigma_G^2 / \sigma_R^2$.

It should be noted that only in GPS-available environments, we can apply GPS-aided TOA (DOA) fusion to localize TNs; while the semi-distributed multi-node TOA-DOA fusion localization technique is not affected by the availability of GPS service.

A. Simulation Assumptions

In order to make a fair comparison across all techniques, we assume: (1) all nodes are uniformly distributed in the MANET; (2) the nodes geometrical distribution is the same for the three localization techniques; (3) in GPS-aided TOA (DOA) fusion, BNs position is determined via GPS receivers; (4) for the first simulation (Figure 3.3), the MANET

coverage radius is αR_{\max} , $0.5 < \alpha \leq 1.6$, there are 5 BNs and the performance is evaluated in terms of the probability of TN being localized; (5) for other simulations, the MANET coverage radius is αR_{\max} , $0 < \alpha \leq 0.5$, i.e., all BNs can estimate other nodes' TOA and (or) DOA in the MANET, and the localization performance is evaluated in terms of average positioning CEP $[P(\Delta r \leq \beta \sigma_r)]$ as a function of β .

B. Simulation Results

1. *Probability of TNs being localized comparison:* Here, we calculate the probability of TNs being localized in a MANET with a radius larger than half of the BN coverage radius ($0.5R_{\max}$). Figure 3.3 depicts: (1) as the MANET coverage radius increases from $0.5R_{\max}$ to $1.6R_{\max}$, the probability of TNs being localized decreases from 1 to about 0.8 (GPS-aided DOA fusion), 0.55 (GPS-aided TOA fusion) and 0.49 (the proposed method); (2) with the same MANETs coverage radius, the probability of TNs being localized in the semi-distributed method is always lower than the other two methods.

2. *Point CEP Verification:* Here, we generate the numerical results of point CEP for three localization techniques and compare them to the corresponding simulation results. Figure 3.4 shows: (1) the simulation results are consistent with the numerical results; (2) there is a very small gap between the simulation and numerical results, because we ignored higher order terms in the computation of the positioning error; (3) the positioning CEP of the multi-node TOA-DOA fusion with raw estimations is consistent with that simulated CEP using true values; (4) the positioning CEP of GPS aided DOA fusion is much lower

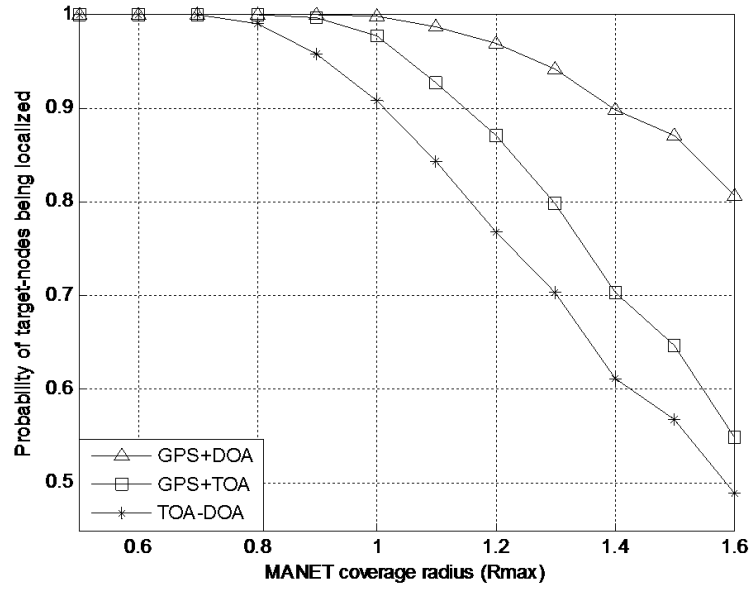


Figure 3.3: probability of TNs being localized vs. MANET radius, with 5 BNs.

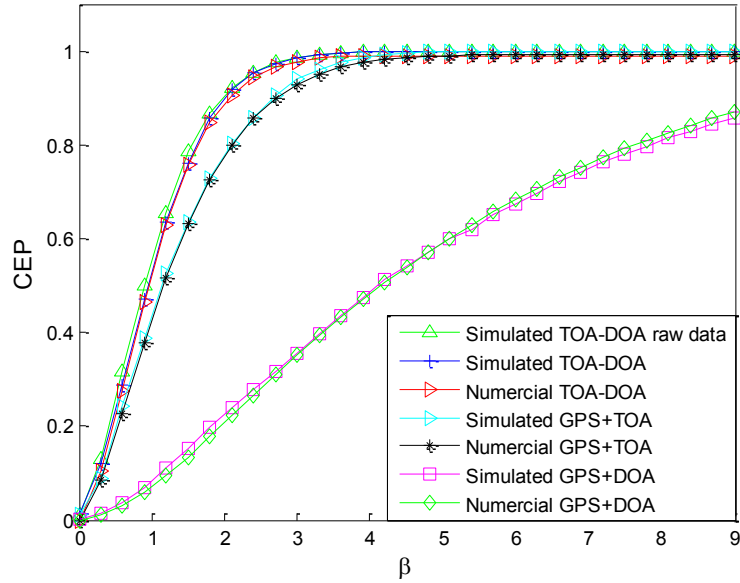


Figure 3.4: point CEP with 5 BNs, $R_{max} = 80\sigma_R$, $\sigma_\theta = 2^\circ$ and the ratio $Z = 0.5$.

than that of the other two methods. Note that the point CEP only represents the system performance at a known (but randomly selected) nodes geometrical distribution. Thus, it might be better or worse than the average CEP. The average CEP is generated over a large number of point CEPs.

3. *Average CEP*: Here, we compare the average CEP of the three localization techniques considering the number of BNs, MANET coverage radius, DOA estimation error and $Z = \sigma_G^2 / \sigma_R^2$. The results in Figures 3.5-3.8 show: (1) all methods perform better with more BNs; (2) the performance of GPS-aided TOA fusion is independent of MANET coverage radius, but the performance of the other two methods decreases as the MANET coverage radius increases; (3) the performance of the semi-distributed multi node TOA-DOA fusion and GPS-aided DOA fusion decreases as the DOA estimation error increases; (4) as $Z = \sigma_G^2 / \sigma_R^2$ increases, the performance of GPS-aided TOA fusion and GPS-aided DOA fusion decreases; and, (5) Considering $R_{\max} = 80\sigma_R$, $\sigma_\theta = 1^\circ$ or 2° and $Z = \sigma_G^2 / \sigma_R^2 \geq 0.5$, semi-distributed multi-node TOA-DOA fusion performs the best and GPS aided DOA fusion performs the worst.

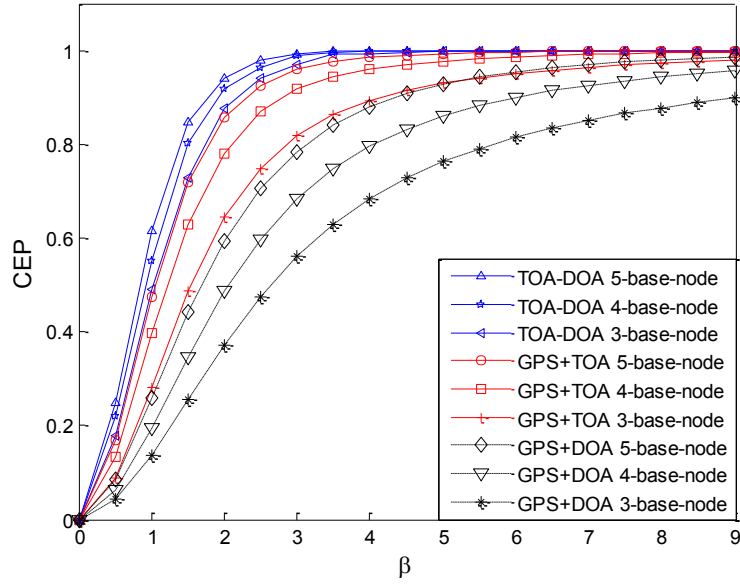


Figure 3.5: Average CEP vs. BNs number with $R_{max} = 80\sigma_R$, $\sigma_\theta = 2^\circ$ and $Z=0.5$.

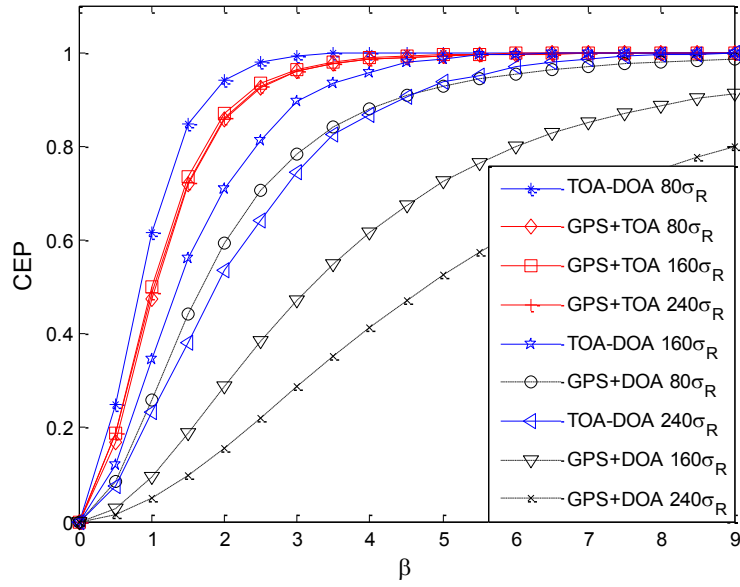


Figure 3.6: Average CEP comparison vs. MANET radius with 5 BNs, $\sigma_\theta = 2^\circ$ and $Z=0.5$.

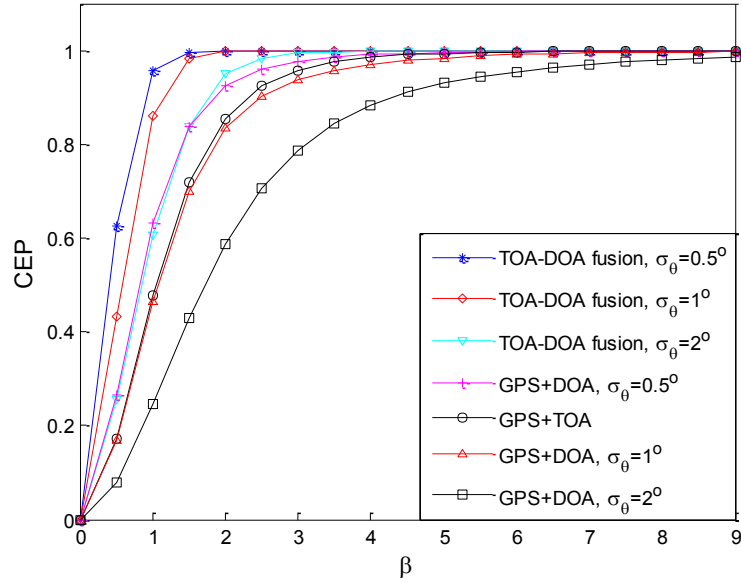


Figure 3.7: Average CEP comparison vs. DOA estimation error with 5 BNs, $R_{max} = 80\sigma_R$,

$\sigma_\theta = 2^\circ$ and $Z=0.5$.

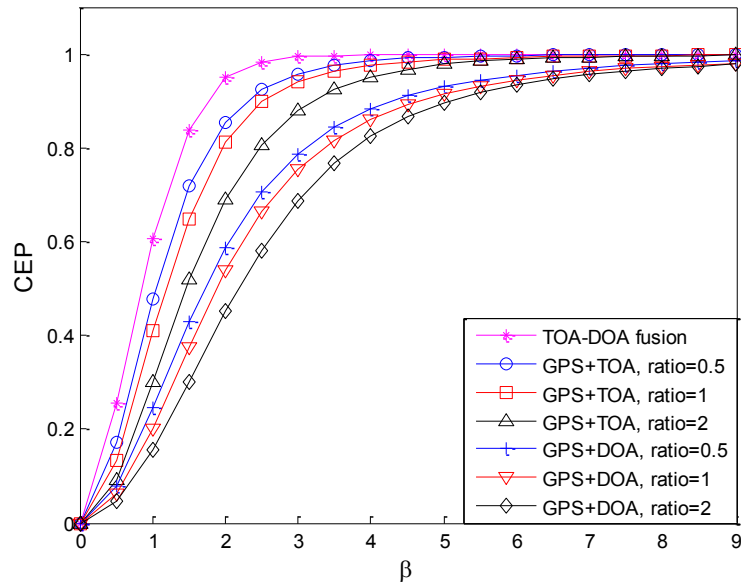


Figure 3.8: Average CEP comparison vs. Z with 5 BNs, $R_{max} = 80\sigma_R$ and $\sigma_\theta = 2^\circ$.

C. Discussions

The semi-distributed multi-node TOA-DOA fusion localization technique takes the advantages of the BNs property, the capability of localizing other nodes independently; hence, it does not depend on GPS to localize BN in MANETs. Accordingly, it is applicable in GPS-denied environments.

The semi-distributed multi-node TOA-DOA fusion localization technique suffers from coordinate transformation: TNs' position should be transformed from BNs local coordinates to the reference BN coordinates (the main coordinates) prior to the fusion. If a TN is not localized by the reference BN via any hop, then the TN position estimated by any BN cannot be transformed to the main coordinates. In this case, the TN cannot be localized in the main coordinates, even if it is localized by multiple BNs.

The probability of TNs being not localized by the reference BN via any hop increases as the MANET coverage radius increases from half of BN coverage radius. In this case, the probability of TNs that are not localized in the main coordinates increases. But GPS aided TOA and GPS-aided DOA fusion methods do not suffer from coordinate transformation. In these two methods, all BNs and TNs are localized in earth-centered earth-fixed (ECEF) Cartesian coordinate; hence, no coordinate transformation is needed. In any MANET scale, as long as a TNs TOA (DOA) is estimated by at least 3 (2) BNs, it would be localized in the ECEF Cartesian coordinate. Finally, because GPS-aided DOA fusion technique needs only two BNs for localization, it is less vulnerable to coverage radius compared to GPS-aided TOA fusion.

The positioning error generated by DOA estimation increases as the TN and BN distance increases; however, the positioning error generated by TOA estimation remains unchanged. Hence, the average positioning performance of the semi-distributed technique would be high (low) in a moderate (large) scale MANET.

The GPS-aided DOA fusion error is high. The reason is explained as follows. In the GPS-aided DOA fusion, the total DOA estimation error is due to two factors: BN DOA estimation error and DOA estimation error generated by GPS positioning error. When the BN and TN distance is low, the DOA estimation error generated by GPS would be high and it leads to a high positioning error. In addition, when the BN and TN distance is high, the BN DOA estimation error would be dominant, which also generate a high positioning error due to high distance.

In GPS-aided TOA fusion, the TOA estimation error includes BN TOA estimation error and TOA estimation error generated by GPS positioning error. These two errors are independent of the distance between BN and TN. Hence, average GPS-aided TOA fusion performance is independent of the MANET scale as long as all BNs can localize all TNs.

The semi-distributed multi-node TOA-DOA fusion can be applied to MANETs in GPS denied environments. In the GPS available environments and all BNs localize all TNs, the semi-distributed localization method is suitable for moderate scale MANETs and GPS-aided TOA fusion is suitable for large scale MANETs.

In this performance evaluation, for simplicity, we assumed TOA and DOA estimation

errors are independent and have identical zero mean Gaussian distributions. However, in general, TOA and DOA estimation errors are functions of many variables including SNR, bandwidth, channel multi-path effects and the availability of LOS [68, 69]. When LOS signal is available and it is stronger than NLOS signal: (a) TOA estimation errors can be considered zero mean Gaussian random variables with its variance normalized with respect to the TN and based-node distance (as distance increases, TOA estimation error variance increases) [70]; and, (b) the PDF of DOA estimation error fits Laplacian distribution [71]. Whereas in the scenario that LOS is not available or LOS and NLOS signal power are comparable, the statistics of TOA and DOA estimation errors are complicated and hard to compute [72]. In addition, depending on the nature of channels, the TOA and DOA estimation errors might become independent [71] or correlated [73].

If the PDF of the TOA and DOA estimation errors are not identical, the joint distribution of $\Delta \hat{x}_j^{(T)}$ and $\Delta \hat{y}_j^{(T)}$ would be hard to compute (in the scenario that the PDF of TOA and DOA estimation errors are identical zero mean Gaussian, we use Equation (3.4) to calculate the joint PDF of $\Delta \hat{x}_j^{(T)}$ and $\Delta \hat{y}_j^{(T)}$). Accordingly, the fusion CEP would be difficult to evaluate. Thus, making any conclusion would not be plausible.

The performance of the semi-distributed multi-node TOA-DOA fusion is altered by the variances of the positioning error over x and y axis defined in (2.14), which depends on BNs localization error variance (calculated in (2.9)) and TN localization error variance (calculated in (2.12)). If TOA and DOA estimation errors are correlated, then an additional term that is a function of their correlation coefficient would appear in the

equations (2.9) and (2.12). This additional term ultimately degrades the performance of the fusion in the proposed semi-distributed technique.

The other two techniques, i.e., GPS-aided TOA fusion and GPS-aided DOA fusion, only need the estimation of TOA or DOA. Therefore, in the first view, one may deduce that the performance of GPS-aided TOA fusion and GPS-aided DOA fusion may not be altered by the correlation of TOA and DOA estimation errors. But, let's see what may impacts (or increase) the correlation of TOA and DOA estimation errors. We predict that multi-path environment impacts (or increases) the correlation of TOA and DOA estimation errors, because the estimation performance of TOA and DOA reduces as the channel multi-path effect increases. Thus, higher correlation might be translated into lower performance of GPS-aided TOA fusion and GPS-aided DOA fusion, as well. Accordingly, it is hard to make a solid conclusion when comparing our technique with GPS-aided TOA fusion and GPS-aided DOA fusion when TOA and DOA estimation errors are considered correlated.

3.5 Conclusions

In this Chapter, we theoretically derive and compare the point CEP of the semi-distributed multi-node TOA-DOA fusion, GPS-aided TOA fusion and GPS-aided DOA fusion localization techniques. In addition, we verify the results via simulation, and compare the average CEP of these three localization techniques under the same nodes' geometrical distribution, and the same TOA and DOA estimation error variance.

Simulation results confirm that the semi-distributed multi-node TOA-DOA fusion localization technique is not suitable for MANETs with radius larger than half of BNs coverage radius. In the condition of MANET coverage radius smaller than or equal to half of BNs coverage radius, the semi-distributed multi-node TOA-DOA fusion localization technique leads to a better performance in moderate scale MANETs. GPS-aided TOA fusion localization technique leads to a better performance in large scale MANETs. Finally, GPS-aided DOA fusion leads to a lower performance compared to the other two techniques.

3.6 Covariance Calculation

The covariance of $\Delta\hat{\mathbf{x}}_j^{(T)}$ and $\Delta\hat{\mathbf{y}}_j^{(T)}$ corresponds to

$$\rho\sigma_{\hat{\mathbf{x}}_j^{(T)}}\sigma_{\hat{\mathbf{y}}_j^{(T)}} = E(\Delta\hat{\mathbf{x}}_j^{(T)} \cdot \Delta\hat{\mathbf{y}}_j^{(T)}). \quad (3.35)$$

Incorporating (2.16) in (3.35) leads to

$$\rho\sigma_{\mathbf{x}_j^{(T)}}\sigma_{\mathbf{y}_j^{(T)}} = \sum_{i=1}^n p_{i,j} q_{i,j} E(\Delta\mathbf{x}_{1i,j}^{(B,T)} \cdot \Delta\mathbf{y}_{1i,j}^{(B,T)}). \quad (3.36)$$

In (3.36), if $i=1$, the TN j 's positioning information is provided by the reference BN and the error is one-hop positioning error calculated in (2.12), which does not include the coordinate transformation error. Accordingly, the one-hop positioning error covariance corresponds to

$$E(\Delta x_{11,j}^{(B,T)} \cdot \Delta y_{11,j}^{(B,T)}) = (\sigma_R^2 - \sigma_\theta^2 R_{1,j}^{(B,T,t)^2}) \sin \theta_{1,j}^{(B,T,t)} \cos \theta_{1,j}^{(B,T,t)}. \quad (3.37)$$

And, if $i \neq 1$, the TN j 's positioning information is provided by non-reference BN and the error is two-hop positioning error, which includes the coordinate transformation error. Considering (2.6), (2.11) and (2.14), the two-hop positioning error covariance would correspond to

$$\begin{aligned} E(\Delta x_{1i,j}^{(B,T)} \cdot \Delta y_{1i,j}^{(B,T)}) &= (\sigma_R^2 - \sigma_\theta^2 R_{1i}^{(B,T)^2}) \sin \theta_{1i}^{(B,T)} \cos \theta_{1i}^{(B,T)} \\ &+ (\sigma_R^2 - \sigma_\theta^2 R_{i,j}^{(B,T,t)^2}) \sin \theta_{i,j}^{(B,T,t)} \cos \theta_{i,j}^{(B,T,t)} \end{aligned} \quad (3.38)$$

Incorporating (3.37) and (3.38) in (3.36), we can calculate the covariance of $\Delta \hat{x}_j^{(T)}$ and $\Delta \hat{y}_j^{(T)}$, and we can achieve

$$\rho \sigma_{\hat{x}_j^{(T)}} \sigma_{\hat{y}_j^{(T)}} \neq 0. \quad (3.39)$$

Hence, $\Delta \hat{x}_j^{(T)}$ and $\Delta \hat{y}_j^{(T)}$ are not independent.

3.7 Point PDF Derivation

From the discussion in Chapter 2, we know that the fused localization errors on x and y axes ($\Delta \hat{x}_j^{(T)}$ and $\Delta \hat{y}_j^{(T)}$) are jointly Gaussian, and $\Delta r_j = \sqrt{\Delta \hat{x}_j^{(T)^2} + \Delta \hat{y}_j^{(T)^2}}$; hence, the CDF of Δr_j corresponds to

$$F_{point, \Delta r_j}(\Delta r_j) = \int_{-\Delta r_j}^{\Delta r_j} \left[\int_{-\sqrt{\Delta r_j^2 - \Delta \hat{y}_j^{(T)2}}}^{\sqrt{\Delta r_j^2 - \Delta \hat{y}_j^{(T)2}}} f_{\Delta \hat{x}_j^{(T)}, \Delta \hat{y}_j^{(T)}}(\Delta \hat{x}_j^{(T)}, \Delta \hat{y}_j^{(T)}) d\Delta \hat{x}_j^{(T)} \right] d\Delta \hat{y}_j^{(T)}. \quad (3.40)$$

Differentiating the CDF with respect to Δr_j leads to the PDF of Δr_j

$$f_{point, \Delta r_j}(\Delta r_j) = \int_{-\Delta r_j}^{\Delta r_j} \frac{\Delta r_j}{\sqrt{\Delta r_j^2 - \Delta y_j^2}} \left[\begin{aligned} & f_{\Delta \hat{x}_j^{(T)}, \Delta \hat{y}_j^{(T)}} \left(\sqrt{\Delta r_j^2 - \Delta \hat{y}_j^{(T)2}}, \Delta \hat{y}_j^{(T)} \right) + \\ & f_{\Delta \hat{x}_j^{(T)}, \Delta \hat{y}_j^{(T)}} \left(-\sqrt{\Delta r_j^2 - \Delta \hat{y}_j^{(T)2}}, \Delta \hat{y}_j^{(T)} \right) \end{aligned} \right] d\Delta \hat{y}_j^{(T)}. \quad (3.41)$$

Let $\Delta \hat{y}_j^{(T)} = \Delta r_j \sin \varphi$, then $\sqrt{\Delta r_j^2 - \Delta \hat{y}_j^{(T)2}} = \Delta r_j \cos \varphi$, $d\Delta y_j = \Delta r_j \cos \varphi d\varphi$, $\varphi \in [-\frac{\pi}{2}, \frac{\pi}{2}]$.

Accordingly, (3.41) leads to

$$f_{point, \Delta r_j}(\Delta r_j) = \int_{-\pi/2}^{\pi/2} \Delta r_j [f_{\Delta \hat{x}_j^{(T)}, \Delta \hat{y}_j^{(T)}}(\Delta r_j \cos \varphi, \Delta r_j \sin \varphi) + f_{\Delta \hat{x}_j^{(T)}, \Delta \hat{y}_j^{(T)}}(-\Delta r_j \cos \varphi, \Delta r_j \sin \varphi)] d\varphi. \quad (3.42)$$

Incorporating (3.4) into (3.42), we have

$$f_{point, \Delta r_j}(\Delta r_j) = \frac{\Delta r_j}{2\pi|\Lambda|^{0.5}} \times \int_{-\frac{\pi}{2}}^{\frac{\pi}{2}} \left[\exp \left(\frac{\sigma_{\hat{y}_j^{(T)}}^2 \cos^2 \varphi - \rho \sigma_{\hat{x}_j^{(T)}} \sigma_{\hat{y}_j^{(T)}} \sin 2\varphi + \sigma_{\hat{x}_j^{(T)}}^2 \sin^2 \varphi}{-2|\Lambda|} \Delta r_j^2 \right) + \exp \left(\frac{\sigma_{\hat{y}_j^{(T)}}^2 \cos^2 \varphi + \rho \sigma_{\hat{x}_j^{(T)}} \sigma_{\hat{y}_j^{(T)}} \sin 2\varphi + \sigma_{\hat{x}_j^{(T)}}^2 \sin^2 \varphi}{-2|\Lambda|} \Delta r_j^2 \right) \right] d\varphi. \quad (3.43)$$

Because, $2\cos^2 \varphi = 1 + \cos 2\varphi$, and $2\sin^2 \varphi = 1 - \cos 2\varphi$, (3.43) corresponds to

$$f_{point, \Delta r_j}(\Delta r_j) = \frac{\Delta r_j}{2\pi|\Lambda|^{0.5}} \exp\left(\frac{\sigma_{\hat{y}_j^{(T)}}^2 + \sigma_{\hat{x}_j^{(T)}}^2}{-4|\Lambda|} \Delta r_j^2\right) \times \int_{-\frac{\pi}{2}}^{\frac{\pi}{2}} \left[\exp\left(\frac{(\sigma_{\hat{y}_j^{(T)}}^2 - \sigma_{\hat{x}_j^{(T)}}^2) \cos 2\phi - 2\rho\sigma_{\hat{x}_j^{(T)}}\sigma_{\hat{y}_j^{(T)}} \sin 2\phi}{-4|\Lambda|} \Delta r_j^2\right) + \exp\left(\frac{(\sigma_{\hat{y}_j^{(T)}}^2 - \sigma_{\hat{x}_j^{(T)}}^2) \cos 2\phi + 2\rho\sigma_{\hat{x}_j^{(T)}}\sigma_{\hat{y}_j^{(T)}} \sin 2\phi}{-4|\Lambda|} \Delta r_j^2\right) \right] d\phi. \quad (3.44)$$

Let $A = \frac{\Delta r_j}{|\Lambda|^{0.5}} \exp\left(\frac{\sigma_{\hat{y}_j^{(T)}}^2 + \sigma_{\hat{x}_j^{(T)}}^2}{-4|\Lambda|} \Delta r_j^2\right)$, $B = \sigma_{\hat{y}_j^{(T)}}^2 - \sigma_{\hat{x}_j^{(T)}}^2$, $C = 2\rho\sigma_{\hat{x}_j^{(T)}}\sigma_{\hat{y}_j^{(T)}}$, $\gamma = \Delta r_j^2 \sqrt{B^2 + C^2} / 4|\Lambda|$,

$\cos \beta = B / \sqrt{B^2 + C^2}$, and $\alpha = 2\phi$, then $d\phi = 1/2 d\alpha$, $\alpha \in [-\pi, \pi]$. Incorporating these parameters in (3.44) leads to

$$f_{point, \Delta r_j}(\Delta r_j) = \frac{A}{4\pi} \int_{-\pi}^{\pi} \{\exp[-\gamma \cdot \cos(\alpha + \beta)] + \exp[-\gamma \cdot \cos(\alpha - \beta)]\} d\alpha. \quad (3.45)$$

Here, $g(\alpha) = \exp(-\gamma \cdot \cos(\alpha))$ is an even periodic function with period of 2π . Hence, (3.45) is simplified to

$$\begin{aligned} f_{point, \Delta r_j}(\Delta r_j) &= A/\pi \cdot \int_0^{\pi} \exp(-\gamma \cdot \cos \alpha) d\alpha \\ &= A/\pi \cdot \int_0^{\pi} \exp(\gamma \cdot \cos \alpha) d\alpha = A \cdot I_0(\gamma). \end{aligned} \quad (3.46)$$

In (3.46), $I_0(\gamma) = 1/\pi \int_0^{\pi} e^{\gamma \cos \phi} d\phi$ is the modified Bessel function of the first kind and zero order. In addition,

$$\begin{aligned}
A &= \frac{\Delta r_j}{|\Lambda|^{0.5}} \exp \left(\frac{\sigma_{\hat{y}_j^{(T)}}^2 + \sigma_{\hat{x}_j^{(T)}}^2}{-4|\Lambda|} \Delta r_j^2 \right), \\
&= \frac{\Delta r_j}{|\Lambda|^{0.5}} \exp \left(\frac{\Lambda_{11} + \Lambda_{12}}{-4|\Lambda|} \Delta r_j^2 \right)
\end{aligned} \tag{3.47}$$

and,

$$\begin{aligned}
\gamma &= \Delta r_j^2 \sqrt{B^2 + C^2} / 4|\Lambda| \\
&= \Delta r_j^2 \sqrt{(\Lambda_{22} - \Lambda_{11})^2 + \Lambda_{12}^2} / 4|\Lambda|.
\end{aligned} \tag{3.48}$$

Hence,

$$f_{point, \Delta r_j}(\Delta r_j) = \frac{\Delta r_j}{|\Lambda|^{0.5}} \exp \left(\frac{\Lambda_{11} + \Lambda_{22}}{-4|\Lambda|} \Delta r_j^2 \right) \cdot I_0 \left(\frac{\Delta r_j^2 \sqrt{(\Lambda_{22} - \Lambda_{11})^2 + \Lambda_{12}^2}}{4|\Lambda|} \right). \tag{68}$$

Chapter 4

Localization with Kalman Filter in LOS Scenario⁴

This Chapter proposes the application of Kalman filter (KF) to further enhance the performance of the multi-node TOA-DOA fusion, and compares it with a traditional method, applying extended Kalman filter (EKF) to multi-node TOA-DOA estimations to localize TN. The comparison criteria include localization accuracy in terms of error CDF and approximate posterior Cramer Rao lower bound (APCRLB), filter stability and computational complexity. The comparison confirms that the proposed method involves minor computational complexity, while it demonstrates slightly larger PCRLB; however, its stability is higher than EKF. This makes it a good candidate for localizing multiple TNs in mobile ad-hoc networks.

4.1 Introduction

KF was originally designed for target tracking purposes [74]. Nowadays, it is widely used for localization fusion applications when measurements are achieved periodically. In [75], KF is applied to fuse GPS, INS (inertial navigation system) and radar data to localize and track a missile and its target. In this system, there are only two localization targets (the missile and the missile target). In [76], TDOA and DOA measurements are fused using constrained KF. Here, the number of targets is small, as well.

⁴© [2010] IEEE. Reprinted, with permission, from [IEEE ICT, A New TOA-DOA Node Localization for Mobile Ad-hoc Networks, Z. Wang and S. A. Zekavat]. See Appendix A for full permission.

When KF is applied to address fusion problems in ad-hoc networks, computational complexity and divergence should be considered. In centralized or semi-distributed localization methods, one BN is usually in charge of localizing multiple TNs. The BN processor capacity is limited. Thus, the computational complexity of localizing one TN should be limited; otherwise, the number of TNs being localized by one BN cannot exceed a certain threshold. In this case, we should increase the number of BNs. However, this increases the system cost. The divergence of a KF is related to the geometrical distribution of BNs and TN. In a MANET, nodes are mobiles, any geometrical may take place. When a KF diverges, large errors would be generated.

In this chapter, we integrate KF with multi-node TOA-DOA fusion, which is stable, applicable in MANETs and exhibits low computational complexity. We compare the integration of KF and multi-node TOA-DOA fusion with a traditional localization method based on EKF (EKF is used to address the non-linear equation set constructed with measurements from multiple BNs) in terms of computational complexity, accuracy, and stability. EKF is usually used to address non-linear localization problems; hence, we select it as the comparison benchmark. Results confirm that the integration of KF and multi-node TOA-DOA fusion possesses considerably low complexity and is stable compared to EKF: EKF may diverge in some scenarios. The approximate posterior Cramer Rao lower bound (APCRLB) of the proposed method is slightly higher than that of EKF. In addition, its reliability and complexity makes it suitable for MANET applications, where a large number of TNs should be localized.

In this chapter, we first introduce the integration of KF and multi-node TOA-DOA fusion and the localization method applying EKF to multi-node TOA-DOA measurements; and, then, we compare two methods in terms of localization accuracy, approximate posterior Cramer Rao lower bound (APCRLB), filter stability and computational complexity; finally, simulations are conducted to confirm the comparison results.

4.2 Localization with the Integration of KF and Multi-node TOA-DOA Fusion and EKF

In this chapter, the proposed MANTE is shown in Figure 4.1. Two localization techniques are considered to localize the TN. The first one is based on multi-node TOA-DOA fusion plus KF and the second one is based on the implementation of EKF to multi-node TOA-DOA estimations, as shown in Figure 4.2. In this system, BNs position is

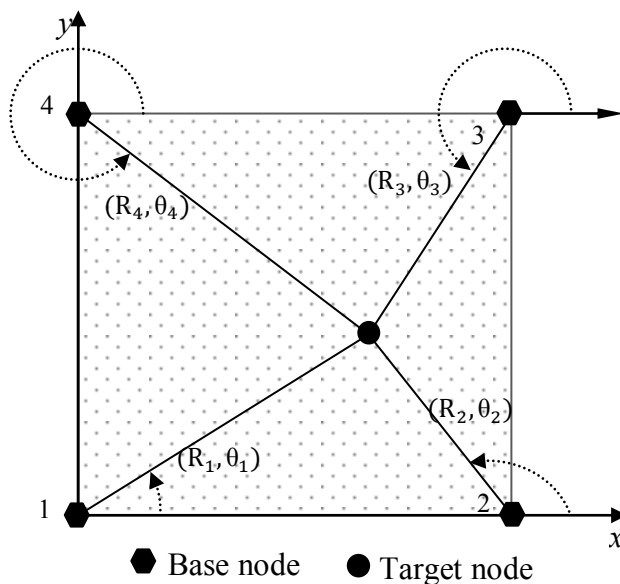


Figure 4.1: Ad-hoc net work configuration.

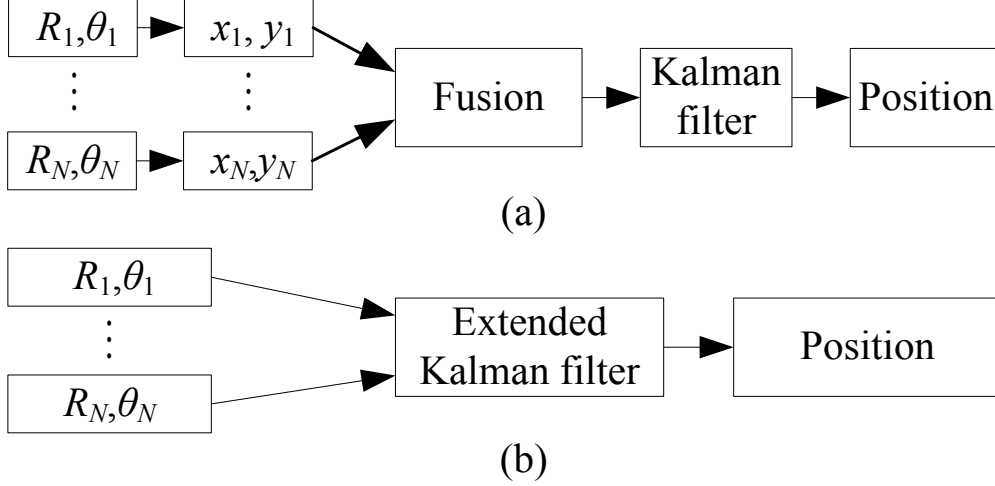


Figure 4.2: Localization techniques. (a) Fusion plus KF. (b) EKF.

given and all BNs periodically estimate TN position via joint TOA-DOA estimation. In the following sub-sections, we introduce the detail of the two methods.

4.2.1 Localization Based on Fusion plus Kalman Filter

At a time instance n ($n = 1, 2, \dots$), when a TN position is estimated via the fusion of multi-node TOA-DOA fusion, we achieve the estimated TN position $(x^{(f)}, y^{(f)})_n$ as that in (2.15), the corresponding localization error variances $(\sigma_{x^{(f)}}^2, \sigma_{y^{(f)}}^2)_n$ as that in (3.3) and the localization error covariance $cov(x^{(f)}, y^{(f)})_n$ as that in (3.36). The corresponding

error covariance matrix is noted as $R_n^{(f)} = \begin{bmatrix} \sigma_{x^{(f)}}^2 & cov(x^{(f)}, y^{(f)}) \\ cov(x^{(f)}, y^{(f)}) & \sigma_{y^{(f)}}^2 \end{bmatrix}_n$.

Given a series of fused target node position $(x^{(f)}, y^{(f)})_n$ and the corresponding error covariance matrix $R_n^{(f)}$, KF can be implemented at a BN to further reduce the localization error. The state transition model corresponds to

$$\mathbf{X}_{n+1} = \mathbf{A}\mathbf{X}_n + \mathbf{W}_{n+1}. \quad (4.1)$$

In (4.1), $\mathbf{X}_n = [x_n \ y_n \ \dot{x}_n \ \dot{y}_n]^T$ is the TN state at time instant n including the TN position (x_n, y_n) and the TN speed (\dot{x}_n, \dot{y}_n) , \mathbf{A} is the state transition matrix, \mathbf{W}_{n+1} is the process noise, and

$$\mathbf{A} = \begin{bmatrix} 1 & 0 & \Delta t & 0 \\ 0 & 1 & 0 & \Delta t \\ 0 & 0 & 1 & 0 \\ 0 & 0 & 0 & 1 \end{bmatrix},$$

$$\mathbf{W}_{n+1} = \begin{bmatrix} \Delta t^2/2 & 0 \\ 0 & \Delta t^2/2 \\ \Delta t & 0 \\ 0 & \Delta t \end{bmatrix} \cdot \begin{bmatrix} a_x \\ a_y \end{bmatrix}_{n+1}. \quad (4.2)$$

In (4.2), Δt is the position update period (the time difference between two neighboring measurements); a_x and a_y are the TN acceleration on x and y axes, and a_x and a_y are assumed to be zero mean Gaussian random variables with the variance of σ_a^2 . In addition, $\mathbf{Q}_{n+1} = E(\mathbf{W}_{n+1} \cdot \mathbf{W}_{n+1}^T)$ is the covariance matrix of the process noise at time instant $n + 1$.

The observation model is

$$\mathbf{Z}_{n+1}^{(fk)} = \mathbf{B}^{(fk)}\mathbf{X}_{n+1} + \mathbf{V}_{n+1}^{(fk)}. \quad (4.3)$$

In (4.3), the superscript (fk) indicates that the parameter is for the fusion plus KF method;

$\mathbf{Z}_{n+1}^{(fk)} = [x^{(f)} \ y^{(f)}]^T_{n+1}$ is the TN position computed via fusion; $\mathbf{B}^{(fk)} = \begin{bmatrix} 1 & 0 & 0 & 0 \\ 0 & 1 & 0 & 0 \end{bmatrix}$ is the

observation matrix; $V_{n+1}^{(fk)} = [\Delta x^{(f)} \Delta y^{(f)}]^T_{n+1}$ is the localization error via fusion; in addition, $R_{n+1}^{(fk)} = E(V_{n+1}^{(fk)} \cdot V_{n+1}^{(fk)T})$ is the fused localization error covariance matrix.

Based on the state transition model and the observation model, we apply KF to improve the localization performance via reducing fusion error. Given the state estimation $\hat{X}_{n|n}^{(fk)}$ and the corresponding error covariance $P_{n|n}^{(fk)} = \text{cov}(X_n - \hat{X}_{n|n}^{(fk)})$ at time instant n , the predicted state $\hat{X}_{n+1|n}^{(fk)}$ and the corresponding error covariance $P_{n+1|n}^{(fk)}$ at time instant $n + 1$ correspond to

$$\begin{aligned}\hat{X}_{n+1|n}^{(fk)} &= A\hat{X}_{n|n}^{(fk)}, \\ P_{n+1|n}^{(fk)} &= AP_{n|n}^{(fk)}A^T + Q_n.\end{aligned}\tag{4.4}$$

Here, the subscript $n+1|n$ depicts that the data at the time instant $n+1$ is calculated based on the measurements from the time instant 1 to the time instant n . Given the measurement information $(Z_{n+1}^{(fk)})$ at time instant $n+1$, the updated estimation and the corresponding error covariance would be

$$\begin{aligned}\hat{X}_{n+1|n+1}^{(fk)} &= A\hat{X}_{n+1|n}^{(fk)} + K_{n+1}^{(fk)}\tilde{Z}_{n+1}^{(fk)}, \\ P_{n+1|n+1}^{(fk)} &= (I - K_{n+1}^{(fk)}B^{(fk)})P_{n+1|n}^{(fk)}.\end{aligned}\tag{4.5}$$

In (4.5), $K_{n+1}^{(fk)} = P_{n+1|n}^{(fk)}B^{(fk)T}(B^{(fk)}P_{n+1|n}^{(fk)}B^{(fk)T} + R_{n+1}^{(fk)})^{-1}$ is the Kalman gain, and $\tilde{Z}_{n+1}^{(fk)} = Z_{n+1}^{(fk)} - \hat{X}_{n+1|n}^{(fk)}$ is the measurement (fusion result) residue at time instant $n+1$.

4.2.2 Localization Based on Extended Kalman Filter

When multiple BNs estimate a TN position via TOA-DOA measurements, EKF can be applied to address the non-linear equations fusing multiple TOA-DOA measurements to localize the TN. In the EKF, we assume the same state transition model as that of (4.1) and the observation model is taken as

$$Z_{n+1}^{(k)} = b(X_{n+1}) + V_{n+1}^{(k)}. \quad (4.6)$$

In (4.6), the superscript (k) indicates that the parameters are for EKF; $Z_{n+1}^{(k)} = [R_1 \cdots R_N \theta_1 \cdots \theta_N]^T$ is the range and angle measurement vector at time instant $n+1$ achieved by BNs 1 to N ; $V_{n+1}^{(k)} = [\Delta R_1 \cdots \Delta R_N \Delta \theta_1 \cdots \Delta \theta_N]^T$ is the error vector and its covariance matrix is $R_{n+1}^{(k)} = \text{cov}(V_{n+1}^{(k)})$; and, $b(X_{n+1}) = [c_1 \cdots c_N c_{N+1} \cdots c_{2N}]$ are a set of nonlinear equations that transform the TN state X_{n+1} to measurement $Z_{n+1}^{(k)}$. These nonlinear equations correspond to

$$c_i = \begin{cases} [(x_{n+1} - x_i^{(B)})^2 + (y_{n+1} - y_i^{(B)})^2]^{0.5}, & 1 \leq i \leq N; \\ \tan^{-1} \frac{y_{n+1} - y_{i-N}^{(B)}}{x_{n+1} - x_{i-N}^{(B)}}, & N + 1 \leq i \leq 2N. \end{cases} \quad (4.7)$$

Given the state estimation $\hat{X}_{n|n}^{(k)}$ and the corresponding error covariance matrix $P_{n|n}^{(k)} = \text{cov}(X_n - \hat{X}_{n|n}^{(k)})$ at the time instant n , the predicted state $\hat{X}_{n+1|n}^{(k)}$ and the corresponding error covariance matrix $P_{n+1|n}^{(k)}$ at the time instant $n + 1$ would be

$$\hat{X}_{n+1|n}^{(k)} = A\hat{X}_{n|n}^{(k)},$$

$$P_{n+1|n}^{(k)} = AP_{n|n}^{(k)}A^T + Q_n. \quad (4.8)$$

When the measurement information $Z_{n+1}^{(k)}$ at the time instant $n+1$ is available, the updated estimation and the error covariance are calculated as

$$\begin{aligned} \hat{X}_{n+1|n+1}^{(k)} &= A\hat{X}_{n+1|n}^{(k)} + K_{n+1}^{(k)} \tilde{Z}_{n+1}^{(k)}, \\ P_{n+1|n+1}^{(k)} &= (I - K_{n+1}^{(k)} B_{n+1}^{(k)}) P_{n+1|n}^{(k)}. \end{aligned} \quad (4.9)$$

In (4.9), $K_{n+1}^{(k)} = P_{n+1|n}^{(k)} B_{n+1}^{(k)T} (B_{n+1}^{(k)} P_{n+1|n}^{(k)} B_{n+1}^{(k)T} + R_{n+1}^{(k)})^{-1}$ is the Kalman gain; $\tilde{Z}_{n+1}^{(k)} = Z_{n+1}^{(k)} - b(\hat{X}_{n+1|n}^{(k)})$ is the measurement residue vector of range and angle at the time instant $n+1$; and, $B_{n+1}^{(k)}$ is the observation matrix calculated via a linearization process as follow,

$$B_{n+1}^{(k)} = \left. \frac{\partial b}{\partial X_{n+1}} \right|_{X_{n+1}=\hat{X}_{n+1|n}^{(k)}}. \quad (4.10)$$

In (4.10), we only considered the first order derivative of $b(X_{n+1})$ with respect to X_{n+1} at the point of $X_{n+1} = \hat{X}_{n+1|n}^{(k)}$ and ignored higher order derivatives. Hence, the observation matrix and therefore the EKF are biased. The biased EKF would not converge to the TNs true position, and when the bias is large (considerable error is ignored) the EKF may diverge. In addition, $B_{n+1}^{(k)}$ is a $2N \times 4$ matrix. Because $b(X_{n+1})$ is only a function of TN position (x_{n+1}, y_{n+1}) ; hence, the last two columns of $B_{n+1}^{(k)}$ are zeros, i.e., $B_{n+1}^{(k)}(:, 3) =$

$B_{n+1}^{(k)}(:, 4) = 0$. Defining $(\hat{R}_i)_{n+1|n} = [(\hat{x}_{n+1|n} - x_i^{(B)})^2 + (\hat{y}_{n+1|n} - y_i^{(B)})^2]^{0.5}$, the first two column elements in $B_{n+1}^{(k)}$ correspond to

$$\begin{aligned} B_{n+1}^{(k)}(i, 1) &= \frac{\hat{x}_{n+1|n}^{(k)} - x_i^{(B)}}{(\hat{R}_i)_{n+1|n}}, 1 \leq i \leq N; \\ B_{n+1}^{(k)}(i, 2) &= \frac{\hat{y}_{n+1|n}^{(k)} - y_i^{(B)}}{(\hat{R}_i)_{n+1|n}}, 1 \leq i \leq N; \\ B_{n+1}^{(k)}(i, 1) &= \frac{\hat{y}_{n+1|n}^{(k)} - y_{i-N}^{(B)}}{(\hat{R}_i)_{n+1|n}^2}, N+1 \leq i \leq 2N; \\ B_{n+1}^{(k)}(i, 2) &= -\frac{\hat{x}_{n+1|n}^{(k)} - x_{i-N}^{(B)}}{(\hat{R}_i)_{n+1|n}^2}, N+1 \leq i \leq 2N. \end{aligned} \quad (4.11)$$

We have introduced the two localization techniques based on fusion plus KF and EKF, respectively. In the following section, we compare their localization accuracy, stability and complexity.

4.3 Localization Accuracy, Stability and Complexity

4.3.1 Localization Accuracy and Filter Stability

As shown in Figure 4.2 (a), in the fusion plus KF method, multiple estimations of the TN x and y coordinates are fused to achieve a better TN position estimation. Then, KF is applied to further reduce localization errors. Taylor series' first order term is used to

approximate localization errors in (2.11); hence, the error contained in H.O.T. is ignored.

In the fusion, we use the error variance to calculate fusion weights; and the fused TN positioning error is taken as the measurement error for KF; hence, in the fusion plus KF, the approximated localization error is applied within both fusion and Kalman Filtering processes. These two sources of error are added on the top of measurement errors, and reduce the performance of TN position estimation. However, the observation matrix calculated in (4.10) is an approximation result, and it is applied once in EKF. Thus, if EKF converges, its accuracy would be higher than that of the fusion plus KF (the error generated by one application of approximation result in (4.10) in EKF is smaller than that generated by twice applications of approximation result in (2.11) in the fusion plus KF).

The main component of the Taylor series H.O.T. that was ignored in (2.11) is the second order term $(\Delta x_{2nd}, \Delta y_{2nd})$, which corresponds to

$$\begin{aligned}\Delta x_{i,j,2nd}^{(B,T)} &= -\Delta\theta_{i,j}^{(B,T)^2} R_{i,j}^{(B,T)} \cos(\theta_{i,j}^{(B,T)}) - 2\Delta\theta_{i,j}^{(B,T)} \Delta R_{i,j}^{(B,T)} \sin(\theta_{i,j}^{(B,T)}), \\ \Delta y_{i,j,2nd}^{(B,T)} &= -\Delta\theta_{i,j}^{(B,T)^2} R_{i,j}^{(B,T)} \sin(\theta_{i,j}^{(B,T)}) + 2\Delta\theta_{i,j}^{(B,T)} \Delta R_{i,j}^{(B,T)} \cos(\theta_{i,j}^{(B,T)}).\end{aligned}\quad (4.12)$$

In (4.12), $R_{i,j}^{(B,T)}$ is the measured distance between BN i and the TN; hence, the ignored component increases with the distance between BN i and the TN. As a result, the fused TN localization accuracy and the KF performance decrease as the distance between BNs and TN increases.

We may refer to a special scenario, in which there is only one BN. In this case, no fusion happens in the proposed method. Approximation result is applied once in both the two methods; hence, fusion plus KF and EKF should perform equivalently.

In the scenario that both KF and EKF converge, their localization accuracy can be compared via posterior Cramer Rao lower bound (PCRLB). According to the derivative in [77], the PCRLB of the above KF and EKF can be iteratively calculated respectively via

$$\mathbf{P}_{n+1}^{(fk)^{-1}} = \mathbf{B}^{(fk)T} \mathbf{R}_{n+1}^{(fk,t)^{-1}} \mathbf{B}^{(fk)} + \left(\mathbf{Q}_n + \mathbf{A} \mathbf{P}_n^{(fk)^{-1}} \mathbf{A}^T \right), \quad (4.13)$$

and,

$$\mathbf{P}_{n+1}^{(k)^{-1}} = \mathbf{B}_{n+1}^{(k,t)T} \mathbf{R}_{n+1}^{(k)^{-1}} \mathbf{B}_{n+1}^{(k,t)} + \left(\mathbf{Q}_n + \mathbf{A} \mathbf{P}_n^{(k)^{-1}} \mathbf{A}^T \right). \quad (4.14)$$

Where $\mathbf{P}_{n+1}^{(fk)}$ and $\mathbf{P}_{n+1}^{(k)}$ are the PCRLB of the KF, and EKF, respectively at the time instance $n + 1$; $\mathbf{P}_0^{(fk)}$ and $\mathbf{P}_0^{(k)}$ are the initial localization error covariance matrix of fusion plus KF and EKF, respectively, and they are assumed calculable; $\mathbf{R}_{n+1}^{(fk,t)}$ is the covariance matrix of the fused TN position and the true TN position that is applied in the calculating process; $\mathbf{B}_{n+1}^{(k,t)}$ is the posterior observation matrix and it is obtainable by calculating $\mathbf{B}_{n+1}^{(k)}$ using the true value to take the place of the estimated TN position; and, other parameters have been defined in previous equations. We applied Taylor series to calculate the localization error in (2.11), and the calculated error is applied in the following fusion and KF; in addition, we applied linearization method in the process of calculating $\mathbf{B}_{n+1}^{(k,t)}$; hence,

the bounds calculated in (4.13) and (4.14) are approximate values, and we call them approximate PCRLB (APCRLB).

In the proposed KF and EKF, all system states have been considered and they are bounded; hence, *true divergence* would not happen. In the localization method based on fusion plus KF, the measurement covariance matrix is calculated using (3.3) and (3.36). It is clear that the covariance matrix would not be unrealistically small and hence *apparent divergence* would not take place in KF. While in EKF, the calculated states covariance matrix may be over-reduced due to the linearization of (4.11) and becomes unrealistically small [78]. In this scenario (e.g., in Figure 4.1, when only BNs 1 and 2 are available, and the TN is close to the line connecting BNs 1 and 2) divergence may occur, and generate considerable localization error. This apparent divergence in EKF cannot be detected theoretically, but it can be detected via monitoring the state covariance matrix. Studying the relationship between EKF divergence and nodes topology, detecting and avoiding EKF divergence form the continuous work of this chapter.

4.3.2 Computational Complexity

We define the computational complexity as the number of multiplications required to create one estimation of the TN position. Here, we assume the values of sine, cosine and inverse tangent functions are available in a lookup table; seven multiplications are required for the inverse operation [57]; Gaussian-Jordan elimination method is used to calculate matrix inverse and $N^3 + 6N^2$ multiplications are needed to calculate the inverse of an $N \times N$ matrix, N refers to the number of BNs that involve the TN localization; and,

Newton method is used to calculate a number's square root and twelve multiplications are needed in one square root calculation. In addition, zero and one multiplied by any number is not taken into account.

The number of multiplications in the localization method based on fusion plus KF is listed in Table 4.1. Adding all multiplications in Table 4.1 leads to

$$C_{com}^{(f)} = 54N + 60. \quad (4.15)$$

Table 4.1: Number of multiplications in fusion plus KF.

<i>Calculation step</i>	<i>Number of multiplications</i>
Localizing TNs	2M
TNs positioning covariance matrix calculation	16M
Fusion weights calculation	28M
TNs position fusion	2M
Fused TN localization covariance matrix calculation	6M
Calculation of $\hat{X}_{n+1 n}^{(f)}$	2
Calculation of $P_{n+1 n}^{(f)}$	4
Calculation of $K_{n+1}^{(f)}$	32
Calculation of $\hat{X}_{n+1 n+1}^{(f)}$	6
Calculation of $P_{n+1 n+1}^{(f)}$	16

The number of multiplications in the localization method based on EKF is listed in Table 4.2. Adding all multiplications in Table 4.2 leads to

$$C_{com}^{(k)} = 8N^3 + 40N^2 + 72N + 28. \quad (4.16)$$

Table 4.2: Number of multiplications in EKF.

<i>Calculation step</i>	<i>Number of multiplications</i>
Calculation of $\hat{\mathbf{X}}_{n+1 n}^{(k)}$	2
Calculation of $\mathbf{P}_{n+1 n}^{(k)}$	4
Calculation of $\tilde{\mathbf{Z}}_{n+1}^{(k)}$	$14M$
Calculation of $\mathbf{B}_{n+1}^{(k)}$	$42M$
Calculation of $\mathbf{K}_{n+1}^{(k)}$	$8M^3 + 40M^2 + 16M$
Calculation of $\hat{\mathbf{X}}_{n+1 n+1}^{(k)}$	6
Calculation of $\mathbf{P}_{n+1 n+1}^{(k)}$	16

Equations (4.15) and (4.16) clearly depict that the computational complexity of the localization method based on fusion plus KF is considerably lower than that of the method based on EKF.

Nowadays, processors can handle more computational load than ever. If we localize a few TNs, the processor may handle the computational load generated by fusion plus KF or EKF in real time. But if there are a large number of TNs to be localized, using fusion plus KF, a processor can localize much higher number of TNs compared to using EKF.

4.4 Simulation and Discussion

In the simulations, we assume: (1) the range estimation error standard deviation is σ_R and the range is normalized to σ_R ; in addition, the angle estimation error standard deviation is 1° ($\sigma_\theta = 1^\circ$); (2) the TN accelerations on x and y axes are zero mean Gaussian random variables with the standard deviation of $\sigma_a = 2\sigma_R/s^2$; (3) the time difference between

two neighboring measurements is 0.5s; (4) the TN speed on x axis is $1.5\sigma_R/s$ and the target trace is determined by

$$y = d + e \cdot \sin(\pi x / 100\sigma_R), \quad (4.17)$$

d and e are constants, and (x, y) is the TN position; (5) BNs appear in the position order of $(0, 0)$, $(500\sigma_R, 0)$, $(0, 500\sigma_R)$, $(500\sigma_R, 500\sigma_R)$ as shown in Figure 4.1, which means if there is one BN, it is at $(0, 0)$, and if the second BN is available, it is at $(500\sigma_R, 0)$, etc.; and, (6) the localization accuracy of the two methods is compared in terms of CDF of the localization error [i.e., $CDF = P(\Delta r \leq \beta\sigma_R)$, Δr is the distance between the true and estimated TN position and $\beta \geq 0$].

In order to maintain simulations, we: (1) generate the TN true position using above assumptions; (2) use the true TN position, σ_R , σ_θ and BNs position to generate the measured range and angle; and (3) apply the two methods to the measured range and angle to localize the TN and repeat the localization process 100 times to calculate the localization error CDF.

Here, we consider two scenarios to compare the two localization methods. In the first scenario, the TN is far away from the upper and lower edges of the dotted area in Figure 4.1, and $y = 250\sigma_R + 240\sigma_R \sin(\pi x / 100\sigma_R)$ is used to generate TN trace. In this case, no divergence occurs in both methods (see Figure 4.3 (a)). In the second scenario, the TN may move closer to the upper and lower edges of the dotted area in Figure 4.1, and $y = 250\sigma_R + 250\sigma_R \sin(\pi x / 100\sigma_R)$ is used to generate TN trace. In this case, when two

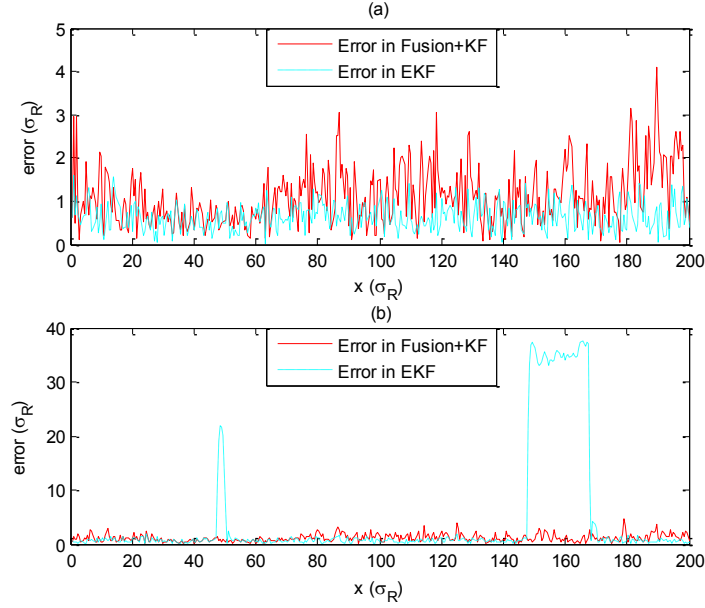


Figure 4.3: Localization error with 4 BNs, (a) $d = 250\sigma_\rho, e = 240\sigma_\rho$; (b) $d = 250\sigma_\rho, e = 250$.

or more BNs are available, apparent divergence occurs in EKF (see Figure 4.3 (b)).

Figure 4.4 compares the localization error CDF of localization methods based on EKF, fusion plus KF and direct fusion (the fusion part in fusion plus KF). There are 1, 2 and 4 BNs in Figure 4.4(a), (b) and (c), respectively. Figure 4.4(a) depicts that with one BN, the performance of the methods based on EKF and fusion plus KF is almost the same and much better than that of the direct fusion. This simulation confirms our analysis on the single BN scenario; it also confirms that the KF does shrink the fused localization error.

Figure 4.4 (b) and (c) depicts that converged EKF ($e = 240\sigma_R$) achieves the best performance, but the performance of diverged EKF ($e = 250\sigma_R$) is the worst. In addition,

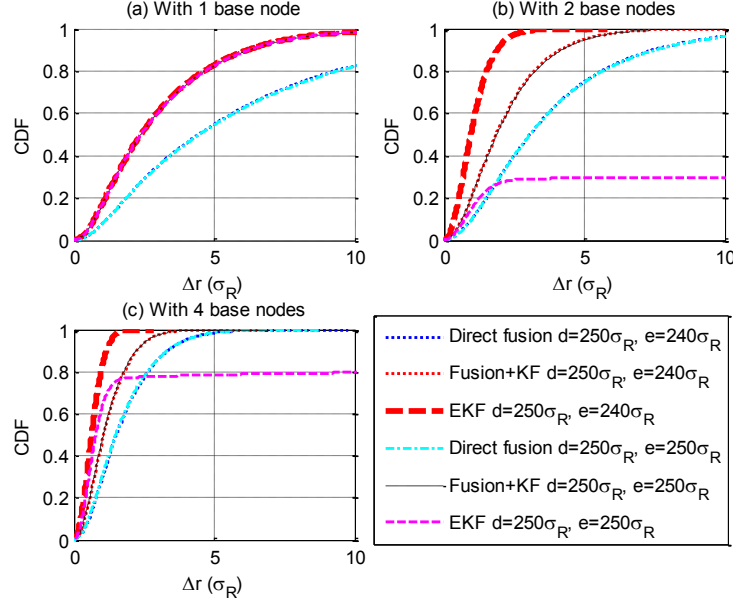


Figure 4.4: Comparison of localization error CDF with 1, 2 and 4 BNs.

fusion plus KF performs better than direct fusion. The small difference of the TN trace parameter ($e = 240\sigma_R$, and $e = 250\sigma_R$) does not affect the performance of fusion plus KF and direct fusion. But in the case $e = 250\sigma_R$, divergence takes place in the EKF and generates considerable localization error. Figure 4.4 (b) shows that only about 30% of the localization error stays below a threshold of $3\sigma_p$. This number is in the order of 80% for Figure 4.4 (c). Though the localization performance is enhanced with two more BNs, but it is still too low in many applications to satisfy the requirement.

Figure 4.5 compares the APCRLB's of the two methods based on fusion plus KF and EKF. The comparison confirms that the performance of EKF is better than that of the fusion plus KF in the scenario that both KF and EKF converge.

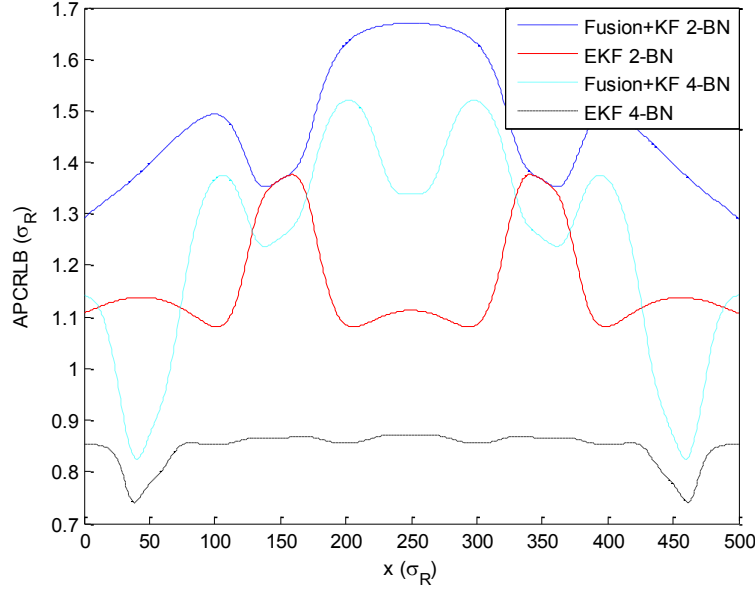


Figure 4.5: Comparison of APCRLB with 2 and 4 BNs.

Figure 4.6 compares the computational complexity of the methods based on fusion plus KF and EKF. Here, we observe that the complexity of the EKF is much higher and increases faster than that of fusion plus KF. If there are 4 (5) BNs, the complexity of EKF would be about 5 (7) times of that of fusion plus KF. Hence, using fusion plus KF, we can localize higher number of TNs compared to using EKF if the processor capability is limited.

Usually the cost of BNs used in ad-hoc network applications is higher than that of TNs. Thus, the number of BNs is kept as small as possible. In addition, their communication range limits the number of BNs that are capable of localizing a TN simultaneously. Moreover, the TN can be anywhere, e.g., a TN may be close to the line connecting two BNs. In these scenarios, we observe that EKF diverges, and localization error would be

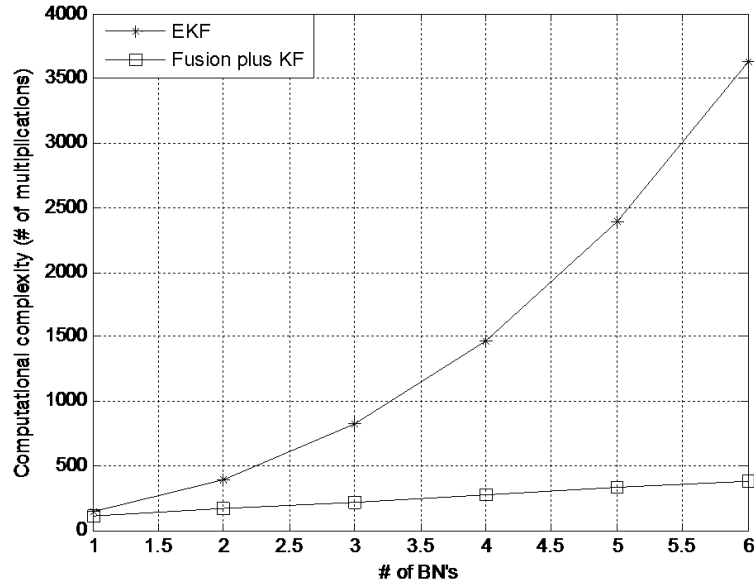


Figure 4.6: Computational complexity comparison.

high. However, fusion plus KF converges and achieves a reasonable performance. In addition, computational complexity of fusion plus KF is low. Therefore, applying fusion plus KF, we can localize more TNs compared to EKF, if the processor capability is limited.

4.5 Conclusions

We propose a stable, low complex localization method – fusion plus KF – and compare it with the localization method based on EKF. If the EKF converges, it performs better than the proposed method except in the scenario that only one BN is available, in which the two methods have almost the same performance. But if the EKF diverges, it performs poorly and its performance is much worse than that of the proposed method. In ad-hoc

networks, nodes can be anywhere, and the number of BNs localizing a TN simultaneously is limited; therefore, convergence cannot be guaranteed in an EKF. Hence, the proposed localization technique performs better than EKF in terms of stability (no divergence). In addition, the proposed method has very low computational complexity, which makes it a good candidate for localizing multiple TNs in MANETs.

Chapter 5

Single Base Node LOS and NLOS Separation⁵

This chapter introduces a LOS and NLOS separation technique based on the statistics of the phase difference of two received signals. The phase difference is achieved via a co-installed synchronized two-receiver system. The variance of the phase difference is related to the wireless channels K-factor (the received signal power ratio of the stable part to the random part) to separate LOS and NLOS between one BN and one TN. The PDF of the received signal phase generated by NLOS component is theoretically derived. The variance of the phase difference is calculated using the derived PDF numerically and verified via simulations. The LOS and NLOS separation performance versus signal power ratio of LOS to NLOS is evaluated via simulations.

5.1 Introduction

In most localization methods based on TOA and (or) DOA measurement [9 – 11, 22 – 27], LOS channel between TN and BNs is necessary to achieve reasonable localization performance. When the LOS between BNs and the TN is blocked by obstacles, the TOA and DOA measurement would involve with significant errors [30, 36], and therefore large localization error would be introduced if we use these traditional localization methods.

⁵ © [2009] IEEE. Reprinted, with permission, from [IEEE DSP/SPE, A New Multi-Antenna Based LOS - NLOS Separation Technique, Z. Wang, W. Xu, and S. A. Zekavat]. See Appendix A for full permission.

If we identify that a signal is received from a NLOS channel, then we can minimize the localization error generated by NLOS signals using proper method, e.g., discarding the associated TOA and/or DOA if the LOS measurements are enough for implementing the localization [30]. Hence, discrimination between LOS and NLOS helps to improve the localization accuracy.

Techniques proposed in the literature to identify NLOS signal include the method based on the root-mean-squared delay spread (RDS) of the received signals [32], and the test of the statistics of the measured range [29]. The method presented in [32] is only applicable to ultra-wideband (UWB) systems. It is not applicable to narrow or wideband systems, because the RDS cannot be properly estimated in these systems. The latency in the method presented in [29] is large: the full statistics of the estimated range should be achieved that requires considerable time.

This chapter introduces a new LOS and NLOS separation technique that is based on the statistics of the phase difference of two signals received by a co-installed synchronized two-receiver system. The phase difference variance is calculated, and related to the wireless channel's K-factor to separate LOS and NLOS between a BN and a TN. In NLOS condition, the phase difference variance is large and it decreases as LOS power increases from 0. In LOS only condition, the variance is zero. The separation technique can be easily applied to multi-input systems, e.g., WLPS [9].

This chapter derives the PDF of the received signal's phase generated by NLOS component (including reflected signals and noise), calculates the phase difference

variance numerically; and, computes the phase difference variance in the condition that a strong LOS component is available. The derived PDF and phase difference variance are verified via simulations. In addition, the chapter proposes a measure for the reliability of the data and evaluates that measure via simulations. Finally, the probability of discriminating LOS and NLOS versus wireless channel K-factor is evaluated via simulations.

5.2 Received Signal Model

A co-installed synchronized two-receiver system shown in Figure 5.1 supports the proposed LOS and NLOS separation method. In this system, the two antennas are installed with fixed relative position, and they are located far enough from each other to maintain independent channels, and the two receivers share the same local oscillator. The

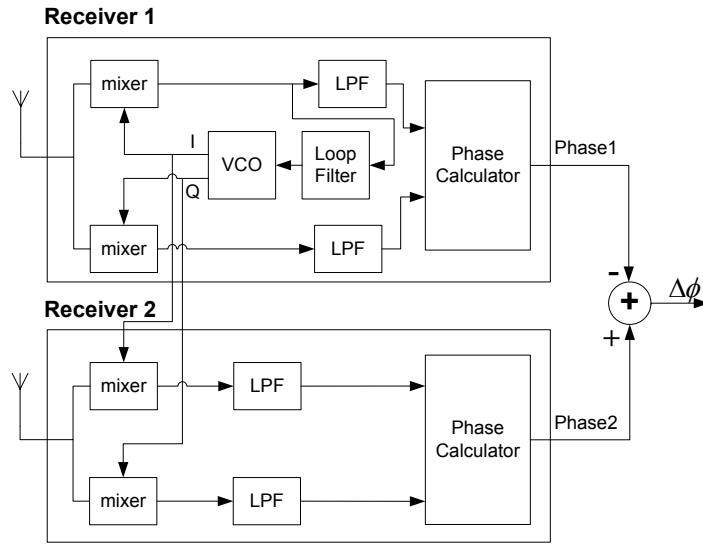


Figure 5.1: Synchronized two-receiver system.

far region scenario is assumed (the two receivers receive signals through wireless channels with the same power but different phases). The only difference between these receivers and smart antenna receivers is the phase calculator. Hence, the proposed structure can be easily implemented in smart antenna systems using the two outer antenna elements (they are far enough from each other to maintain channel independency).

The LOS signal received by Receiver 1 is modeled as

$$\begin{aligned} r_{LOS1} &= x_{LOS1} + jy_{LOS1} \\ &= A \cos \varphi' + jA \sin \varphi'. \end{aligned} \quad (5.1)$$

In (5.1), $x_{LOS1} = A \cos \varphi'$ is the real part and $y_{LOS1} = A \sin \varphi'$ is the imaginary part of the received signal at Receiver 1; A and φ' are the received signal's amplitude and phase, respectively. Considering the source is located very far from the receivers, the LOS signal received by Receiver 2 would have the same amplitude of A but different phase φ'' . The LOS signal received by Receiver 2 is modeled as

$$\begin{aligned} r_{LOS2} &= x_{LOS2} + jy_{LOS2} \\ &= A \cos \varphi'' + jA \sin \varphi''. \end{aligned} \quad (5.2)$$

Here, the phase of the received signal at Receiver 2 is $\varphi'' = \varphi' + 2\pi d \cos \theta / \lambda$; d is the distance between the two antennas; λ is the carrier wavelength; and, θ is the DOA of the received LOS signal (see Figure 5.2). In addition, $x_{LOS2} = A \cos \varphi''$ is the real part and $y_{LOS2} = A \sin \varphi''$ is the imaginary part of the received signal at Receiver 2.

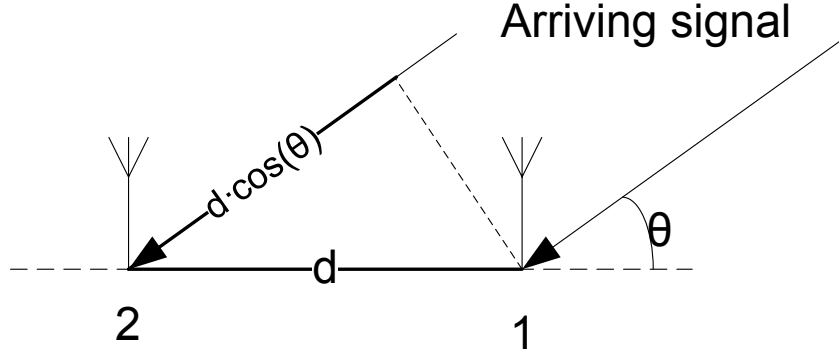


Figure 5.2: Signals' phase difference at antennas 1 and 2.

The NLOS signal (the summation of reflected signal and noise) can be modeled as Rayleigh random variable [79]; hence, the NLOS signal received by Receiver 1 is modeled as

$$r_{NLOS1} = x_{NLOS1} + jy_{NLOS1}. \quad (5.3)$$

In (5.3), x_{NLOS1} and y_{NLOS1} are independent zero mean Gaussian random variables with the same variance (σ_1^2). In addition, we define $K_1 = A^2 / E(x_{NLOS1}^2 + y_{NLOS1}^2) = A^2 / 2\sigma_1^2$ as the signal power ratio of LOS to NLOS (wireless channel's K-factor); here, $E(\cdot)$ denotes expectation operation and A^2 is the power of LOS signal. Similarly, the NLOS signal received by Receiver 2 is modeled as

$$r_{NLOS2} = x_{NLOS2} + jy_{NLOS2}. \quad (5.4)$$

Here, x_{NLOS2} and y_{NLOS2} are independent zero mean Gaussian random variables with the

same variance (σ_2^2). We define $K_2 = A^2 / E(x_{NLOS2}^2 + y_{NLOS2}^2) = A^2 / 2\sigma_2^2$. Assuming antennas 1 and 2 are located far from each other, x_{NLOS1} , y_{NLOS1} , x_{NLOS2} and y_{NLOS2} would be independent. Knowing that the two antennas receive the same signal power, $\sigma_1^2 = \sigma_2^2 = \sigma^2$. Thus, $K_1 = K_2 = K$.

The total received signals at receivers 1 (r_1) and 2 (r_2) correspond to

$$\begin{aligned} r_1 &= x_1 + jy_1 \\ &= r_{LOS1} + r_{NLOS1}, \\ r_2 &= x_2 + jy_2 \\ &= r_{LOS2} + r_{NLOS2}. \end{aligned} \tag{5.5}$$

5.3 Phase Difference Variance

The phases of the signals received by receivers 1 and 2 ($\varphi_1^{(in)}$ and $\varphi_2^{(in)}$) are calculated as

$$\begin{aligned} \varphi_1^{(in)} &= \tan^{-1}(y_1 / x_1), \\ \varphi_2^{(in)} &= \tan^{-1}(y_2 / x_2). \end{aligned} \tag{5.6}$$

Assuming the phase of the local oscillator is φ_o , the phase of the output signals of receivers 1 and 2 ($\varphi_1^{(out)}$ and $\varphi_2^{(out)}$) would correspond to

$$\begin{aligned} \varphi_1^{(out)} &= \varphi_1^{(in)} - \varphi_o, \\ \varphi_2^{(out)} &= \varphi_2^{(in)} - \varphi_o. \end{aligned} \tag{5.7}$$

The phase difference ($\Delta\varphi$) between the two output signals of receivers 1 and 2 is

$$\begin{aligned}\Delta\varphi &= \varphi_2^{(out)} - \varphi_1^{(out)} \\ &= \varphi_2^{(in)} - \varphi_1^{(in)}.\end{aligned}\tag{5.8}$$

The received signal's phase ($\varphi_1^{(in)}$) at Receiver 1 includes two parts: (a) φ' that is generated by the LOS component introduced in (5.1), and (b) $\Delta\varphi_1$ that is generated by the NLOS component. The relationship between these two components is shown in Figure 5.3, and

$$\varphi_1^{(in)} = \varphi' + \Delta\varphi_1.\tag{5.9}$$

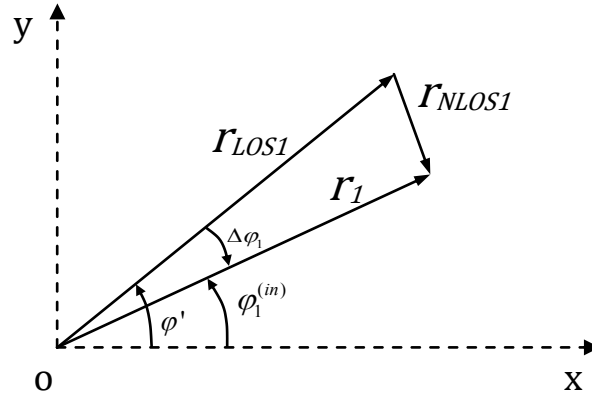


Figure 5.3: Received signal phase at Receiver 1.

Similarly,

$$\varphi_2^{(in)} = \varphi'' + \Delta\varphi_2.\tag{5.10}$$

Here, φ'' has been introduced in (5.2), and $\Delta\varphi_2$ is the phase shift generated by the NLOS component at Receiver 2. Incorporating (5.9) and (5.10) in (5.8), we achieve

$$\Delta\varphi = (\varphi'' - \varphi') + (\Delta\varphi_2 - \Delta\varphi_1). \quad (5.11)$$

Assuming the DOA of the LOS signal (θ) keeps unchanged, i.e., $\varphi'' - \varphi' = 2\pi d \cos \theta / \lambda$ is a constant. The phase difference variance ($\sigma_{\Delta\varphi}^2$) would be determined by $\Delta\varphi_1$ and $\Delta\varphi_2$. The two antennas locate far from each other. Hence, the NLOS signals at receivers 1 and 2 and accordingly $\Delta\varphi_1$ and $\Delta\varphi_2$ are assumed independent. $\Delta\varphi_1$ and $\Delta\varphi_2$ have the same variance, because the variance of $\Delta\varphi_i$ ($\sigma_{\Delta\varphi_i}^2$), $i \in \{1, 2\}$, is only a function of K_i (see (5.17) and (5.18)) and $K_1 = K_2 = K$. If we calculate $\sigma_{\Delta\varphi_1}^2$, then $\sigma_{\Delta\varphi_2}^2$ can be easily evaluated.

The statistics of $\Delta\varphi_1$ is independent of the LOS signal phase (φ') (see Figure 5.3). Hence, in the process of calculating the PDF of $\Delta\varphi_1$, we assume $\varphi' = 0$. In this case, $x_{LOS1} = A$, $y_{LOS1} = 0$ and $\Delta\varphi_1 = \varphi_1^{(in)}$ falls within $(-\pi, \pi)$. Let B_1 represent the amplitude of r_1 (calculated in (5.5)), then we have

$$\begin{aligned} x_1 &= A + x_{NLOS1} \\ &= B_1 \cos \Delta\varphi_1, \\ y_1 &= 0 + y_{NLOS1} \\ &= B_1 \sin \Delta\varphi_1. \end{aligned} \quad (5.12)$$

Here, x_1 and y_1 are independent Gaussian random variables. x_1 follows the distribution of $N(A, \sigma^2)$ and y_1 follows the distribution of $N(0, \sigma^2)$. In addition, $\Delta\varphi_1$ is a zero mean random variable. The joint distribution of x_1 and y_1 corresponds to

$$f_{X_1, Y_1}(x_1, y_1) = \frac{1}{2\pi\sigma^2} \exp\left(-\frac{(x_1 - A)^2 + y_1^2}{2\sigma^2}\right). \quad (5.13)$$

Considering (5.12), we calculate the joint distribution of B_1 and $\Delta\varphi_1$ using bivariate transformation

$$f_{B_1, \Delta\varphi_1}(B_1, \Delta\varphi_1) = f_{X_1, Y_1}(B_1 \cos \Delta\varphi_1, B_1 \sin \Delta\varphi_1) \cdot |J(B_1, \Delta\varphi_1)|. \quad (5.14)$$

Where,

$$J(B_1, \Delta\varphi_1) = \begin{vmatrix} \frac{\partial x_1}{\partial B_1} & \frac{\partial x_1}{\partial \Delta\varphi_1} \\ \frac{\partial y_1}{\partial B_1} & \frac{\partial y_1}{\partial \Delta\varphi_1} \end{vmatrix} = B_1. \quad (5.15)$$

Incorporating (5.13) and (5.15) into (5.14) leads to

$$f_{B_1, \Delta\varphi_1}(B_1, \Delta\varphi_1) = \frac{B_1}{2\pi\sigma^2} \exp\left(-\frac{B_1^2 + A^2 - 2AB_1 \cos \Delta\varphi_1}{2\sigma^2}\right). \quad (5.16)$$

The marginal PDF of $\Delta\varphi_1$ corresponds to

$$\begin{aligned} f(\Delta\varphi_1) &= \int_0^\infty f_{B_1, \Delta\varphi_1}(B_1, \Delta\varphi_1) dB_1 \\ &= \frac{\exp(-B_1^2 \sin^2 \Delta\varphi_1 / 2\sigma^2)}{2\pi\sigma^2} \times \int_0^\infty B_1 \exp[-(B_1 - A \cos \Delta\varphi_1)^2 / 2\sigma^2] dB_1 \\ &= \frac{\exp(-K)}{2\pi} + \sqrt{\frac{K}{\pi}} \cos \Delta\varphi_1 \exp(-K \sin^2 \Delta\varphi_1) \times Q(-\sqrt{2K} \cos \Delta\varphi_1). \end{aligned} \quad (5.17)$$

In (5.17), $Q(x) = \int_x^\infty \frac{1}{2\pi} \exp(-\frac{u^2}{2}) du$ and K is the signal power ratio of LOS to NLOS

(wireless channel's K-factor). The variance of $\Delta\varphi_1$ corresponds to

$$\sigma_{\Delta\varphi_1}^2 = \int_{-\pi}^{\pi} \Delta\varphi_1^2 f(\Delta\varphi_1) d\Delta\varphi_1. \quad (5.18)$$

There is a Q function in $f(\Delta\varphi_1)$; hence, we numerically evaluate (5.18).

In the extreme condition that there is no LOS component, K would be equal to 0, $r_1 = r_{NLOS1}$ and $\Delta\varphi_1$ would be uniformly distributed between $-\pi$ and π . $\Delta\varphi_2$ and $\Delta\varphi_1$ are assumed independent and having the same variance. Hence, in this scenario, the variance of $\Delta\varphi$ reaches its upper bound of

$$\begin{aligned} \sigma_{\Delta\varphi,ub}^2 &= 2\sigma_{\Delta\varphi_1}^2 \\ &= 2\pi^2 / 3. \end{aligned} \quad (5.19)$$

On the other hand, when a strong LOS component is available, K would be large ($x_{LOS1} \gg x_{NLOS1}$, $y_{LOS1} \gg y_{NLOS1}$, $x_{LOS2} \gg x_{NLOS2}$ and $y_{LOS2} \gg y_{NLOS2}$). In this case, using Taylor expansion of (5.6) and ignoring higher order terms, $\varphi_1^{(in)}$ and $\varphi_2^{(in)}$ are calculated and the phase difference ($\Delta\phi = \varphi_2^{(in)} - \varphi_1^{(in)}$) corresponds to

$$\begin{aligned} \Delta\varphi &= [\tan^{-1} y_{LOS2}/x_{LOS2} - \tan^{-1} y_{LOS1}/x_{LOS1}] \\ &\quad + [y_{NLOS2} \cos \varphi'' - x_{NLOS2} \cos \varphi'' - y_{NLOS1} \cos \varphi' + x_{NLOS1} \cos \varphi'] / A. \end{aligned} \quad (5.20)$$

In (5.20), the first term, $\tan^{-1} y_{LOS2}/x_{LOS2} - \tan^{-1} y_{LOS1}/x_{LOS1}$, is equal to $2\pi d \cos \theta / \lambda$, which is a constant assuming the LOS signal's DOA keeps unchanged. Moreover, x_{NLOS1} , y_{NLOS1} , x_{NLOS2} and y_{NLOS2} are assumed independent zero mean Gaussian random variables; hence, the second term in (5.20), $[y_{NLOS2} \cos \varphi'' - x_{NLOS2} \cos \varphi'' - y_{NLOS1} \cos \varphi' + x_{NLOS1} \cos \varphi'] / A$, is a zero mean Gaussian random variable. Thus, the variance of $\Delta\phi$ corresponds to

$$\begin{aligned}\sigma_{\Delta\phi}^2 &= E[(y_{NLOS2} \cos \varphi'' - x_{NLOS2} \cos \varphi'' - y_{NLOS1} \cos \varphi' + x_{NLOS1} \cos \varphi')^2 / A^2] \\ &= 2\sigma^2 / A^2 \\ &= 1 / K.\end{aligned}\tag{5.21}$$

In the extreme condition that there is only a strong LOS signal, $K \rightarrow \infty$ and $\sigma_{\Delta\phi}^2 = 0$. Based on the two extreme cases of $K \rightarrow 0$ and $K \rightarrow \infty$, it is concluded that $\sigma_{\Delta\phi}^2$ should vary between 0 and $2\pi^2 / 3$ as K changes from ∞ (LOS only) to 0 (NLOS only).

5.4 Data Reliability and LOS and NLOS Separation

Not all TOA and DOA estimation are reliable: when LOS component is not available, the estimated TOA is biased [36] and the estimated DOA includes large error [30]. In this case, the estimation would not be reliable. If a strong LOS component is available, the TOA and DOA estimation errors would be mainly determined by the received noise, and the estimation would be reliable. This is specifically important in the process of data (TOA-DOA) fusion in cooperative localization techniques [62]. If a measure of data

reliability is provided in TOA and/or DOA fusion, better performance would be achieved.

In Section 3, we calculated the phase difference variance ($\sigma_{\Delta\varphi}^2$). In NLOS only scenario, $\sigma_{\Delta\varphi}^2$ reaches its upper bound ($2\pi^2/3$). As the signal power ratio of LOS to NLOS increases from 0 (no LOS), the phase difference variance decreases. When only LOS is available, the phase difference variance equals to 0. TOA and DOA estimation in the case of NLOS only are not reliable, while the one estimated in LOS only scenario is fully reliable. Hence, the measure of data reliability (Re) can be calculated as:

$$Re = \frac{\sigma_{\Delta\varphi,ub}^2 - \sigma_{\Delta\varphi}^2}{\sigma_{\Delta\varphi,ub}^2}. \quad (5.22)$$

Here, $\sigma_{\Delta\varphi,ub}^2 = 2\pi^2/3$ refers to the upper bound of $\sigma_{\Delta\varphi}^2$. According to (5.22), $Re = 0$ when there is no LOS component, which means that the data is not reliable; and, $Re = 1$ when there is only LOS component, which means that the data is fully reliable. This measure of reliability can be used in the fusion of TOA and/or DOA to assign fusion weights.

In some applications, e.g., localization via joint TOA-DOA estimation [9], a threshold is needed to discriminate LOS and NLOS. In general, there are both LOS and NLOS components in the received signal, and the power ratio K can be any value between zero and infinity. Thus, there is not a clear threshold to separate LOS and NLOS. If power ratio K is used to separate LOS and NLOS, the threshold would depend on applications.

For example, we have a uniform linear antenna (ULA) array, and apply delay and sum [58] to estimate the received signal's DOA. When the power ratio K is smaller than 1.5, the root mean squared error (RMSE) of the DOA estimation would be larger than 6.2° . While if K increases to 2.5, the DOA estimation RMSE would be 2.1° . DOA RMSE verses K simulation results are sketched in Figure 5.4. To sketch this figure, we assume the ULA array includes six elements; the distance between neighboring elements is $\lambda/2$; one sample is captured to calculate DOA (no averaging technique is applied to decrease the DOA estimation error). Based on this figure, there is always a threshold K_{th} , if $K < K_{th}$, as K decreases, the DOA estimation error increases fast; while if $K > K_{th}$, as K increases, the DOA estimation error decreases slowly. When the ULA array includes six elements, $K_{th} = 2$ can be considered as the threshold: when $K < K_{th}$, large DOA estimation error is experienced and the received signal is considered as NLOS signal; while $K \geq K_{th}$, small DOA error is achievable and the received signal is considered LOS signal.

5.5 Simulation and Discussion

In this section, we verify the derived PDF of the received signal's phase generated by NLOS component and the calculated variance, and evaluate the performance of LOS and NLOS separation via simulations.

Here, we assume: (1) transmitter and reflectors are located far from the co-installed

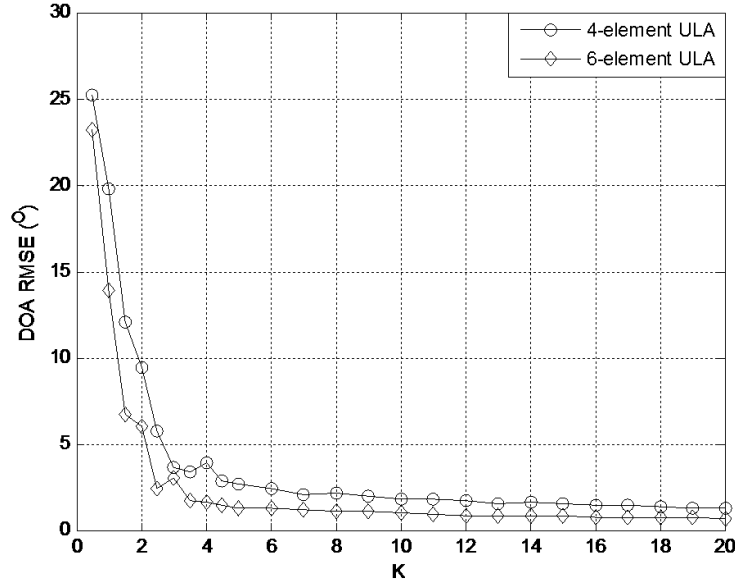


Figure 5.4: DOA estimation error vs. power ratio K .

synchronized two-receiver system, receivers 1 and 2 receive signals with the same power and different phase from transmitter and reflectors; (2) there are twenty reflectors uniformly distributed around the two-receiver system (the DOA of NLOS signals is uniformly distributed between 0 and 2π), and the NLOS signal power is uniformly distributed across these paths; (3) the distance between the two receive antennas is 2λ ; (4) a set of samples (e.g., 50 or 100) are captured to calculate the phase difference variance ($\sigma_{\Delta\varphi}^2$) as the two-receiver system moves; (5) the received signals' power and DOA remain unchanged in the process of capturing these samples; (6) the threshold of the phase difference variance ($\sigma_{\Delta\varphi,th}^2$) is calculated at $K_{th}=2$. If the calculated $\sigma_{\Delta\varphi}^2$ is larger than $\sigma_{\Delta\varphi,th}^2$, the signal is considered received through a NLOS channel; and if the calculated

$\sigma_{\Delta\varphi}^2$ is smaller than or equal to $\sigma_{\Delta\varphi,th}^2$, the received signal is considered coming through a LOS channel; and, (7) the LOS and NLOS separation performance is evaluated in terms of the probability of false alarm (P_f) given the power ratio K , i.e., $P_f = P(NLOS|LOS, K)$; and the probability of misdetection (P_m) given the power ratio K , i.e., $P_m = P(LOS|NLOS, K)$.

Figure 5.5 depicts the consistency of the simulated and derived PDF's of the received signal phase ($\Delta\varphi_1$) generated by the NLOS component. The data used to calculate $\Delta\varphi_1$ is independently generated. When $K = 0$, there is only NLOS component and $\Delta\varphi_1$ is uniformly distributed between $-\pi$ and π . As K increases, the phase generated by NLOS component tends to zero, which means the variance of $\Delta\varphi_1$ decreases.

Figure 5.6 shows the consistency of the simulated and numerically calculated phase difference variances with respect to K . The phase difference variance decreases as K increases; the variance decreases fast from $K = 0$ to $K = 2$ and decreases slowly when $K > 2$. When $K = 0$, the phase difference variance reaches its upper bound of $2\pi^2/3$. When K is larger than 6, the phase difference variance is about equal to $1/K$ (see (5.21)).

Figure 5.7 represents the simulated P_f and P_m . The pair of curves marked with *circle* are generated with independent samples. And the other three pairs of curves are generated with correlated samples captured as the two-receiver system moves; the spatial distance between neighboring samples is 0.1λ or λ . Figure 5.7 depicts that: (1) the best separation performance (the lowest P_f and P_m) is achieved with samples generated independently;

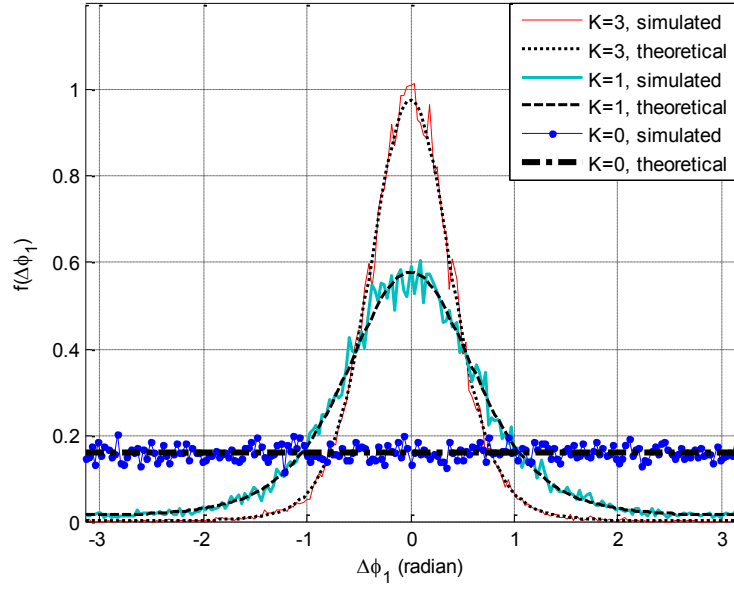


Figure 5.5: Verification of $f(\Delta\phi_1)$ with different K .

the reason is that the true statistics of the phase difference is obtained when independent samples are captured. 2) The separation performance increases as the number of samples increases; that is as the number of samples increases, both P_f and P_m decrease (the calculated variance tends to its true value as more samples are captured); (3) the separation performance increases as the spatial distance between samples increases (the correlation between samples decreases); and (4) the method performs with small spatial distance between samples (e.g., 0.1λ) and small number of samples (e.g., 50).

The spatial sampling distance can be very small (down to 0.1λ) and the number of samples can be very small (down to 50); hence, the latency in the proposed method is small. For example, at 2.4GHz, a TN with a speed of 10km per hour can be identified

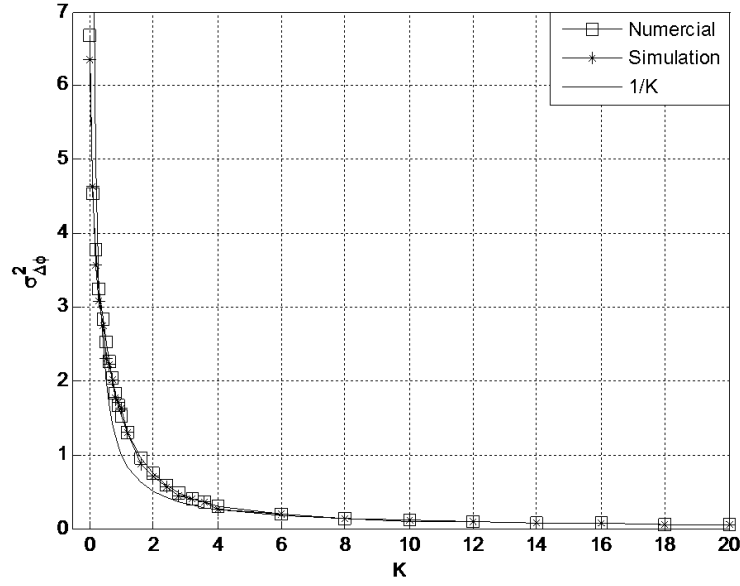


Figure 5.6: Verification of phase difference variance ($\sigma_{\Delta\phi}^2$).

having LOS or NLOS with BN in a distance of 0.625m (5λ), which corresponds to 0.225 seconds. Using this method, we can identify LOS and NLOS very fast.

In NLOS scenario, if there is a strong NLOS component, the received signal phase might be dominantly determined by the strong NLOS component. In addition, the strong NLOS component might be considered as LOS component. This is the shortcoming of the presented separation method. But this scenario does not happen frequently. In downtown area, the size of buildings is comparable and there is no dominant reflector; in rural area, there are only houses, trees and crops, but no large reflectors. Thus, the probability of NLOS being considered as LOS is low in downtown and rural area. While in hilly area, a hill may be a dominant reflector, the probability of NLOS is considered as LOS is high.

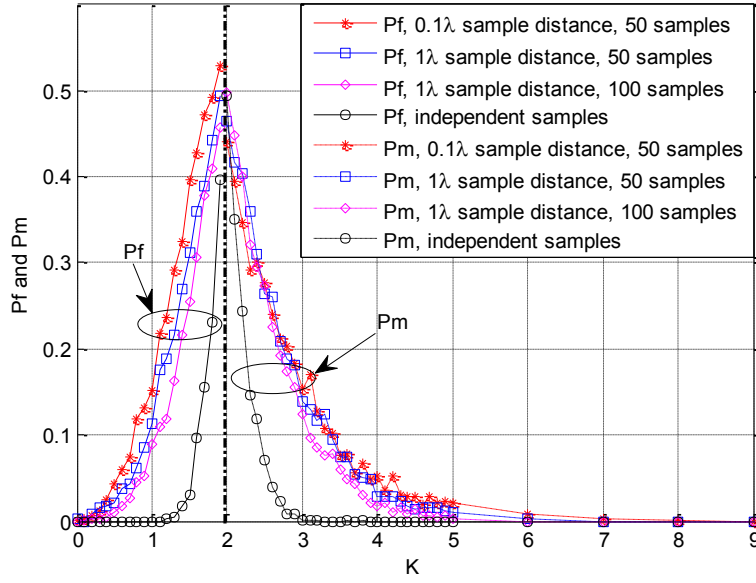


Figure 5.7: LOS and NLOS separation performance.

5.6 Conclusions

In this chapter, we presented a novel LOS and NLOS separation method, which is based on the received signals' phase difference statistics. The presented separation method can be conveniently implemented in smart antenna systems; only two phase calculators are added to the receivers. The method only needs the received signals' phase difference variance, it is applicable to narrow or wide band systems (e.g., cellular system). The latency of this system is small, because the required spatial sampling distance and the number of samples can be small.

We theoretically derived the PDF of the received signal's phase shift generated by NLOS component at one receiver and calculated the variance of the received signals' phase

difference between two co-installed synchronized receivers. The derived PDF and calculated phase difference variance were verified via simulations. The LOS and NLOS separation performance were evaluated via simulation with respect to the number of paths, the number of samples and the sampling spatial distance. Simulations confirm the efficiency of the presented LOS and NLOS separation method.

Chapter 6

Localization in NLOS Scenario⁶

This chapter presents an Omni mobile (simple transceiver with Omni directional antenna) TN localization technique in NLOS scenarios based on TOA-DOA measurements. Moreover, we propose NLOS identification, shared reflectors determination and localization technique to support the NLOS TN localization. This chapter assumes BNs are equipped with antenna arrays and capable of TOA-DOA estimation. In addition, single bounce reflection NLOS channel between BNs and TNs is considered. In NLOS scenario, when there are three or more reflectors shared by a TN and multiple sets of BNs, the shared reflectors are localized via DOA fusion, and then the TN is localized via TOA fusion based on the shared reflectors localization. The equations for NLOS identification, shared reflectors determination and localization and NLOS TN localization are theoretically derived. Simulations are conducted to evaluate the efficiency of the proposed technique. Simulations show that the probability of LOS is taken as NLOS and the shared reflector is taken as non-shared reflector is low with a reasonable threshold, while the probability of NLOS is taken as LOS and the non-shared reflector is taken as shared reflector is slightly high; the NLOS TN localization accuracy is acceptable if the system coverage area is not too large and the DOA estimation error is small.

⁶ © [2009] IEEE. Reprinted, with permission, from [IEEE *Transactions on Mobile Computing*, Omni-Directional Mobile NLOS Identification and Localization via Multiple Cooperative Nodes, Z. Wang, and S. A. Zekavat]. See Appendix A for full permission.

6.1 Introduction

In a real application, LOS channel between BNs and TNs may be available or blocked by obstructers. Thus, a localization system should consider both LOS localization and NLOS localization. Many localization technique have been designed for LOS application (LOS channel between BNs and TNs are assumed) [9-11, 22-27]. But only a few localization methods have been designed for NLOS application, i.e., using NLOS measurement to implement localization [38-40]. But their limitations are obvious: the signature mapping in [38] needs a RSS map of the application environment, which may be unavailable in some scenarios; the leveraging LPMD in [39] assumes the reflectors are either parallel or perpendicular to each other, this is not reasonable in an area with irregular distribution of buildings; and, the multiple lines crossing in [40] requires each node being equipped with antenna array, which are expensive and power consuming, it is not possible to install antenna array on TN if cost and power consumption are critical.

In this chapter, we propose an Omni-directional TN localization technique that directly applies NLOS TOA-DOA measurements to the localization process. Here, only BNs are equipped with antenna arrays to estimate other nodes' TOA and DOA; TNs are equipped with Omni-directional antennas (i.e., simple transceivers) and respond inquiring signals of BNs to support the TOA-DOA measurements at BNs. Hence, if the system includes a large number of TNs and a small number of BNs, the cost would not be high, and TNs consume much less power than BNs. The method would be applicable in an ad-hoc network, where cost and power consumption are critical. In addition, it is assumed that

either LOS or single bouncing reflection NLOS channel is available between BNs and TNs. We also propose NLOS identification between multiple BNs and a TN, shared reflectors determination and localization techniques to support NLOS TN localization. The equations for NLOS identification, shared reflectors determination and localization, and NLOS TN localization are theoretically derived. Simulations are conducted to evaluate the performance of NLOS identification and shared reflectors determination in terms of false alarm and miss detection, and the NLOS TN localization accuracy in terms of localization circular error CDF.

6.2 System Model and Problem Definition

The localization system is composed of two categories of nodes, BNs and TNs, as shown in Figure 6.1. BNs are equipped with antenna arrays and capable of estimating other nodes' TOA and DOA. In addition, BNs DOA measurements are made with respect to a reference direction, e.g., with respect to the east. TNs are simple transceivers equipped with Omni-directional antennas responding inquiring signals of BNs to support TOA-DOA measurements. BNs position is known or computed using LOS localization method presented in Chapter 2 or NLOS localization method presented in [40]. The wireless channel between BNs and TNs is assumed to be LOS or single bounce reflection NLOS. Here, we reasonably assume that signals that go through multiple bounces are weaker than single bounce signals; thus, they are ignorable. This assumption is typically fare for urban areas [80]. Practically, we can design our receiver such that it only considers signals received with power larger than a specific threshold for this problem. Finding the

threshold at the receiver to resolve single bounce signals from multiple bounce with a high probability-of-detection and low probability-of-false-alarm is a problem that will be addressed in our future works.

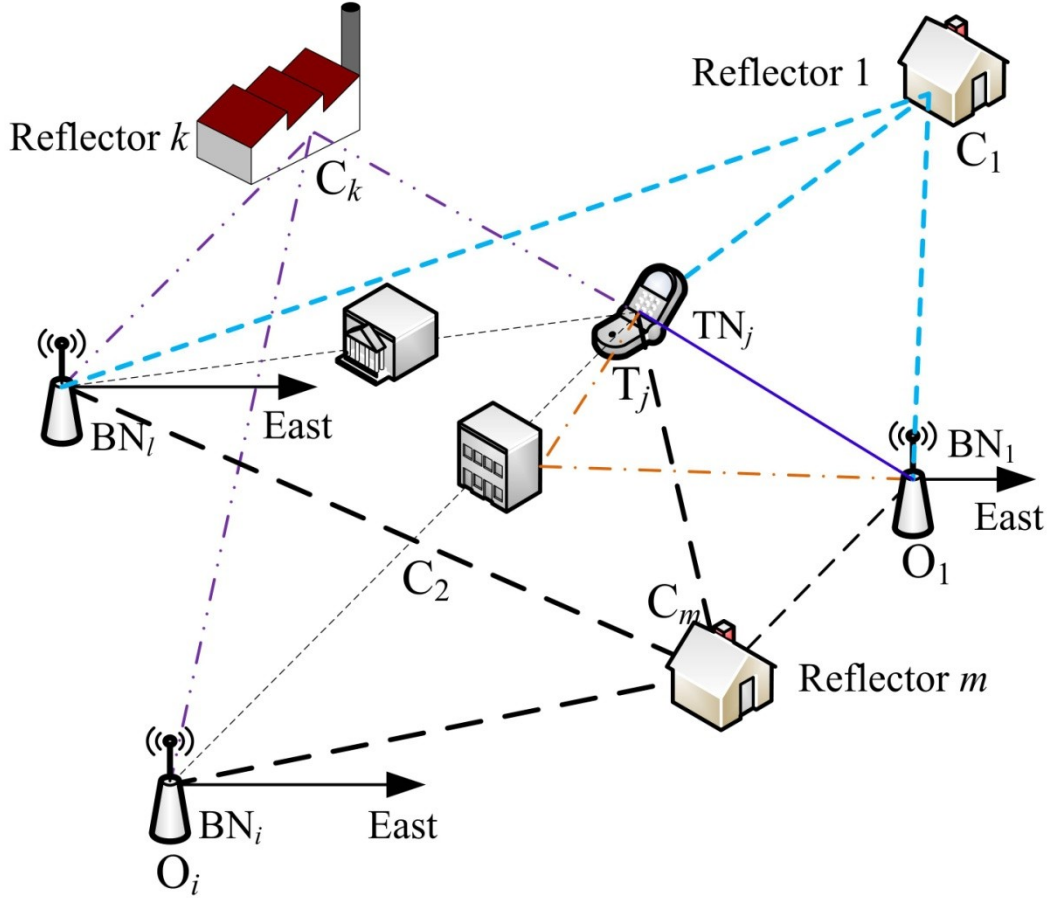


Figure 6.1: NLOS localization system model.

Considering a TOA-DOA based localization, Figure 6.2 summarizes all the TNs localization scenarios. A TN may be localized by only one BN or multiple BNs due to the communication range limitation and shadowing effect. When a TN is localized by multiple BNs, there are two sub-scenarios: 1) There are two or more LOS BNs; and, 2)

There is one or no LOS BN.

This chapter addresses the localization problem in the second sub-scenario: TNs localization with multiple BNs but there is one or no LOS BN (highlighted in Figure 6.2).

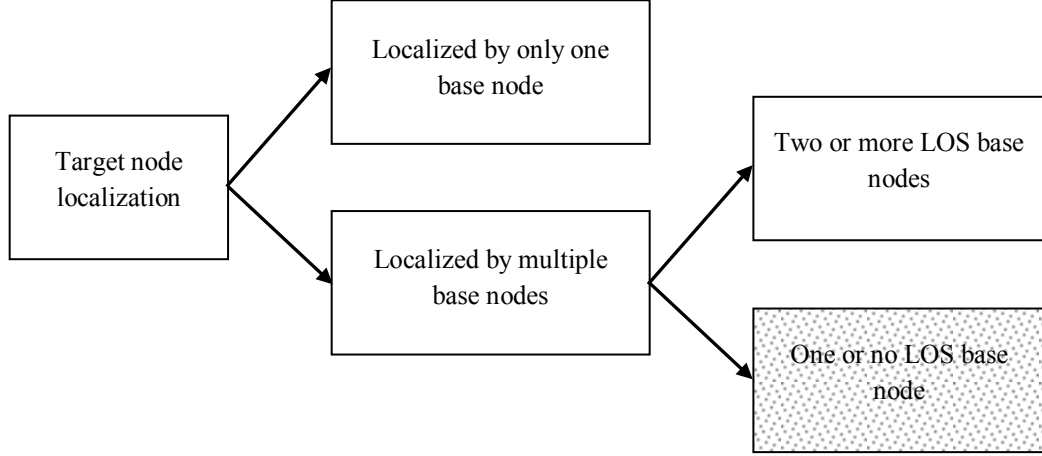


Figure 6.2: TN localization categorization.

When a TN is localized by multiple LOS BNs, the multi-node TOA-DOA fusion presented in Chapter 2 can be applied. In addition, when a TN is localized by only one BN, the set of TOA-DOA measurement that possesses the smallest TOA would be used to estimate the TN position [9], and the LOS-NLOS separation technique based on phase difference variance presented in Chapter 5 can be applied to generate a reliability parameter, which indicates how much we can depend on the estimation.

Here, we design a NLOS Omni-directional TN localization technique directly using the NLOS measurements achieved at BNs when multiple BNs localize a TN simultaneously and there is one or no LOS BN. It needs at least three reflectors to be shared by the TN and

multiple sets of BNs (each set includes two or more BNs). These reflectors can be localized by BNs via DOA fusion. The TN is localized via TOA fusion based on the shared reflectors' localization.

In the process of localizing reflectors, it should be known which set of BNs are sharing a reflector. Accordingly, we present a method to find the set of BNs that share a reflector. Here, we assume that the DOA resolution is high enough to resolve the signals received by BNs from different reflectors. When multiple BNs engage in the localization of a TN, they should decide which localization method should be applied (e.g., the LOS localization method presented in Chapter 2 and the proposed NLOS localization method). In order to do so, they should identify whether the LOS channel between TN and BNs is detectable. Accordingly, the first step is NLOS identification between BNs and TN.

6.3 Localization in NLOS Scenario

Based on the discussion in subsection 6.2, the NLOS TN localization technique includes four steps: (a) NLOS identification; (b) shared reflectors determination; (c) shared reflectors localization; and, (d) TN localization. Here, it is more convenient to first present steps (c) and (d) (see subsections 6.3.1 and 6.3.2), and then use the results to present steps (a) and (b) (see subsections 6.3.3 and 6.3.4). The theoretical results developed for shared reflectors localization are applied for NLOS identification and shared reflectors determination. The TOA and DOA measurement errors are assumed to be independent zero mean Gaussian random variables with the variances of σ_t^2 (the corresponding range

measurement error variance is $\sigma_R^2 = c^2 \sigma_t^2$, where c is the wave propagation speed) and σ_θ^2 , respectively.

6.3.1 Shared Reflectors Localization

The simplified system model for BNs i and l , TN j , reflectors k and m is shown in Figure 6.3. Here, the signal transmitted from TN j can arrive at BNs i and l through reflector k or reflector m , i.e., the reflector k (m) is shared by BNs i and l . At BNs i and l , we obtain two sets of measurements $(R_{ikj}^{(B,R,T)}, \theta_{ikj}^{(B,R,T)})$ and $(R_{lkj}^{(B,R,T)}, \theta_{lkj}^{(B,R,T)})$ due to the reflector k . The superscript (B, R, T) indicates that the range and angle are measured at a BN (B), through a reflector (R), and the source is a TN (T); the three subscript digits are the corresponding index of the superscript. For example, $R_{lkj}^{(B,R,T)}$ is the distance measured at the BN l , through the reflector k , and the source is the TN j .

Based on Figure 6.3, we have

$$R_{ikj}^{(B,R,T)} = R_{ik}^{(B,R)} + R_{kj}^{(R,T)},$$

$$R_{lkj}^{(B,T)} = R_{lk}^{(B,R)} + R_{kj}^{(R,T)},$$

$$\theta_{ikj}^{(B,R,T)} = \theta_{ik}^{(B,R)},$$

$$\theta_{lkj}^{(B,R,T)} = \theta_{lk}^{(B,R)}. \quad (6.1)$$

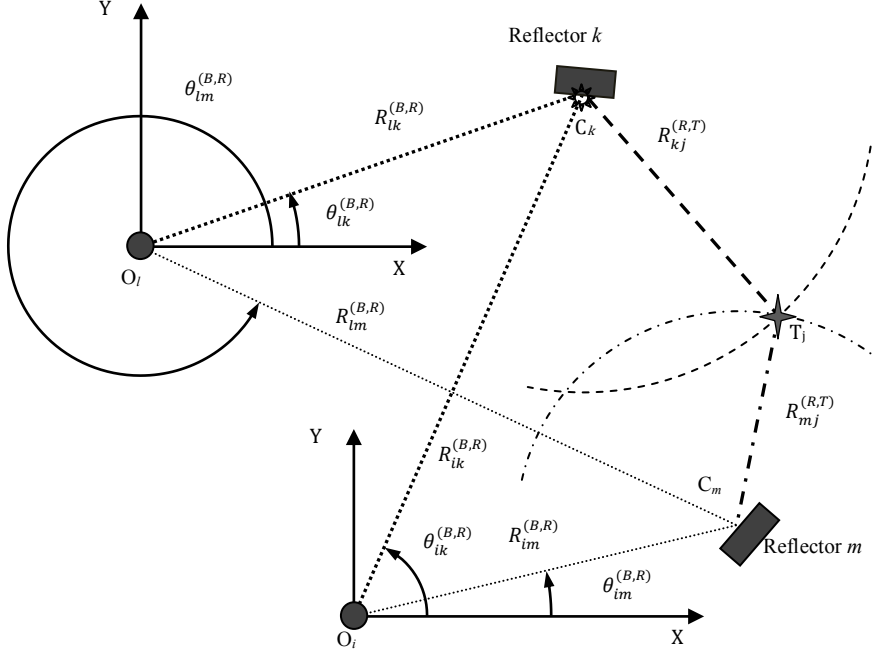


Figure 6.3: Reflector and TN localization.

Here, the superscript (B, R) indicates that the range or direction is for the reflector with respect to BN; the superscript (R, T) indicates that the range is for the TN with respect to the reflector; in addition, the first subscript digit is the index of the first superscript letter and the second digit is the index of the second superscript letter, e.g., $R_{kj}^{(R,T)}$ corresponds to the range between reflector k and TN j .

We have BNs position and we have computed the DOA's of reflector k with respect to BNs i and l . Using the positions of BNs i $(x_i^{(B,t)}, y_i^{(B,t)})$ and l $(x_l^{(B,t)}, y_l^{(B,t)})$ and the measurement of reflector k 's angles $(\theta_{ik}^{(B,R)}$ and $\theta_{lk}^{(B,R)})$ with respect to the two BNs, we can localize reflector k at $(x_k^{(R)}, y_k^{(R)})$ via DOA fusion. The superscript (t) indicates the

true value. Assuming the reflector k 's true position is $(x_k^{(R,t)}, y_k^{(R,t)})$, we have

$$\begin{aligned}\theta_{ik}^{(B,R,t)} &= \tan^{-1} \frac{y_k^{(R,t)} - y_i^{(B,t)}}{x_k^{(R,t)} - x_i^{(B,t)}}, \\ \theta_{lk}^{(B,R,t)} &= \tan^{-1} \frac{y_k^{(R,t)} - y_l^{(B,t)}}{x_k^{(R,t)} - x_l^{(B,t)}}.\end{aligned}\tag{6.2}$$

It should be noted that we use a pair of DOA's $(\theta_{ik}^{(B,R,t)}$ and $\theta_{lk}^{(B,R,t)})$ in (6.2), which are all coming from the shared reflector k . The approach for determining this pair of DOA's (that are computed based on signals coming from a shared reflector) would be introduced in subsection 6.3.4. Considering (6.1), and replacing the true values in (6.2) with the measured DOA values (i.e., $\theta_{ik}^{(B,R)}$ and $\theta_{lk}^{(B,R)}$), we have

$$\begin{aligned}\theta_{ik}^{(B,R)} &= g_i(x_k^{(R)}, y_k^{(R)}) = \tan^{-1} \frac{y_k^{(R)} - y_i^{(B,t)}}{x_k^{(R)} - x_i^{(B,t)}}, \\ \theta_{lk}^{(B,R)} &= g_l(x_k^{(R)}, y_k^{(R)}) = \tan^{-1} \frac{y_k^{(R)} - y_l^{(B,t)}}{x_k^{(R)} - x_l^{(B,t)}}.\end{aligned}\tag{6.3}$$

Using extended Kalman filter (EKF) or iterative linearization method [10], we can calculate the position of reflector k $(x_k^{(R)}, y_k^{(R)})$ from (6.3). Using the same method, we can calculate other shared reflectors' position, e.g., reflectors m , k , and 1 in Figure 6.1. The positions of these reflectors would be used for localizing TN j . We should mention that the reflector should be shared by at least two BNs in order to be localized.

Applying iterative linearization method to (6.3), the approximated localization error would be [28]

$$\Delta \mathbf{X}_k^{(R)} = (\mathbf{B}^T \mathbf{B})^{-1} \mathbf{B}^T \cdot \Delta \boldsymbol{\theta}. \quad (6.4)$$

In (6.4), $\Delta \mathbf{X}_k^{(R)}$ is the reflector k 's localization error and $\Delta \mathbf{X}_k^{(R)} = [\Delta x_k^{(R)}, \Delta y_k^{(R)}]^T$;

$\mathbf{B} = \begin{bmatrix} b_{x,i} & b_{y,i} \\ b_{x,l} & b_{y,l} \end{bmatrix}$ is the error transformation matrix, $b_{x,i} = \frac{\partial g_i(x_k^{(R)}, y_k^{(R)})}{\partial x_k^{(R)}}$, $b_{y,i} =$

$\frac{\partial g_i(x_k^{(R)}, y_k^{(R)})}{\partial y_k^{(R)}}$, $b_{x,l} = \frac{\partial g_l(x_k^{(R)}, y_k^{(R)})}{\partial x_k^{(R)}}$ and $b_{y,l} = \frac{\partial g_l(x_k^{(R)}, y_k^{(R)})}{\partial y_k^{(R)}}$; and, $\Delta \boldsymbol{\theta} = [\Delta \theta_{ik}^{(B,R)} \quad \Delta \theta_{lk}^{(B,R)}]^T$,

$\Delta \theta_{ik}^{(B,R)}$ ($\Delta \theta_{lk}^{(B,R)}$) is the measurement error of the DOA of reflector k with respect to BN i

(l). The corresponding reflector localization error covariance matrix is [28]

$$\text{cov}(\mathbf{X}_k^{(R)}) = (\mathbf{B}^T \mathbf{B})^{-1} \mathbf{B}^T \cdot \text{cov}(\Delta \boldsymbol{\theta}) \mathbf{B} (\mathbf{B}^T \mathbf{B})^{-1}. \quad (6.5)$$

Defining $\mathbf{E} \mathbf{R} = \text{cov}(\mathbf{X}_k^{(R)})$, the shared reflector's localization error variance on x and y axes and the error covariance would be

$$\sigma_{x_k^{(R)}}^2 = \mathbf{E} \mathbf{R}(1,1),$$

$$\sigma_{y_k^{(R)}}^2 = \mathbf{E} \mathbf{R}(2,2),$$

$$\text{cov}(\Delta x_k^{(R)} \Delta y_k^{(R)}) = \mathbf{E} \mathbf{R}(1,2). \quad (6.6)$$

6.3.2 Targe Node Localization

Assuming the BNs position is known, and the location of shared reflectors has been calculated, the distance between the shared reflector (e.g., reflector k) and BNs (e.g., BN i) corresponds to

$$\begin{aligned}
R_{ik}^{(B,R)} &= f_i(x_i^{(B,t)}, y_i^{(B,t)}, x_k^{(R)}, y_k^{(R)}) \\
&= \sqrt{(x_k^{(R)} - x_i^{(B,t)})^2 + (y_k^{(R)} - y_i^{(B,t)})^2}.
\end{aligned} \tag{6.7}$$

The approximated error of the distance between the shared reflector k and BN i is calculated using Taylor series' first order terms, which is

$$\Delta R_{ik}^{(B,R)} = \frac{x_k^{(R)} - x_i^{(B,t)}}{R_{ik}^{(B,R)}} \Delta x_k^{(R)} + \frac{y_k^{(R)} - y_i^{(B,t)}}{R_{ik}^{(B,R)}} \Delta y_k^{(R)}. \tag{6.8}$$

The corresponding error variance of $\Delta R_{ik}^{(B,R)}$ is

$$\begin{aligned}
\sigma_{R_{ik}^{(B,R)}}^2 &= \left(\frac{x_k^{(R,t)} - x_i^{(B,t)}}{R_{ik}^{(B,R,t)}} \right)^2 \sigma_{x_k^{(R)}}^2 + \left(\frac{y_k^{(R,t)} - y_i^{(B,t)}}{R_{ik}^{(B,R,t)}} \right)^2 \sigma_{y_k^{(R)}}^2 + \\
&\quad 2 \left(\frac{x_k^{(R,t)} - x_i^{(B,t)}}{R_{ik}^{(B,R,t)}} \cdot \frac{y_k^{(R,t)} - y_i^{(B,t)}}{R_{ik}^{(B,R,t)}} \right) \text{cov}(\Delta x_k^{(R)} \Delta y_k^{(R)}).
\end{aligned} \tag{6.9}$$

In (6.9), $\sigma_{x_k^{(R)}}^2$, $\sigma_{y_k^{(R)}}^2$ and $\text{cov}(\Delta x_k^{(R)} \Delta y_k^{(R)})$ are defined in (6.6). Considering (6.1), when a shared reflector k is localized and the distances between reflector k and the two BNs i and l are calculated, we achieve two estimations of the distance between the shared reflector k and the TN j , i.e., $R_{ikj}^{(B,R,T)} - R_{ik}^{(B,R)}$ and $R_{lkj}^{(B,R,T)} - R_{lk}^{(B,R)}$, and assuming the same error variances across the TN l and i , a better estimation is calculated that corresponds to

$$R_{kj}^{(R,T)} = \frac{(R_{ikj}^{(B,R,T)} - R_{ik}^{(B,R)}) + (R_{lkj}^{(B,R,T)} - R_{lk}^{(B,R)})}{2}. \tag{6.10}$$

The errors in $R_{ikj}^{(B,R,T)}$, $R_{lkj}^{(B,R,T)}$, $R_{ik}^{(B,R)}$ and $R_{lk}^{(B,R)}$ are assumed to be independent and identically distributed zero mean Gaussian random variables. In addition, the error variance of $R_{ikj}^{(B,R,T)}$ and $R_{lkj}^{(B,R,T)}$ is σ_R^2 and the error variance of $R_{ik}^{(B,R)}$ and $R_{lk}^{(B,R)}$ can be calculated using (6.9). Accordingly, the error variance of $R_{kj}^{(R,T)}$ corresponds to

$$\sigma_{R_{kj}^{(R,T)}}^2 = \frac{\left(2\sigma_R^2 + \sigma_{R_{ik}^{(B,R)}}^2 + \sigma_{R_{lk}^{(B,R)}}^2\right)}{4}. \quad (6.11)$$

If there are three or more shared reflectors for a TN, then we can obtain multiple distance estimations from the TN to these shared reflectors ($R_{1j}^{(R,T)}$, $R_{2j}^{(R,T)}$, \dots , $R_{Kj}^{(R,T)}$), K is the number of reflectors shared by TN j and K sets of BNs. In addition, we have localized these shared reflectors via DOA fusion. Therefore, TN can be localized at $(x_j^{(T)}, y_j^{(T)})$ via TOA (range) fusion. Assuming the TN is at $(x_j^{(T,t)}, y_j^{(T,t)})$, the shared reflectors' true positions are $(x_1^{(R,t)}, y_1^{(R,t)})$, $(x_2^{(R,t)}, y_2^{(R,t)})$, \dots , $(x_K^{(R,t)}, y_K^{(R,t)})$, and the true distances between the TN and shared reflectors are $R_{1j}^{(R,T,t)}$, $R_{2j}^{(R,T,t)}$, \dots , $R_{Kj}^{(R,T,t)}$, we have

$$\begin{aligned} R_{1j}^{(R,T,t)} &= f_1(x_j^{(T,t)}, y_j^{(T,t)}) = \sqrt{\left(x_1^{(R,t)} - x_j^{(T,t)}\right)^2 + \left(y_1^{(R,t)} - y_j^{(T,t)}\right)^2}, \\ R_{2j}^{(R,T,t)} &= f_2(x_j^{(T,t)}, y_j^{(T,t)}) = \sqrt{\left(x_2^{(R,t)} - x_j^{(T,t)}\right)^2 + \left(y_2^{(R,t)} - y_j^{(T,t)}\right)^2}, \\ &\vdots \\ R_{Kj}^{(R,T,t)} &= f_K(x_j^{(T,t)}, y_j^{(T,t)}) = \sqrt{\left(x_K^{(R,t)} - x_j^{(T,t)}\right)^2 + \left(y_K^{(R,t)} - y_j^{(T,t)}\right)^2}. \end{aligned} \quad (6.12)$$

Using shared reflectors' positions $[(x_1^{(R)}, y_1^{(R)})$, $(x_2^{(R)}, y_2^{(R)})$, \dots , $(x_K^{(R)}, y_K^{(R)})]$ calculated in

subsection 6.3.1 and the calculated distances between shared reflectors and the TN j ($R_{1j}^{(R,T)}, R_{2j}^{(R,T)}, \dots, R_{Kj}^{(R,T)}$) to take the places of the corresponding true values in (6.12) and solve it using EKF or iterative linearization method [10], we can calculate the TN position ($x_j^{(T)}, y_j^{(T)}$).

If we apply iterative linearization method to calculate TN j 's position, the localization error ($\Delta \mathbf{X}_j^{(T)} = [x_j^{(T,t)} \ y_j^{(T,t)}]^T$) is calculated as [10]

$$\Delta \mathbf{X}_j^{(T)} = (\mathbf{C}^T \mathbf{C})^{-1} \mathbf{C}^T \cdot \Delta \mathbf{R}_j^{(R,T)}. \quad (6.13)$$

In (6.13), $\Delta \mathbf{R}_j^{(R,T)} = [\Delta R_{1j}^{(R,T)} \ \Delta R_{2j}^{(R,T)} \ \dots \ \Delta R_{Kj}^{(R,T)}]^T$ and $\mathbf{C} = \begin{bmatrix} c_{x,1} & c_{y,1} \\ \vdots & \vdots \\ c_{x,K} & c_{y,K} \end{bmatrix}$. In

addition, $\Delta R_{kj}^{(R,T)}$, $1 \leq k \leq K$, is the error of the range between the shared reflector k and

TN j , whose variance is calculated in (6.11); in \mathbf{C} , $c_{x,k} = \frac{\partial f_k(x_j^{(T)}, y_j^{(T)})}{\partial x_j^{(T)}}$ and $c_{y,k} =$

$\frac{\partial f_k(x_j^{(T)}, y_j^{(T)})}{\partial y_j^{(T)}}$. The localization error covariance matrix corresponds to

$$\text{cov}(\Delta \mathbf{X}_j^{(T)}) = (\mathbf{C}^T \mathbf{C})^{-1} \mathbf{C}^T \cdot \text{cov}(\Delta \mathbf{R}_j^{(R,T)}) \cdot \mathbf{C}(\mathbf{C}^T \mathbf{C})^{-1}. \quad (6.14)$$

In (6.14), $\text{cov}(\Delta \mathbf{R}_j^{(R,T)}) = \text{diag}(\sigma_{R_{1j}^{(R,T)}}^2 \ \sigma_{R_{2j}^{(R,T)}}^2 \ \dots \ \sigma_{R_{Kj}^{(R,T)}}^2)$ assuming the calculated

distances between shared reflectors and the TN j are independent, i.e., $R_{1j}^{(R,T)}, R_{2j}^{(R,T)}, \dots,$

$R_{Kj}^{(R,T)}$ are independent.

6.3.3 NLOS Identification

In subsections 6.3.1 and 6.3.2, we applied multiple NLOS measurements coming from the shared reflectors achieved at multiple BNs to localize the shared reflectors and then localize the TN. However, when these TOA-DOA measurements are achieved at BNs, we do not know which measurements are associated to LOS channel and which measurements are associated to NLOS channel. In addition, we do not know which sets of measurements are associated to the same shared reflector. The NLOS identification between BNs and TN is discussed in this subsection, and the shared reflectors determination would be discussed in the next subsection 6.3.4.

When multiple (N) BNs localize a TN simultaneously, at each BN n ($1 \leq n \leq N$), we achieve K_n (the number of separable reflectors saw by BN n) sets of NLOS TOA-DOA measurements and 1 set of LOS TOA-DOA measurement, if LOS is available. The measurement set with the smallest TOA is selected at each BN n and marked as $(R_{nj}^{(B,T)}, \theta_{nj}^{(B,T)})$. Therefore, we achieve N sets of measurements, i.e., $(R_{1j}^{(B,T)}, \theta_{1j}^{(B,T)})$, \dots , $(R_{ij}^{(B,T)}, \theta_{ij}^{(B,T)})$, \dots , $(R_{Nj}^{(B,T)}, \theta_{Nj}^{(B,T)})$. For example, in Figure 6.4, $(R_{2j}^{(B,T)}, \theta_{2j}^{(B,T)})$, $(R_{3j}^{(B,T)}, \theta_{3j}^{(B,T)})$, $(R_{45j}^{(B,R,T)}, \theta_{45j}^{(B,R,T)})$, $(R_{imj}^{(B,R,T)}, \theta_{imj}^{(B,R,T)})$ and $(R_{lkj}^{(B,R,T)}, \theta_{lkj}^{(B,R,T)})$ would be selected and marked as $(R_{2j}^{(B,T)}, \theta_{2j}^{(B,T)})$, $(R_{3j}^{(B,T)}, \theta_{3j}^{(B,T)})$, $(R_{4j}^{(B,T)}, \theta_{4j}^{(B,T)})$, $(R_{ij}^{(B,T)}, \theta_{ij}^{(B,T)})$ and $(R_{lj}^{(B,T)}, \theta_{lj}^{(B,T)})$, respectively.

Using these N sets of measurements, we can achieve N estimations of the TN position

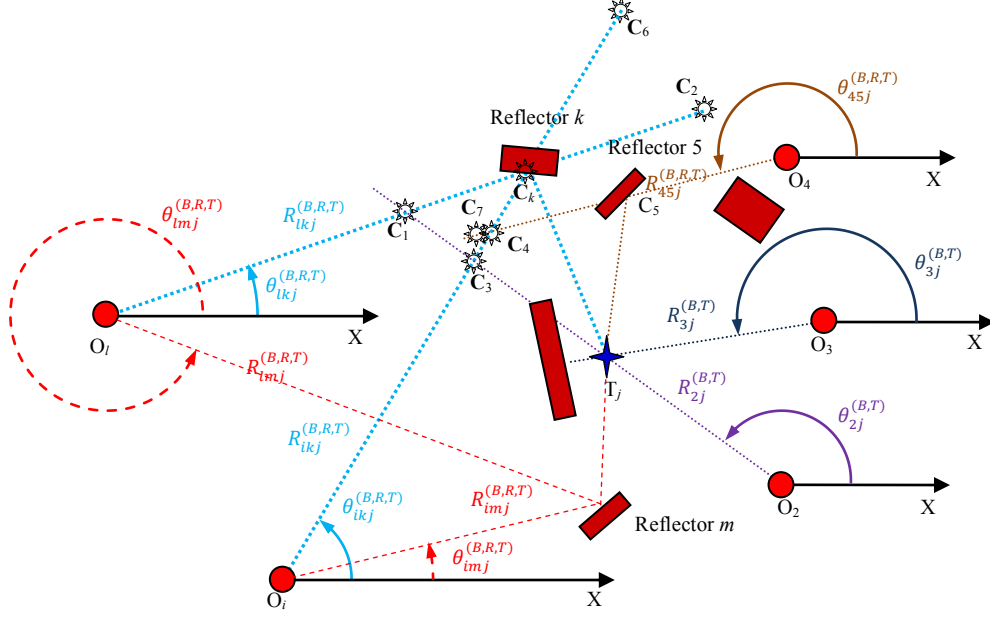


Figure 6.4: NLOS identification and shared reflector determination.

$$\hat{x}_{ij}^{(T)} = R_{ij}^{(B,T)} \cos\left(\theta_{ij}^{(B,T)}\right) + x_i^{(B,t)},$$

$$\hat{y}_{ij}^{(T)} = R_{ij}^{(B,T)} \sin\left(\theta_{ij}^{(B,T)}\right) + y_i^{(B,t)}, 1 \leq i \leq N. \quad (6.15)$$

The corresponding localization errors are assume to be zero mean Gaussian random variables and their variances are calculated as

$$\sigma_{\hat{x}_{ij}^{(T)}}^2 = \sigma_R^2 \cos^2\left(\theta_{ij}^{(B,T,t)}\right) + \sigma_\theta^2 \left(R_{ij}^{(B,T,t)}\right)^2 \sin^2\left(\theta_{ij}^{(B,T,t)}\right),$$

$$\sigma_{\hat{y}_{ij}^{(T)}}^2 = \sigma_R^2 \sin^2\left(\theta_{ij}^{(B,T,t)}\right) + \sigma_\theta^2 \left(R_{ij}^{(B,T,t)}\right)^2 \cos^2\left(\theta_{ij}^{(B,T,t)}\right). \quad (6.16)$$

We calculate the difference between two estimations coming from two BNs o and p , and

obtain

$$\begin{aligned}\Delta\hat{x}_{op}^{(T)} &= \hat{x}_{oj}^{(T)} - \hat{x}_{pj}^{(T)}, \\ \Delta\hat{y}_{op}^{(T)} &= \hat{y}_{oj}^{(T)} - \hat{y}_{pj}^{(T)}.\end{aligned}\tag{6.17}$$

If the two BNs o and p are in LOS of the TN j , (e.g., $o = 2, p = 3$, BNs 2 and 3 are both in LOS of the TN j in Figure 6.4), the two TN position estimations would be close to the true TN position. Mathematically, $\hat{x}_{oj}^{(T)} = x_j^{(T,t)} + \Delta\hat{x}_{oj}^{(T)}$, $\hat{y}_{oj}^{(T)} = y_j^{(T,t)} + \Delta\hat{y}_{oj}^{(T)}$, $\hat{x}_{pj}^{(T)} = x_j^{(T,t)} + \Delta\hat{x}_{pj}^{(T)}$ and $\hat{y}_{pj}^{(T)} = y_j^{(T,t)} + \Delta\hat{y}_{pj}^{(T)}$. Here, $(\Delta\hat{x}_{oj}^{(T)}, \Delta\hat{y}_{oj}^{(T)})$ and $(\Delta\hat{x}_{pj}^{(T)}, \Delta\hat{y}_{pj}^{(T)})$ are the TN j 's localization errors achieved by BNs o and p , respectively. Applying these four equations to (6.17), we have

$$\begin{aligned}\Delta\hat{x}_{op}^{(T)} &= \Delta\hat{x}_{oj}^{(T)} - \Delta\hat{x}_{pj}^{(T)}, \\ \Delta\hat{y}_{op}^{(T)} &= \Delta\hat{y}_{oj}^{(T)} - \Delta\hat{y}_{pj}^{(T)}.\end{aligned}\tag{6.18}$$

In (6.18), $(\Delta\hat{x}_{oj}^{(T)}, \Delta\hat{y}_{oj}^{(T)})$ and $(\Delta\hat{x}_{pj}^{(T)}, \Delta\hat{y}_{pj}^{(T)})$ are the TN localization errors, and assumed to be zero mean Gaussian random variables.

When one or none of the two selected BNs is in the LOS of the TN j , the TN j 's position estimation made by the NLOS BN would have a large error. All the three categories of examples are shown in Figure 6.4:

- 1) One BN (e.g., $o = 2$) is in the LOS of TN and estimates the TN close to point T_j ,

i.e., $\hat{x}_{oj}^{(T)} = x_j^{(T,t)} + \Delta\hat{x}_{oj}^{(T)}$, $\hat{y}_{oj}^{(T)} = y_j^{(T,t)} + \Delta\hat{y}_{oj}^{(T)}$; and, the other BN (e.g., $p = l$) is in the NLOS of TN and estimates the TN close to point C_2 , i.e., $\hat{x}_{pj}^{(T)} = x_{C_2}^{(T,t)} + \Delta\hat{x}_{pj}^{(T)}$ and $\hat{y}_{pj}^{(T)} = y_{C_2}^{(T,t)} + \Delta\hat{y}_{pj}^{(T)}$. There is a large distance between the points T_j and C_2 , i.e., $\sqrt{\left(x_j^{(T,t)} - x_{C_2}^{(T,t)}\right)^2 + \left(y_j^{(T,t)} - y_{C_2}^{(T,t)}\right)^2} \gg 0$.

2) The two BNs are both in the NLOS of TN and they share the same reflector. For example, $o = i$, $p = l$, BNs o and p share reflector k . BN o estimates the TN close to point C_6 , i.e., $\hat{x}_{oj}^{(T)} = x_{C_6}^{(T,t)} + \Delta\hat{x}_{oj}^{(T)}$, $\hat{y}_{oj}^{(T)} = y_{C_6}^{(T,t)} + \Delta\hat{y}_{oj}^{(T)}$; and BN p estimates the TN close to point C_2 , i.e., $\hat{x}_{pj}^{(T)} = x_{C_2}^{(T,t)} + \Delta\hat{x}_{pj}^{(T)}$ and $\hat{y}_{pj}^{(T)} = y_{C_2}^{(T,t)} + \Delta\hat{y}_{pj}^{(T)}$. Figure 6.4 shows that $\sqrt{\left(x_{C_6}^{(T,t)} - x_{C_2}^{(T,t)}\right)^2 + \left(y_{C_6}^{(T,t)} - y_{C_2}^{(T,t)}\right)^2} \gg 0$.

3) The two BNs are both in the NLOS of the TN and they do not share reflector. For example, $o = i$, $p = 4$, BNs o and p do not share any reflector. BN o estimates the TN close to point C_6 , i.e., $\hat{x}_{oj}^{(T)} = x_{C_6}^{(T,t)} + \Delta\hat{x}_{oj}^{(T)}$, $\hat{y}_{oj}^{(T)} = y_{C_6}^{(T,t)} + \Delta\hat{y}_{oj}^{(T)}$; and, BN p estimates the TN close to point C_7 , i.e., $\hat{x}_{pj}^{(T)} = x_{C_7}^{(T,t)} + \Delta\hat{x}_{pj}^{(T)}$, $\hat{y}_{pj}^{(T)} = y_{C_7}^{(T,t)} + \Delta\hat{y}_{pj}^{(T)}$. Figure 6.4 shows that $\sqrt{\left(x_{C_6}^{(T,t)} - x_{C_7}^{(T,t)}\right)^2 + \left(y_{C_6}^{(T,t)} - y_{C_7}^{(T,t)}\right)^2} \gg 0$.

In the above three scenarios, $(\Delta\hat{x}_{oj}^{(T)}, \Delta\hat{y}_{oj}^{(T)})$ and $(\Delta\hat{x}_{pj}^{(T)}, \Delta\hat{y}_{pj}^{(T)})$ are localization errors of the TN (e.g., $o = 2$) or the image of the target node due to reflectors (e.g., $p = l$), and

they are assumed to be zero mean Gaussian random variables. Therefore, when one or none of the two BNs is in the LOS of the TN j , in general, there is a large difference between the two TN location estimations. Considering (6.17) and the equations in the above three scenarios, we get

$$\begin{aligned}\Delta\hat{x}_{op}^{(T)} &= \Delta x_{NLOS} + \Delta\hat{x}_{oj}^{(T)} - \Delta\hat{x}_{pj}^{(T)}, \\ \Delta\hat{y}_{op}^{(T)} &= \Delta y_{NLOS} + \Delta\hat{y}_{oj}^{(T)} - \Delta\hat{y}_{pj}^{(T)}.\end{aligned}\tag{6.19}$$

In (6.19), $\sqrt{\Delta x_{NLOS}^2 + \Delta y_{NLOS}^2} \gg 0$ is the distance between the two estimations of the TN position achieved by BNs o and p . When one BN is in the LOS of the TN and one BN is in the NLOS of the TN, it is the distance between the true TN position and the image of the TN due to the reflector; and, when two BNs are both in the NLOS of the TN, it is the distance of the two images of the TN due to the reflector(s). Because $\sqrt{\Delta x_{NLOS}^2 + \Delta y_{NLOS}^2} \gg 0$; thus, one or both of Δx_{NLOS} and Δy_{NLOS} are not zero. In addition, Δx_{NLOS} and Δy_{NLOS} are determined by the geometrical distribution of the two BNs, the TN and the reflector(s).

Comparing (6.18) and (6.19), we obtain: (1) in LOS case (both selected BNs are in the LOS of the TN), the differences between the two estimations of the TN position ($\Delta\hat{x}_{op}^{(T)}$ and $\Delta\hat{y}_{op}^{(T)}$) are zero mean Gaussian random variables; and, (2) in NLOS case (one or none of the two selected BNs is in LOS of the TN), at least one of $\Delta\hat{x}_{op}^{(T)}$ and $\Delta\hat{y}_{op}^{(T)}$ is non zero mean Gaussian random variable. In addition, the variance of $\Delta\hat{x}_{op}^{(T)}$ ($\Delta\hat{y}_{op}^{(T)}$) can be

calculated using the summation of the variances of $\Delta\hat{x}_{oj}^{(T)}$ and $\Delta\hat{x}_{pj}^{(T)}$ ($\Delta\hat{y}_{oj}^{(T)}$ and $\Delta\hat{y}_{pj}^{(T)}$), assuming the two BNs localize the TN independently. Thus, the difference between the two estimations of the TN position can be applied to identify NLOS between two BNs and TN: If $|\Delta\hat{x}_{oj}^{(T)} - \Delta\hat{x}_{pj}^{(T)}| < \alpha \sqrt{\sigma_{\hat{x}_{oj}^{(T)}}^2 + \sigma_{\hat{x}_{pj}^{(T)}}^2}$ and $|\Delta\hat{y}_{oj}^{(T)} - \Delta\hat{y}_{pj}^{(T)}| < \alpha \sqrt{\sigma_{\hat{y}_{oj}^{(T)}}^2 + \sigma_{\hat{y}_{pj}^{(T)}}^2}$, the two selected BNs would be in the LOS of the TN; otherwise, only one or none of the two selected BNs is in the LOS of the TN. Here, $|\cdot|$ refers to the absolute value; α is a positive number determined by the tradeoff between false alarm (LOS is taken as NLOS) and miss-detection (NLOS is taken as LOS). Because $\Delta\hat{x}_{oj}^{(T)}$, $\Delta\hat{x}_{pj}^{(T)}$, $\Delta\hat{y}_{oj}^{(T)}$ and $\Delta\hat{y}_{pj}^{(T)}$ are assumed to be independent zero mean Gaussian random variables; thus, α can be theoretically calculated given a probability of false alarm. For example, if we make the probability of the false alarm equal to 0.3% [i.e., $P(NLOS/LOS) = 0.3\%$], according to the Gaussian distribution, α would be 3.

It should be noted that there is a special scenario, in which the two BNs do not share a reflector, but the position of the images of the TN due to the two reflectors are close to each other. In this case, NLOS scenario would be taken as LOS scenario. But this scenario takes place with small probability.

According to the above discussions, the limitation of this method is that it can only discriminate two scenarios: (a) two or more BNs are in the LOS of a TN; and, (b) one or no BN is in the LOS of a TN. When multiple NLOS BNs and a LOS BN localize a TN simultaneously, the proposed identification technique assumes NLOS and applies NLOS

localization method presented in subsections 6.3.1 and 6.3.2 to localize the TN. The simulations in subsection 6.4 show that the localization accuracy with one LOS BN is much better than that with multiple (e.g., four or five) shared reflectors. How to discriminate the two scenarios: there is only one LOS BN and there is no LOS BN, forms the future work of this chapter.

6.3.4 Shared Reflectors Determination

Sets of TOA-DOA measurements obtained through shared reflectors computed by multiple BNs are applied to the proposed NLOS TN localization method. In this subsection, we present how to find the shared reflectors based on NLOS identification.

In NLOS scenarios, each BN i may compute K_i (the number of separable reflectors observed by BN i) sets of NLOS TOA-DOA measurements. The DOA resolution and reflector distribution with respect to the BN and TN determine the number of separable reflectors. From the K_i sets of measurements, we select one set of TOA-DOA measurement, e.g., $(R_{ikj}^{(B,R,T)}, \theta_{ikj}^{(B,R,T)})$, k is the index of reflector; and, from the K_l sets of measurements achieved at another BN l that localizes the same TN j , we select $(R_{lmj}^{(B,R,T)}, \theta_{lmj}^{(B,R,T)})$, m is the index of reflector. Then, we fuse the two selected DOA measurements $\theta_{ikj}^{(B,R,T)}$ and $\theta_{lmj}^{(B,R,T)}$ to find a point $(\hat{x}_{km}^{(R)}, \hat{y}_{km}^{(R)})$, and compute the distances $(\hat{R}_i^{(B,R)}$ and $\hat{R}_l^{(B,R)})$ between the calculated point $(\hat{x}_{km}^{(R)}, \hat{y}_{km}^{(R)})$ and the two selected BNs position. Then, we calculate the differences between the calculated distances $(\hat{R}_i^{(B,R)}$ and

$\hat{R}_l^{(B,R)}$) and the selected range measurements ($R_{ikj}^{(B,R,T)}$ and $R_{lmj}^{(B,R,T)}$), and achieve

$$\begin{aligned} R_i^{(R,T)} &= R_{ikj}^{(B,R,T)} - \hat{R}_i^{(B,R)}, \\ R_l^{(R,T)} &= R_{lmj}^{(B,R,T)} - \hat{R}_l^{(B,R)}. \end{aligned} \quad (6.20)$$

In (6.20), the variances of $\hat{R}_i^{(B,R)}$ and $\hat{R}_l^{(B,R)}$ can be calculated using (6.9), and the variance of $R_{ikj}^{(B,R,T)}$ and $R_{lmj}^{(B,R,T)}$ is σ_R^2 .

If the two selected sets of measurements are coming from the same reflector (e.g., both $\theta_{ikj}^{(B,R,T)}$ and $\theta_{lmj}^{(B,R,T)}$ come from reflector k in Figure 6.4), i.e., $m = k$, the point $(\hat{x}_{km}^{(R)}, \hat{y}_{km}^{(R)})$ obtained by DOA fusion would be the estimation of the shared reflector's position. The range differences ($R_i^{(R,T)}$ and $R_l^{(R,T)}$) computed in (6.20) would be two estimations of the distance between the shared reflector and TN j . Assuming the shared reflector's localization error is zero mean, the mean of the two estimations ($R_i^{(R,T)}$ and $R_l^{(R,T)}$) would be the distance between the shared reflector and TN j , and we obtain

$$E(R_i^{(R,T)}) = E(R_l^{(R,T)}) = C_k T_j > 0. \quad (6.21)$$

In (6.21), $C_k T_j$ is the true distance between reflector k and TN j as shown in Figure 6.4.

But if the two selected measurement sets come from different reflectors, i.e., $m \neq k$, (e.g., $\theta_{ikj}^{(B,R,T)}$ comes from reflector k and $\theta_{lmj}^{(B,R,T)}$ comes from reflector m in Figure 6.4),

The range differences ($R_i^{(R,T)}$ and $R_l^{(R,T)}$) achieved in (6.20) would have different mean, i.e.,

$$E(R_i^{(R,T)}) \neq E(R_l^{(R,T)}). \quad (6.22)$$

In general, there is an obvious difference between $E(R_i^{(R,T)})$ and $E(R_l^{(R,T)})$. But there is a special scenario for non-shared reflectors, in which the two selected measurement sets come from different reflectors, but the distances from the calculated point ($\hat{x}_{km}^{(R)}, \hat{y}_{km}^{(R)}$) to BNs i and l (i.e., $\hat{R}_i^{(B,R)}$ and $\hat{R}_l^{(B,R)}$) satisfy

$$R_{ikj}^{(B,R,T)} - \hat{R}_i^{(B,R)} = R_{lmj}^{(B,R,T)} - \hat{R}_l^{(B,R)}. \quad (6.23)$$

In this case, we may mistakenly take the calculated point ($\hat{x}_{km}^{(R)}, \hat{y}_{km}^{(R)}$) as the shared reflector's position. But this scenario takes place with a small probability.

A special scenario for shared reflector should be noted [40], in which, the included angle between the two lines connecting the shared reflector and BNs i and l is small (e.g., less than a threshold θ_{th}), in other words, the selected DOAs satisfy one of the following three in-equations

$$|\theta_{ikj}^{(B,R,T)} - \theta_{lmj}^{(B,R,T)}| < \theta_{th},$$

$$\pi - \theta_{th} < |\theta_{ikj}^{(B,R,T)} - \theta_{lmj}^{(B,R,T)}| < \pi + \theta_{th},$$

$$2\pi - \theta_{th} < \left| \theta_{ikj}^{(B,R,T)} - \theta_{lmj}^{(B,R,T)} \right|. \quad (6.24)$$

In this case, the localization error generated by DOA fusion is large and the two selected measurement sets are considered not sharing a reflector. The value of θ_{th} is determined by the tradeoff between localization error of the shared reflectors and the probability of localizing TN. As the value of θ_{th} increases, the shared reflectors localization accuracy would be enhanced, but the probability of achieving three or more qualified shared reflectors decreases, because the number of shared reflectors is limited in a real application.

Summarizing the above analysis, the following shared reflectors determination algorithm is deductable:

- 1) Select two sets of TOA-DOA measurements from the NLOS measurements of two different BNs i and l , and $(R_{ikj}^{(B,R,T)}, \theta_{ikj}^{(B,R,T)})$ and $(R_{lmj}^{(B,R,T)}, \theta_{lmj}^{(B,R,T)})$ are achieved;
- 2) If the selected DOAs do not satisfy any in-equation in (6.24), go to Step 3; otherwise, select a new pair of NLOS measurement sets achieved by different BNs and return to Step 2;
- 3) Fuse $\theta_{ikj}^{(B,R,T)}$ and $\theta_{lmj}^{(B,R,T)}$ to find a point $(\hat{x}_{km}^{(R)}, \hat{y}_{km}^{(R)})$ and calculate the corresponding localization error variances $(\sigma_{\hat{x}_{km}^{(R)}}^2, \sigma_{\hat{y}_{km}^{(R)}}^2)$;

- 4) Calculate the distances ($\hat{R}_i^{(B,R)}$ and $\hat{R}_l^{(B,R)}$) between the point $(\hat{x}_{km}^{(R)}, \hat{y}_{km}^{(R)})$ and the positions of BNs i and l using (6.7) and the corresponding ranging variances ($\sigma_{\hat{R}_i^{(B,R)}}^2$ and $\sigma_{\hat{R}_l^{(B,R)}}^2$) using (6.9);
- 5) If $R_{ikj}^{(B,R,T)} < \hat{R}_i^{(B,R)}$ or $R_{lmj}^{(B,R,T)} < \hat{R}_l^{(B,R)}$ (based on the in-equation part of (6.21)), select a new pair of NLOS measurement sets collected by different BNs and go to Step 2; otherwise, go to Step 6;
- 6) If $\left| \left(R_{ikj}^{(B,R,T)} - \hat{R}_i^{(B,R)} \right) - \left(R_{lmj}^{(B,R,T)} - \hat{R}_l^{(B,R)} \right) \right| < \alpha \sqrt{2\sigma_R^2 + \sigma_{\hat{R}_i^{(B,R)}}^2 + \sigma_{\hat{R}_l^{(B,R)}}^2}$ (based on the equation part of (6.21) and (6.22)), a shared reflector is found and it is localized at $(\hat{x}_{km}^{(R)}, \hat{y}_{km}^{(R)})$; otherwise, select a new pair of NLOS measurement sets attained by different BNs and repeat steps 2 to 6.

In Step 6, α is a positive number determined by the tradeoff between false alarm and miss detection. The ranging errors in $R_{ikj}^{(B,R,T)}$ and $R_{lmj}^{(B,R,T)}$ are assumed to be independent and identically distributed (i.i.d.) zero mean Gaussian random variables with variance of σ_R^2 . The errors in $\hat{R}_i^{(B,R)}$ and $\hat{R}_l^{(B,R)}$ are assumed to be independent zero mean Gaussian random variables (see (6.8)) with variances calculated using (6.9). In addition, the errors in $R_{ikj}^{(B,R,T)}$, $R_{lmj}^{(B,R,T)}$, $\hat{R}_i^{(B,R)}$ and $\hat{R}_l^{(B,R)}$ are assumed to be independent. Hence, the value of α can be theoretically calculated given a probability of miss detection [$P(\text{non-shared reflector/shared reflector})$]. For example, if we set $P(\text{non-shared reflector/shared reflector}) = 0.3\%$, according to the Gaussian distribution, α would be equal to 3.

It should be noted that each NLOS BN i computes K_i sets of NLOS TOA-DOA measurements. For each combination of the two sets of NLOS measurements from different BNs, the above determination processes would be implemented once. Therefore, in the worst case scenario, the above determination processes would be repeated $\sum_{1 \leq i, l \leq N_j, i \neq l} K_i K_l$ (the number of combinations including two sets of NLOS measurements from different BNs) times. Here, N_j is the number of BNs that localize the TN j simultaneously; K_i (K_l) is the number of NLOS measurement sets achieved by BN i (l).

For example, if we have four BNs 1, 2, 3 and 4, and they find 2, 3, 4 and 5 sets of NLOS measurements, respectively, (i.e., $K_1 = 2$, $K_2 = 3$, $K_3 = 4$ and $K_4 = 5$), and there are only two BNs sharing a reflector. In the worst case, the shared reflector would be determined after $K_1K_2 + K_2K_3 + K_3K_4 + K_1K_3 + K_1K_4 + K_2K_4 = 71$ repetitions of the above determination process.

6.4 Simulations

Simulations are conducted to evaluate the performance of the proposed NLOS identification and shared reflectors determination in terms of false alarm and miss detection, and the NLOS TN localization accuracy in terms of localization error CDF. Simulation assumptions include: (1) 10,000 sets of positions of BNs, TN and reflectors with random geometrical distribution are generated to calculate the probability of false alarm and miss-detection, and the CDF of the TNs localization error; (2) BNs position is

computed without error; (3) range estimation error standard deviation is 1m, and angle estimation error standard deviation is 1° or 2° ; (4) all nodes are uniformly distributed in an area with corners $(-d, -d)$, $(-d, d)$, (d, d) and $(d, -d)$, $d = 100\sigma_R$ for Figures 6.5 and 6.7, and $d = 50\sigma_R$ for Figure 6.6; (5) In the shared reflectors determination process, we set $\theta_{th} = 18^\circ$ to compare the performance of the proposed method to that of the NLOS localization method presented in [40] (we call it *crossing method*); and, (6) miss-detection occurs when NLOS is mistakenly categorized as LOS (shared reflector is taken as non-shared reflector), and false alarm occurs when LOS is mistakenly categorized as NLOS (non-shared reflector is taken as shared reflector).

Figure 6.5 shows the probability of the miss-detection and false alarm of the proposed NLOS identification and shared reflectors determination with respect to parameter α (x axis) and DOA estimation error standard deviation σ_θ . In Figure 6.5, we observe that the probability of the miss detection of NLOS identification (NLOS \rightarrow LOS) and the false alarm of shared reflector determination (non-shared \rightarrow shared reflector) is much higher than the theoretical value (0.3%) when $\alpha = 3$. The reason is that we assume BNs, TNs and reflectors are uniformly distributed in the area, and their size is not considered, BNs and TNs may be closely located, and reflectors may be located close to the line connecting BN and TN or close to BN or TN. In these cases, the NLOS may be considered as LOS and non-shared reflectors may be considered as shared reflectors. But these scenarios do not occur in real applications for the size of obstructions. In addition, when the included angle between the two lines connecting the shared reflector and BNs i and l

is smaller than the threshold θ_{th} , the shared reflector is considered as non-shared reflector. The probability of the false alarm of NLOS identification (LOS \rightarrow NLOS) and the miss detection of shared reflector determination (shared \rightarrow non-shared reflector) does not change considerable as the DOA error standard deviation, σ_θ , increases from 1° to 2° . However, the probability of the miss detection of NLOS identification (NLOS \rightarrow LOS) and the false alarm of shared reflector determination (non-shared \rightarrow shared reflector) increases as σ_θ increases from 1° to 2° . The reason is that when σ_θ increases, the localization error increases, and therefore the threshold for NLOS identification

$(\alpha \sqrt{\sigma_{\hat{x}_{oj}}^2 + \sigma_{\hat{x}_{pj}}^2})$ and the threshold for shared reflectors determination

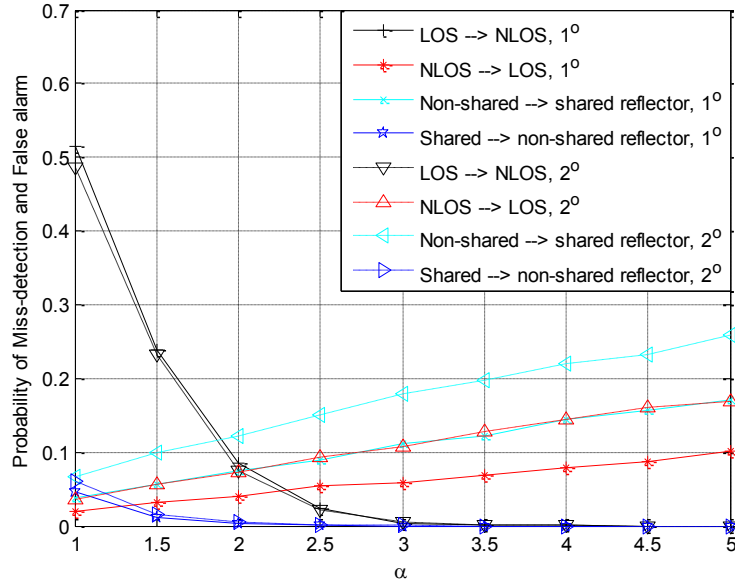


Figure 6.5: Miss-detection and false alarm for NLOS identification and shared reflectors

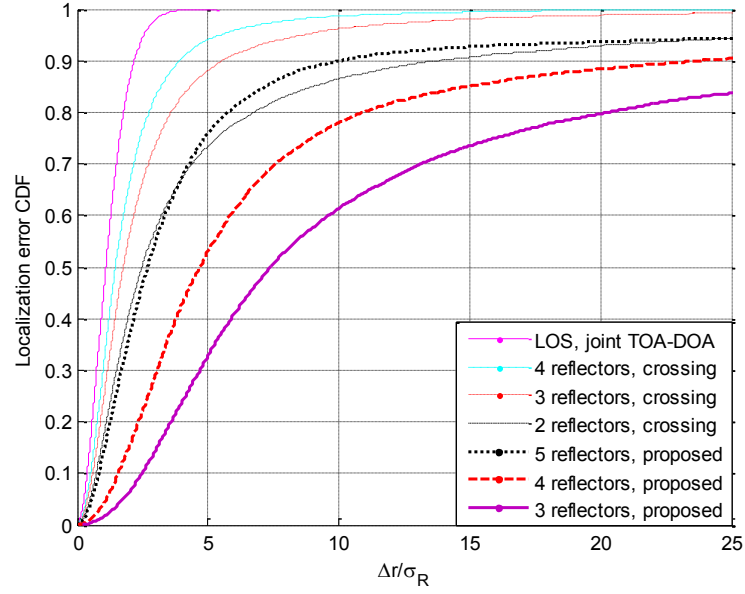
determination with $d = 100\sigma_R$, $\sigma_\theta = 1^\circ$ and $\sigma_\theta = 2^\circ$.

$(\alpha \sqrt{2\sigma_R^2 + \sigma_{\hat{R}_i^{(B,R)}}^2 + \sigma_{\hat{R}_i^{(B,R)}}^2})$ increases. Thus, more NLOS is taken as LOS, and more non-shared reflectors are taken as shared reflectors. In real applications, α and θ_{th} should be carefully selected based on the consideration mainly on the miss detection of NLOS identification and the false alarm of shared reflectors determination, because the false alarm of NLOS identification and the miss detection of shared reflectors determination are relative low and not affected by the DOA estimation error too much as shown in Figure 6.5.

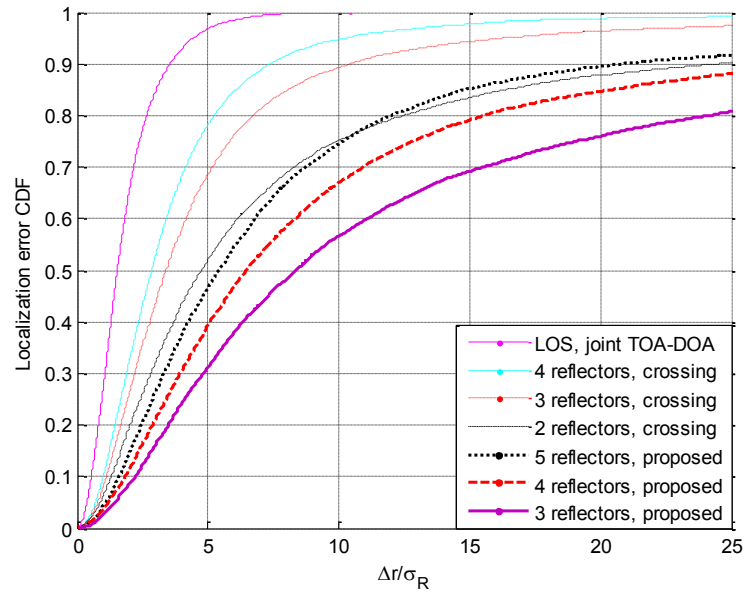
Figures 6.6 and 6.7 represent the CDF of the TN localization circular error (the distance between the estimated and true TNs position) of the proposed NLOS localization method with 3, 4 and 5 shared reflectors. The results are compared with the crossing NLOS localization method presented in [40] with 2, 3, and 4 reflectors. The comparison results confirm that the localization accuracy of the crossing method is better than that of the proposed method with the same number of reflectors. The performance of the proposed method with 5 shared reflectors is comparable to that of the crossing method with 2 reflectors (the two black curves in Figures 6.6 and 6.7). But one important point should be noted, in the crossing method, all nodes need to be equipped with antenna arrays. Antenna array is expensive and costs more power than Omni directional antenna system. It is not implementable in many applications, in which cost and power consumption are critical and the number of TNs is large.

The performance of the proposed NLOS localization technique is acceptable, especially

in the case that the network coverage area is not large, the DOA estimation error is small and there are enough shared reflectors. For example, when $d = 50\sigma_R$, with 4 shared



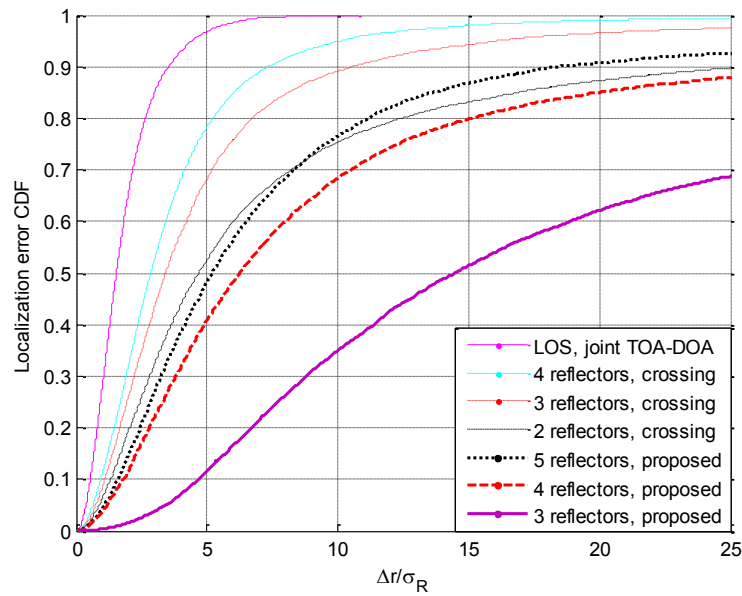
(a)



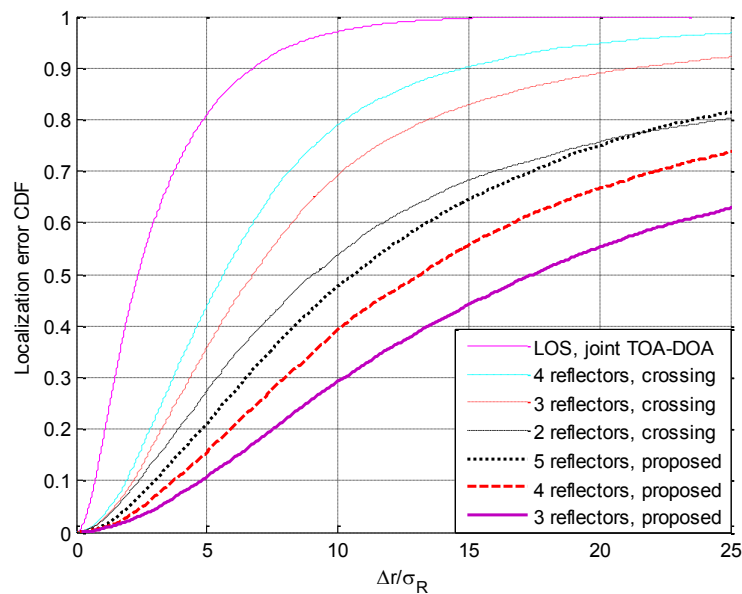
(b)

Figure 6.6: Target node localization error CDF, $d = 50\sigma_R$, (a) $\sigma_\theta = 1^\circ$, (b) $\sigma_\theta = 2^\circ$.

reflectors, $P(\Delta r < 5\sigma_R) = 0.53$, and with 5 shared reflectors, $P(\Delta r < 5\sigma_R) = 0.76$. The reason is that the shared reflectors' localization error via DOA fusion is transformed to



(a)



(b)

Figure 6.7: Target node localization error CDF, $d = 100\sigma_R$, (a) $\sigma_\theta = 1^\circ$, (b) $\sigma_\theta = 2^\circ$.

the TN localization error, and DOA fusion error increases as the the network coverage area and DOA estimation error increase. Comparing the simulation results in Figures 6.6 and 6.7 also confirms that as the DOA estimation error increases the impact of adding more reflectors on the performance decreases. This result is due to the fact that higher DOA estimation error reduces the capability of the BN to resolve one reflector from the other. It should be noted that in many DOA estimation techniques, DOA performance decreases as the number of reflection increases. Thus, it is anticipated that while higher number of reflectors improve the performance of this technique; however, the reduced performance of DOA estimation technique may inversely impact the performance of the proposed technique.

6.5 Conclusions

In this chapter, we presented an Omni directional TN NLOS identification and localization scheme. In this scheme, multiple BNs cooperate to identify NLOS between BNs and TN, and then in NLOS case, NLOS measurements are directly used to localize the TN. We also presented a shared reflector determination and localization method to support the NLOS identification and NLOS TN localization. The equations for NLOS identification, shared reflector determination and localization, and NLOS TN localization were derived. Simulations were conducted to verify the efficiency of the proposed NLOS localization approach. Simulations depict that the probability of LOS being taken as NLOS and shared reflector being taken as non-shared reflector is low with a reasonable threshold, while the probability of NLOS being taken as LOS and non-shared reflector

being taken as shared reflector is slightly high due to the simulation setup (the size of obstacles is not considered); the NLOS TN localization accuracy increases as the DOA estimation error and/or the system coverage area decreases, and the number of shared reflectors increases, it is acceptable if the system coverage area is not too large, the DOA estimation error is small and there are enough shared reflectors.

Chapter 7

Conclusions and Open Problems

This dissertation investigates techniques of improving the accuracy and the reliability of cooperative node localization: localized (target) nodes cooperate with localizing (base) nodes that are equipped with antenna arrays to allow single node localization via DOA and TOA estimation. Thus, essentially, each node is capable of independently localizing other cooperating nodes that are located in its coverage area. The proposed system does not depend on GPS: it works in the GPS-denied environments, and when the GPS is jittered.

The proposed localization is periodic, i.e., DOA and TOA estimations are updated periodically. Therefore, multiple observations across each base node might be applied to a filter such as Kalman filter to improve the localization performance. In addition, when multiple localizing nodes are available, they can fuse TOA-DOA estimations to improve the localization accuracy. Moreover, NLOS identification, mitigation and localization techniques are implemented to improve the localization reliability. Techniques applicable to single node and techniques that need the availability of multiple nodes are developed.

Accordingly, first, we propose a semi-distributed multi-node TOA-DOA fusion localization technique, which is applicable to MANETs, performs in LOS scenario, and achieves high localization accuracy and low computational complexity. Then, we

evaluate its performance in terms of localization CEP, and compare it with two localization techniques, GPS-aided TOA fusion and GPS-aided DOA fusion, which are applicable to MANETs, as well. Next, we integrate KF and multi-node TOA-DOA fusion to further improve its accuracy, and compare its accuracy and complexity with the EKF when it is applied to multiple TOA-DOA measurements.

In wireless channels such as urban or indoor areas, LOS channel may not be available. NLOS channel leads to unreliable localization. Hence, we propose a method that allows a single node equipped with antenna arrays to independently identify the availability of LOS and accordingly the reliability of localization. The proposed method is based on the phase difference variance of the signals received by two antenna elements in an antenna array.

To further improve NLOS identification performance, we propose a multi-node NLOS identification and localization scheme. In a multi-path wireless environment, the proposed technique allows shared reflectors determination and NLOS target localization as well.

7.1 Conclusions

Chapter 2 proposes a semi-distributed localization method based on multi-node TOA-DOA fusion. The method can independently localize target nodes (TN) without known position of base nodes (BN) or without incorporating other localization systems. Thus, it is suitable for MANETs. In this technique, a node should be optimally selected as the

reference node. The selection procedure impacts the positioning accuracy. We proposed a sub-optimal reference node selection method to minimize the computational complexity and maintain reasonable localization accuracy. Simulations confirm that: (1) compared to optimal reference-node selection, using the sub-optimal reference-node selection method, less than 1.6% extra localization error is introduced; (2) the localization method leads to higher positioning accuracy with higher number of BNs; (3) the positioning error increases fast as the MANET radius increases; thus, it is suitable for moderate scale MANET; (4) the TOA-only method positioning error would not change considerably if the MANET radius is larger than some value (e.g., $160\sigma_R$), and it is suitable for large scale MANET; (5) the positioning error of the proposed method increases as the TOA estimation error increases.

Chapter 3 evaluates the localization accuracy of the above semi-distributed multi-node TOA-DOA fusion localization method in terms of TN localization CEP, and compares it with that of GPS-aided TOA fusion and GPS-aided TOA fusion, which are applicable to MANETs when GPS service is available. It also evaluates the probability of TNs being localized in a MANET with different coverage radius. Simulation results confirm that the semi-distributed multi-node TOA-DOA fusion localization technique is not suitable for MANETs with radius larger than half of BN coverage radius in terms of the probability of TNs being localized compared with GPS-aided TOA fusion and GPS-aided DOA fusion. When MANET coverage radius is smaller than or equal to half of BN's coverage radius, the semi-distributed multi-node TOA-DOA fusion localization technique leads to

a better performance; thus, it is suitable for moderate scale MANETs. GPS-aided TOA fusion localization technique leads to a better performance in large scale MANETs. In addition, GPS-aided DOA fusion performs poorer than semi-distributed multi-node TOA-DOA fusion and GPS-aided TOA fusion.

Chapter 4 integrates KF with multi-node TOA-DOA fusion to further improve the TN localization accuracy. In addition, the integration of KF and multi-node TOA-DOA fusion is compared to a traditional localization method, which applies EKF to multiple TOA-DOA measurements. Results confirm that the localization accuracy of the integration of KF and multi-node TOA-DOA fusion is slightly lower than that of EKF, but the KF is stable (no divergence takes place) compared to EKF (EKF may diverge in some scenarios). In addition, the chapter shows that the computational complexity of the integration of KF and multi-node TOA-DOA fusion is much lower than EKF. This makes the proposed KF-Fusion integration a good candidate for multiple nodes localization in ad-hoc networks.

Chapter 5 proposes a LOS and NLOS separation technique based on the phase difference variance of the signals received by a co-installed synchronized bi-receiver system. The proposed system is simply implantable when an antenna array is available at the receiver. In this chapter, the PDF of the received signal's phase difference generated by the NLOS component is derived and verified via simulation. The phase difference is mapped into wireless channel's K-factor, and used to identify the availability of LOS or NLOS between the BN and the source TN. It is shown that the LOS and NLOS

separation method has small latency, because the method performs with small number of samples. In addition, because only phase information is used in the separation process, the method can be applied in narrowband or wideband systems. The proposed technique can identify the unavailability of LOS between the BN and the source TN with some probability that is called probability-of-detection, i.e., $P(NLOS/NLOS)$. This probability is a function of channel dispersion. As channel dispersion increases, the probability-of-detecting NLOS increases. When there is no LOS between the BN and the source TN, but there is a strong reflected signal, the proposed LOS and NLOS separation method would mistakenly take the NLOS channel as LOS channel. Thus, while *single node* NLOS identification is required when only one BN localizes a TN, its performance is affected by wireless channel.

Chapter 6 proposes a *multi-node* NLOS identification and NLOS Omni directional TN localization scheme. In addition, the proposed scheme allows shared reflectors determination and localization. In this scheme, multiple BNs cooperate to identify the NLOS between multiple BNs and a TN. In NLOS cases, if three or more reflectors are shared by the TN and a number of BNs, the shared reflectors are localized via DOA fusion, and then the TN is localized by TOA fusion based on the localization of shared reflectors' localization. The equations for NLOS identification, shared reflectors determination and localization, and NLOS TN localization are derived. Simulations depict that the probability of LOS being taken as NLOS and shared reflector being taken as non-shared reflector is low, while the probability of NLOS being taken as LOS and

non-shared reflector being taken as shared reflector is slightly high. The NLOS TN localization accuracy increases as the DOA estimation error and/or the system coverage area decreases, and the number of shared reflectors increases. The TN localization error is acceptable if the system coverage area is not too large, the DOA estimation error is small and there are enough shared reflectors.

7.2 Open Problems

This dissertation proposes node localization techniques based on multi-node TOA-DOA fusion and addresses some challenging open problems. However, there are still many relevant open problems that need investigation. In the following subsections, we detail these open problems.

7.2.1 Base Node Set Selection in the Fusion Process

In a real MANET application, a BN may not directly be localized by a reference node: it might be in multi-hop of the reference node. Large localization errors would be involved in the estimation due to multi-hop localization. For example, in Fig. 7.1, the error of the target node position in the main coordinate estimated by BN 1 (one-hop) is smaller than the one achieved in the estimation via BN 3 (two-hop), and smaller than the one achieved in the estimation via BN 4 (three-hop). When one more set of TOA-DOA measurement is involved in a fusion, the fusion performance would be enhanced; but at the same time, the computational complexity increases.

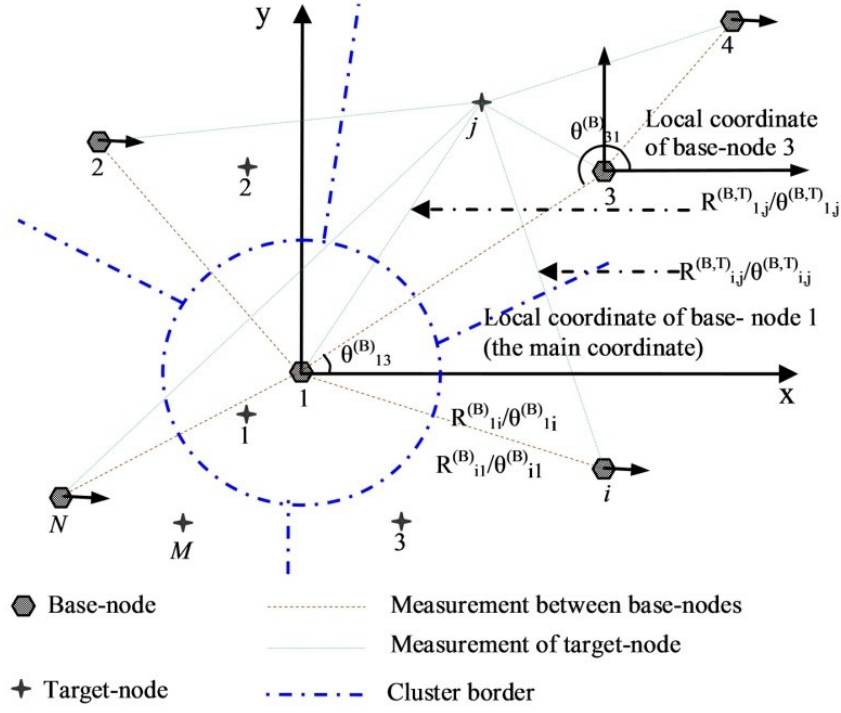


Figure 7.1: Base node selection in the fusion process.

If the newly involved TOA-DOA measurement set is coming from a multi-hop (three or more hops) BN (e.g., BN 4 in Figure 7.1) and other measurement sets are coming from one or two-hop BN's, the localization performance might not be highly improved, but the computational complexity may unlimitedly increased.

Hence, in the fusion process, to maintain a tradeoff between fusion complexity and localization accuracy, we should investigate which set of measurement should be used and which set of measurement should be discarded. In other words, a BN selection scheme is needed, especially when one BN is in charge of localizing a number of target nodes, computational complexity is critical.

7.2.2 Tradeoff between Multi-node TOA-DOA Fusion and TOA-only Fusion

The simulation in Figure 2.5 (Chapter 2) depicts that the localization error of TOA method [43] does not highly change as the MANET coverage radius increases, but the localization error of the semi-distributed multi-node TOA-DOA fusion increases with the MANETs' radius. In the proposed semi-distributed multi-node TOA-DOA fusion, each BN has the capability of TOA estimation; hence, TOA only method can be implemented in the proposed system and the tradeoff between the semi-distributed multi-node TOA-DOA fusion and TOA only method should be studied. Here, a threshold for BN's DOA estimation error and MANETs coverage radius can be found. When the DOA estimation error and/or the MANETs coverage radius are larger than the threshold, higher localization accuracy can be achieved using TOA only method; however, when both the DOA estimation error and MANETs coverage radius are smaller than the threshold, higher localization accuracy can be achieved using semi-distributed multi-node TOA-DOA fusion. This study should take into account the complexity of the DOA estimation on one hand and the bandwidth required by TOA on the other hand.

7.2.3 Localization via Intermediate Target Node

In chapters 2 and 6, we assumed BN's can localize each other or their position is given. In a MANET, BNs and TNs are both mobiles. Accordingly, the scenario that two BNs (e.g., BN's i and l) cannot localize each other but they can communicate via other node (e.g., a TN) and localize the same TN (e.g., TN j) simultaneously may take place. An example is shown in Figure 7.2. In Figure 7.2, BNs i and l cannot localize each other, BN

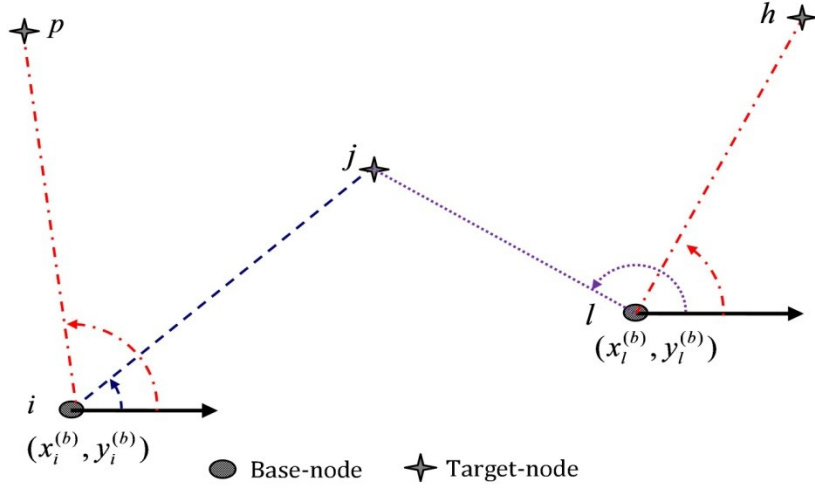


Figure 7.2: Localization through an intermediate TN.

i can localize TNs j and p , BN l can localize TNs j and h , and BNs i and l can communicate with each other via TN j . Thus, both BNs i and l localize TN j . In BN i 's local coordinate, TN j 's position is $(x_{i,j}^{(B,T)}, y_{i,j}^{(B,T)})$. In BN l 's local coordinate, TN j 's position is $(x_{l,j}^{(B,T)}, y_{l,j}^{(B,T)})$. Then considering the relative position of TN j , BNs i and l , in BN i 's local coordinate, BN l 's position is $(x_{l,j}^{(B,T)} - x_{i,j}^{(B,T)}, y_{l,j}^{(B,T)} - y_{i,j}^{(B,T)})$; and, in BN l 's local coordinate, BN i 's position is $(x_{i,j}^{(B,T)} - x_{l,j}^{(B,T)}, y_{i,j}^{(B,T)} - y_{l,j}^{(B,T)})$. Thus, in the following case: (1) a TN (e.g., TN h in Figure 7.2) is directly localized by a BN (e.g., BN l) but not directly localized by another BN (e.g., BN i), (2) these two BNs localize a intermediate TN (e.g., TN j) simultaneously and the two BNs can communicate with each other, the position of the TN (i.e., TN h) would be able to be transformed to another BN's (i.e., BN i 's) local coordinate. In other words, a BN can localize a TN

that is not in its coverage area with the help of a BN and an intermediate TN, if two BNs can communicate with each other and localize the intermediate TN simultaneously. Hence, an intermediate TN can increase the probability that a TN is localized by multiple BNs, and therefore the accuracy of TNs localization increases.

7.2.4 Monitoring and Avoiding the Divergence of EKF

The analysis and simulation in Figure 4.3 (Chapter 4) show that in some scenarios, the EKF would diverge and considerable localization error is generated. The simulation (Figure 4.4) also shows that the localization accuracy of EKF is better than the

integration of KF and multi-node TOA-DOA fusion in the case that EKF converges and there are multiple BNs involved in the localization process. Hence, when localization accuracy is critical, if the divergence of EKF can be avoided, we can achieve better localization accuracy using EKF. Thus, Monitoring and avoiding the divergence of EKF should be studied.

7.2.5 Finding LOS BN when Multiple NLOS BNs and One LOS BN Localize a TN Simultaneously

The scenarios a TN is localized by multiple BN's can be divided into three categories:

- (a) There are two or more LOS BN's;
- (b) There is no LOS BN;
- (c) There is one LOS BN as shown in Figure 7.3.

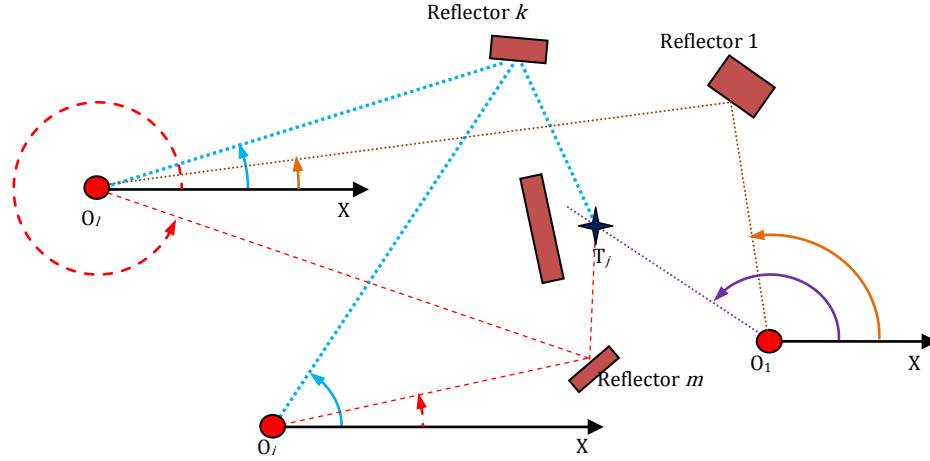


Figure 7.3: Determine the LOS BN in multiple NLOS BN's plus one LOS BN.

In Chapter 5, we proposed a method to discriminate LOS and NLOS channel between a BN and a TN, and in Chapter 6, we proposed a method to discriminate category (a) and categories (b) and (c). But we do not have a method to separate categories (b) and (c), and we considered both of them as NLOS scenarios and use NLOS localization method to localize TN. Simulations conducted in Chapter 6 (Figures 6.6 and 6.7) show that localization performance with one LOS BN is better than the one with multiple NLOS BNs. Hence, in a group of BNs localizing a target node, if only LOS BN is available, better performance would be achievable. The methods proposed in chapters 5 and 6 can be merged to find the LOS BN when multiple NLOS BNs and one LOS BN localize a TN simultaneously.

7.2.6 Discriminate Single Bounce and Multiple Bounces NLOS Channels

In the NLOS localization technique proposed in Chapter 6, we assumed single bounce

NLOS channel between BN's and TN's is available. In fact here, we ignored the effect of multiple bounce reflections when compared to the single one. While in real application, multiple bounce NLOS channel may not be ignorable due to the size and material of reflectors. In the multiple bounces NLOS case, large localization error would be generated if the NLOS localization method proposed in Chapter 6 is applied. An example is shown in Fig. 7.4, the crossing points of the two circles determined by the position of reflectors k and m and the distances between the TN and the two reflectors are not close to the TN position. This is due to fact that the channel, through which the signal travels from TN to BN's i and l , is not a single bounce NLOS channel, it is a two bounces NLOS channel (the signal travels from TN j through reflector 1 and then reflector k to BN's i and l). Hence, single bounce NLOS channel and multiple bounces NLOS channel should be separated to mitigate the localization error generated by the multiple bounces NLOS channel.

7.2.7 Extension of the Multi-node TOA-DOA Fusion from Two-Dimensional to Three-Dimensional

For space-based applications such as satellite formation for solar power transfer via satellites [81-84], or multiple unmanned aerial vehicles (UAVs) conducting a collaborative task, it is important to precisely localize satellites or UAVs in the space. Assuming each satellite is equipped with both BN and TN devices, similar to WLPS [9], the proposed multi-node fusion scheme can be extended from 2D scenario to a 3D case. The relevant equations can be developed and its performance and complexity can be

investigated.

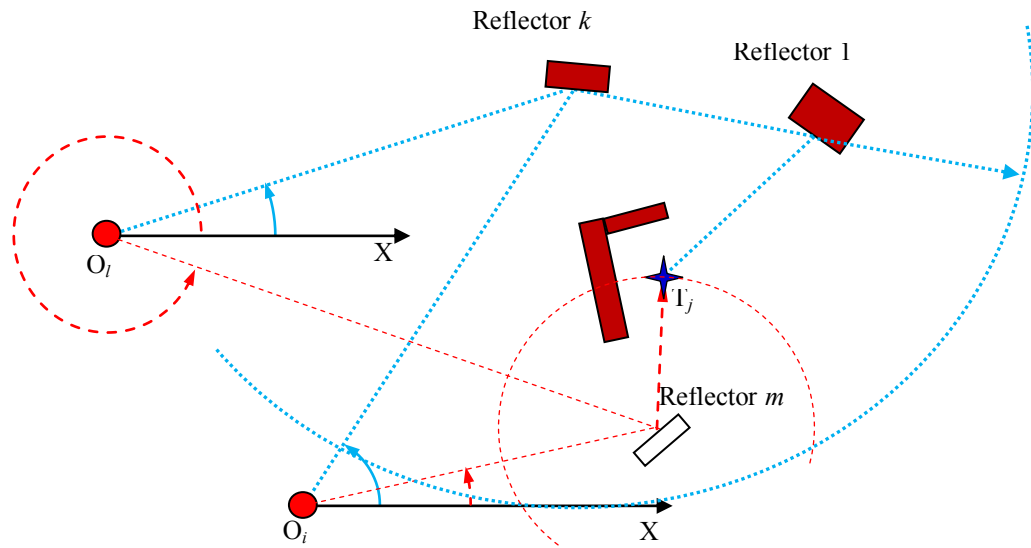


Figure 7.4: The impact of multiple bounces NLOS on NLOS TN localization.

Appendix A

Republish Permission

Dear Jacqueline,

I have inserted my university's name in the bracket in the paragraph 2.

Thank you very much,

Zhonghai Wang

----- Original Message -----

From: "j hansson" j.hansson@ieee.org

To: wzhongha@mtu.edu

Sent: Tuesday, January 26, 2010 10:07:22 AM GMT -05:00 US/Canada Eastern

Subject: Re: Fw: paper reuse permission

Dear Zhonghai Wang :

We are happy to grant you this permission to reprint your below described IEEE copyrighted papers in your thesis and, if you wish, have it placed on your university's website. We have only two requirements that must be satisfied before we can consider this permission final:

(1) The following copyright/credit notice must appear prominently either on the first page of the reprinted material or prominently in the references of the reprinted paper, with the

appropriate details filled in: © [year] IEEE. Reprinted, with permission, from [IEEE publication title, paper title, and author names].

(2) Additionally, if your thesis is to appear on the university's website, the following message should be displayed either at the beginning of the credits or in an appropriate and prominent place on the website: This material is posted here with permission of the IEEE. Such permission of the IEEE does not in any way imply IEEE endorsement of any of the [Michigan Technological University]'s products or services. Internal or personal use of this material is permitted. However, permission to reprint/republish this material for advertising or promotional purposes or for creating new collective works for resale or redistribution must be obtained from the IEEE by writing to pubs-permissions@ieee.org. By choosing to view this material, you agree to all provisions of the copyright laws protecting it.

If applicable, University Microfilms, Inc. or ProQuest may supply single copies of the dissertation.

This letter is your permission grant, but for it to be valid, please send this email back to me with name of your university inserted in the brackets in paragraph 2. Thank you

Sincerely,

Jacqueline Hansson

IEEE Intellectual Property Rights Coordinator

IEEE Intellectual Property Rights Office

445 Hoes Lane

Piscataway, NJ 08855-1331 USA

+1 732 562 3828 (phone)
+1 732 562 1746(fax)
e-mail: j.hansson@ieee.org

IEEE Fostering technological innovation and excellence for the benefit of humanity.

From: William Hagen/PUBS/STAFF/US/IEEE
To: Jacqueline Hansson/PUBS/STAFF/US/IEEE@IEEE
Date: 01/25/2010 05:13 PM
Subject: Fw: paper reuse permission

----- Forwarded by William Hagen/PUBS/STAFF/US/IEEE on 01/25/2010 05:12 PM -----

From: Zhonghai Wang <wzhongha@mtu.edu>
To: w.hagen@ieee.org
Cc: wzhongha <wzhongha@mtu.edu>
Date: 01/25/2010 02:00 PM
Subject: paper reuse permission

Dear Sir/madam,

I am preparing my dissertation and need your permission for the reuse of papers published in IEEE Transactions and conferences.

I am with Michigan Technological University. My address is: Zhonghai Wang 1809B Woodmar Dr. Houghton, Mi. 49931, my phone number is 906-281-2157, and my fax is 906-487-2949.

My dissertation title is "Multi-Node TOA-DOA Cooperative LOS-NLOS Localization: Enabling High Accuracy and Reliability".

The first author of the papers that I will fully use in my dissertation is me. The following are the papers:

- (1) Z. Wang, and S. A. Zekavat, “Omni-Directional Mobile NLOS Identification and Localization via Multiple Cooperative Nodes”, submitted to *IEEE Transactions on Mobile Computing*.
- (2) Z. Wang, and S. A. Zekavat, “A Novel Semi-distributed Localization via Multi-node TOA-DOA Fusion”, *IEEE Transactions on Vehicular Technology*, vol. 58, issue 7, pp. 3426-3435, Sep. 2009.
- (3) Z. Wang and S. A. Zekavat, “A New TOA-DOA Node Localization for Mobile Ad-hoc Networks”, *IEEE ICT 2010*.
- (4) Z. Wang, W. Xu, and S. A. Zekavat, “A New Multi-Antenna Based LOS - NLOS Separation Technique,” *IEEE DSP/SPE 2009*.

Sincerely,

Zhonghai Wang

References

- [1] I. Amundson and X.D. Koutsoukos, "A Survey on Localization for Mobile Wireless Sensor Networks", in *Mobile Entity Localization and Tracking in GPS-less Environments*, published by Springer Berlin / Heidelberg, vol. 5801/2009, pp. 235-254.
- [2] S. J. Ingram, D. Harmer, and M. Quinlan, "Ultra-wideband indoor positioning systems and their use in emergencies," *Position Location and Navigation Symposium, 2004, PLANS 2004*, pp. 706-715, 26-29 Apr. 2004, Rome, Italy.
- [3] M. Carlos Leonel Flores, D. R. Francescantonio, W. Satya Ardhy, S. Gianluca, R. Marie Claire Naima, F. Joao and F. Simone, "Cooperative Positioning Techniques for Mobile Localization in 4G Cellular Networks," *IEEE International Conference on pervasive services*, pp. 39-44, Jul. 2007.
- [4] C.T. Cai, C.S. Yang, Q.D. Zhu and Y.H. Liang, "Collision Avoidance in Multi-Robot Systems", *Mechatronics and Automation, 2007. ICMA 2007. International Conference on*. pp. 2795-2800, Aug. 2007.
- [5] W.D. Jones, "Keeping cars from crashing", *Spectrum, IEEE*, vol. 38, no. 9, pp. 40-45, Sep. 2001.
- [6] K. Amouris, "Position-Based Broadcast TDMA Scheduling for Mobile Ad-Hoc Networks (MANETS) with Advantaged Nodes", *Military Communications*

- Conference 2005, MILCOM IEEE*, pp. 1-6, Oct. 2005.
- [7] V. Sumathy, P. Narayanasmy, K. Baskaran, T. Purusothaman, "GLS with secure routing in ad-hoc networks", *TENCON, Conference on Convergent Technologies for Asia-Pacific Region*, vol. 3, pp. 1072-1076, Oct. 2003.
 - [8] S.M.M. Rahman, M. Mambo, A. Inomata, E. Okamoto, "An Anonymous On-Demand Position-Based Routing in Mobile Ad Hoc Networks", *Applications and the Internet, 2006. International Symposium on SAINT 2006*, pp. 300-306, Jan. 2006.
 - [9] H. Tong and S. A. Zekavat, "A Novel Wireless Local Positioning System via Asynchronous DS-CDMA and Beam-forming: Implementation and Perturbation Analysis," *IEEE Transactions on Vehicular Technology*, vol. 56, no. 3, pp. 1307-1320, May 2007.
 - [10] Elliott D.Kaplan, "Understanding GPS: Principles and Applications", Artech House Telecommunications Library, 1996.
 - [11] Y. Fukuju, M. Minami, H. Morikawa, and T. Aoyama, "DOLPHIN: an autonomous indoor positioning system in ubiquitous computing environment", *IEEE Workshop on Software Technologies for Future Embedded Systems*, pp. 53-56, May. 2003.
 - [12] P.Z. Peebles, "Radar Principles", John Wiely and Sons, Inc. 1998.

- [13] T. Ohira and K. Gyoda, "Electronically steerable passive array radiator antennas for low-cost analog adaptive beam-forming", *IEEE International Conference on Phased Array Systems and Technology, 2000, Proceedings*, pp. 101-104, May. 2000, Dana Point, CA, USA.
- [14] J. Liberti and T.S. Rappaport, "Smart Antennas for Wireless Communications: IS-95 and Third Generation CDMA Applications", Prentice Hall, 1999.
- [15] R.O. Schmidt, "Multiple emitter location and signal parameter estimation", *Antennas and Propagation, IEEE Transactions on*, vol. 34, no. 3, pp. 276-280, 1986.
- [16] A.J. Barabell, "Improving the resolution performance of eigenstructure-based direction-finding algorithms", *IEEE International Conference on Acoustics, Speech, and Signal Processing*, vol. 8, pp. 336-339, 1983.
- [17] T. Ohira and K. Gyoda, "Hand-held microwave direction-of-arrival finder based on varactor-tuned analog aerial beamforming", *Microwave Conference, 2001, APMC 2001, 2001 Asia-Pacific*, vol. 2, pp. 585-588, Dec. 2001.
- [18] Z. Wang, C. Li, and S. A. Zekavat, "A Novel Smart Antenna Calibration Technique," *Virginia Tech Annual Wireless Symposium*, Jun. 2008, VA. USA.
- [19] V. Erceg, L.J. Greenstein, S.Y. Tjandra, S.R. Parkoff, A. Gupta, B. Kulic, A.A. Julius, and R. Bianchi, "An empirically based path loss model for wireless

- channels in suburban environments”, *Selected Areas in Communications, IEEE Journal on*, vol. 17, no. 7, pp. 1205-1211, Jul. 1999.
- [20] F. Ikegami, S. Yoshida, T. Takeuchi and M. Umehira, “Propagation factors controlling mean field strength on urban streets”, *Antennas and Propagation, IEEE Transactions on*, vol. 32, no. 8, pp. 822-829, Aug. 1984.
- [21] Masashi Sugano, Tomonori Kawazoe, Yoshikazu Ohta, and Masayuki Murata, "Indoor Localization System Using RSSI Measurement of Wireless Sensor Network Based on ZigBee Standard," *The IASTED International Conference on Wireless Sensor Networks (WSN 2006)* , Banff (Canada), Jul. 2006.
- [22] S. S. Ghidary, T. Tani, T. Takamori, and, M. Hattori, “A new home robot positioning system (HRPS) using IR switched multi ultrasonic sensors”, *IEEE SMC '99 Conference Proceedings on Systems, Man, and Cybernetics*, vol. 4, pp. 737-741, Oct. 1999.
- [23] J. M. Lee, D. H. Lee, H. T. An, N. Huh, M. K. Kim and M. H. Lee, “Ultrasonic satellite system for the positioning of mobile robots”, *IEEE Proceedings on Industrial Electronics Society*, vol. 1, pp. 448-453, 2-6 Nov. 2004.
- [24] A. Savvides, C.C. Han and M. Srivastava, “Dynamic fine-grained localization in ad-hoc networks of sensors,” *ACM MOBICOM*, 2001.
- [25] M. A. Spirito, A. G. Mattioli, “On the hyperbolic positioning of GSM mobile

- stations”, *Signals, Systems, and Electronics*, pp. 173-177, 29 Sep.-2 Oct. 1998.
- [26] D. Niculescu, and Badri Nath, "Ad hoc positioning system (APS) using AOA", *INFOCOM 2003. Twenty-Second Annual Joint Conference of the IEEE Computer and Communications. IEEE Societies.* vol. 3, pp. 1734-1743, 30 Mar.-3 Apr. 2003.
 - [27] L. Girod, M. Lukac, V. Trifa, and D. Estrin, “The design and implementation of a self calibrating distributed acoustic sensing platform”, *In Proc. of SenSys 2006*, Nov. 2006, Boulder, CO, USA.
 - [28] A. G. Dempster, “Dilution of precision in angle-of-arrival positioning systems”, *IEEE Electronics Letters*, vol. 42, no. 5, pp. 291-292, March 2006.
 - [29] S. Venkatraman and J.Jr. Caffery, “A statistical approach to non-line-of-sight BS identification”, *the 5th IEEE International Symposium on Wireless Personal Multimedia Communications*, vol. 1, pp. 296-300, Oct. 2002.
 - [30] L. Xiong, “A selective model to suppress NLOS signals in angle-of-arrival AOA location estimation”, *IEEE International Symposium on Personal, Indoor and Mobile Radio Communications*, vol. 1, pp. 461–465, Sep. 1998.
 - [31] P.C. Chen, “A non-line-of-sight error mitigation algorithm in location estimation”, *IEEE Wireless Communications Networking Conference*, vol. 1, pp. 316-320, 1999.

- [32] S. Venkatesh, and R.M. Buehrer, “Non-line-of-sight identification in ultra-wideband systems based on received signal statistics”, *IET Microwaves, Antennas & Propagation*, vol. 1, no. 6, pp. 1120-1130, Dec. 2007.
- [33] Y.T. Chan, W.Y. Tsui, H.C. So and P.C. Ching, “Time-of-arrival based localization under NLOS conditions”, *IEEE Transactions on Vehicular Technology*, vol. 55, Issue 1, pp. 17 – 24, Jan. 2006.
- [34] B. Alavi and K. Pahlavan, “Modeling of the TOA-based distance measurement error using UWB indoor radio measurements”, *IEEE Communications Letters*, vol. 10, no. 4, pp. 275- 277, 2006.
- [35] Giovanni Bellusci, Gerard J. M. Janssen, Junlin Yan, and Christian C. J. M. Tiberius, “Modeling Distance and Bandwidth Dependency of TOA-Based UWB Ranging Error for Positioning,” *Research Letters in Communications*, vol. 2009, Article ID 468597, 4 pages, 2009. doi:10.1155/2009/468597.
- [36] I. Güvenç, C.C. Chong, F. Watanabe, and H. Inamura, “NLOS Identification and Weighted Least-Squares Localization for UWB Systems Using Multipath Channel Statistics”, *EURASIP Journal on Advances in Signal Processing*, 2008, Article ID 271984, 14 pages, 2008. doi:10.1155/2008/271984.
- [37] L. Cong and W.H. Zhuang, “Non-line-of-sight error mitigation in mobile location”, *IEEE Transactions on Wireless Communications*, vol. 4, no. 2, pp. 560-573, 2005.

- [38] L. Konrad and W. Matt, "Motetrack: A robust, decentralized approach to RF-based location tracking", *International Workshop on Location-and Context-Awareness*, vol. 3479, pp. 63-82, 2005.
- [39] C.K. Seow and S.Y. Tan, "Non-line-of-sight unidirectional mobile localization in multipath environment", *Electronics Letters*, vol. 44, no. 2, pp. 141-142, Jan. 2008.
- [40] C.K. Seow and S.Y. Tan, "Non-Line-of-Sight Localization in Multipath Environments", *IEEE Transactions on Mobile Computing*, vol. 7, no. 5, pp. 647-660, May. 2008.
- [41] R.R. Skidmore, A. Verstak, N. Ramakrishnan, T.S. Rappaport, L.T. Watson, J. He, S. Varadarajan, C.A. Shaffer, J. Chen, K. Bae, J. Jiang and W.H. Tranter, "Towards integrated PSEs for wireless communications: experiences with the S4W and Site Planner \ text registered projects", *ACM SIGMOBILE Mobile Computing and Communications Review*, vol. 8, no. 2, pp. 20-34, 2004.
- [42] J. Caffery Jr. and G.L. Stuber, "Subscriber location in CDMA cellular networks", *IEEE Transactions on Vehicular Technology*, vol. 47, no. 2, pp. 406-416, May. 1998.
- [43] S. Capkun, M. Hamdi and J.P. Hubaux, "GPS-free positioning in mobile ad-hoc networks", *Proceedings of the 34th Annual Hawaii International Conference on System Science*, pp. 3-6, Jan. 2001.

- [44] K.F. Ssu, C.H. Ou and H.C. Jiau, "Localization with mobile anchor points in wireless sensor networks", *IEEE Transactions on Vehicular Technology*, vol. 54, no. 3, pp. 1187 – 1197, May. 2005.
- [45] E. Falletti, L.P. Letizia and F. Sellone, "SAM LOST smart antennas-based movable localization system", *IEEE Transactions on Vehicular Technology*, vol. 55, no. 1, pp. 25 – 42, Jan. 2006.
- [46] Z.L. Shan and T.S.P. Yum, "Precise Localization with Smart Antennas in Ad-Hoc Networks", *GLOBECOM'07*, pp. 1053 – 1057, Nov. 2007.
- [47] T. Li, A. Ekpenyong and Y.-F. Huang, "Source Localization and Tracking Using Distributed Asynchronous Sensors", *IEEE Transactions on Signal Processing*, vol. 54, no. 10, pp. 3911 – 4003, Oct. 2006.
- [48] M.D. Gillette and H.F. Silverman, "A Linear Closed-Form Algorithm for Source Localization from Time-Differences of Arrival", *IEEE signal Processing Letters*, vol. 15, pp. 1 – 4, 2008.
- [49] B. Li, A.G. Dempster, C. Rizos and J. Barnes, "Hybrid method for localization using WLAN", *Spatial Sciences Conference*, pp. 341-350, CD-ROM proc., 12 -16 Sep. 2006, Melbourne, Australia.
- [50] B.F. Rolfe, S.W. Ekanayake, P.N. Pathirana and M. Palaniswami, "Localization with orientation using RSSI measurements: RF map based approach", *the 3rd*

International Conference on Intelligent Sensors, Sensor Networks and Information, pp. 311 – 316, 3 - 6 Dec. 2007.

- [51] Y.T. Wu, H.C. So, C.H. Hou and J. Li, “Passive Localization of Near-Field Sources with a Polarization Sensitive Array”, *IEEE Transactions on Antennas and Propagation*, vol. 55, no. 8, pp. 2402 – 2408, Aug. 2007.
- [52] R. Huang and G.V. Zaruba, “Incorporating Data from Multiple Sensors for Localizing Nodes in Mobile Ad Hoc Networks”, *IEEE Transactions on Mobile Computing*, vol. 6, no. 9, pp. 1090 – 1104, Sep. 2007.
- [53] A. Brown and J. Nordlie, “Integrated GPS/TOA Navigation using a Positioning and Communication Software Defined Radio”, *Position, Location, And Navigation Symposium, 2006 IEEE/ION*, pp. 147-152, 25-27 Apr. 2006.
- [54] T. Eren, “Using Angle of Arrival (Bearing) information for Localization in Robot Networks”, *Turkish Journal of Electrical Engineering & Computer Science*, vol. 15, no. 2, 2007.
- [55] M.L. Sichitiu and V. Ramadurai, “Localization of wireless sensor networks with a mobile beacon”, *IEEE International Conference on Mobile Ad-hoc and Sensor Systems*, pp. 174 – 183, 25-27 Oct. 2004.
- [56] K. A. Redmill, T. Kitajima, U. Ozguner, “DGPS/INS Integrated Positioning for Control of Automated Vehicle”, *ITSC'01*, Aug. 2001.

- [57] X. Li, X. Chen, G. Goldfarb, E. Mateo, I. Kim, F. Yaman, and G. Li, "Electronic post-compensation of WDM transmission impairments using coherent detection and digital signal processing," *Opt. Express* 16, pp. 880-888, 2008.
- [58] S. A. Zekavat, A. Kolbus, X. Yang, Z. Wang, J. Pourrostam and M. Pourkhaatoon, "A Novel Implementation of DOA Estimation for Node Localization on Software Defined Radios: Achieving High Performance with Low Complexity", *ICSPC'07*, Nov. 2007.
- [59] M. Pesavento, A.B. Gershman and M. Haardt, "Unitary root-MUSIC with a real-valued Eigen decomposition: a theoretical and experimental performance study", *IEEE Transactions on Signal Processing*, vol. 48, no. 5, pp. 1306-1314, May. 2000.
- [60] N. Bulusu, J. Heidemann and D. Estrin, "GPS-less low-cost outdoor localization for very small devices," *IEEE Personal Communications*, vol. 7, no. 5, pp. 287–34, Oct. 2000.
- [61] S. Zhou and J. K. Pollard, "Position measurement using Bluetooth", *Consumer Electronics, IEEE Transactions on*, vol. 52, pp. 555-558, May 2006.
- [62] Z. Wang, and S. A. Zekavat, "MANET Localization via Multi-node TOA-DOA Optimal Fusion," *proceedings on IEEE Milcom'06*, Oct. 2006, Washington DC, USA.

- [63] K. C. Ho, Y. T. Chan, "Solution and performance analysis of geo-location by TDOA", *Aerospace and Electronic Systems, IEEE Transactions on*, vol. 29, no. 4, pp. 1311-1322, Oct. 1993.
- [64] J.T. Gillis, "Computation of the circular error probability integral", *Aerospace and Electronic Systems, IEEE Transactions on*, vol. 27, no. 6, pp. 906 - 910, Nov. 1991.
- [65] D. H. Shin and T. K. Sung, "Comparisons of error characteristics between TOA and TDOA positioning", *IEEE Aerospace and Electronic Systems*, vol. 38, no. 1, pp. 307 – 311, Jan. 2002.
- [66] John G. Proakis, "Digital Communications: Fourth edition", the McGraw-Hill Companies, Inc. 2001.
- [67] D.J. Torrieri, "Statistical Theory of Passive Location Systems", *Aerospace and Electronic Systems, IEEE Transactions on*, vol. AES-20, no. 2, pp. 183-198, Mar. 1984.
- [68] S. Gezici, H. Kobayashi, and H.V. Poor, "Non-parametric non-line-of-sight identification", *IEEE proceedings on Vehicular Technology Conf.*, vol.4, pp.2544–2548, Oct. 2003.
- [69] M. Heidari and K. Pahlavan, "A New Statistical Model for the Behavior of Ranging Errors in TOA-Based Indoor Localization", *IEEE WCNC'07*, 11-15

March, 2007, Hong Kong, China.

- [70] B. Alavi and K. Pahlavan, "Modeling of the distance error for indoor geolocation", *IEEE WCNC 2003*, vol. 1, pp. 668-672, Mar. 2003.
- [71] Q.H. Spencer, B.D. Jeffs, M.A. Jensen and A.L. Swindlehurst, "Modeling the statistical time and angle of arrival characteristics of an indoor multipath channel", *IEEE Journal on Selected Areas in Communications*, vol. 18, no. 3, pp. 347-360, Mar. 2000.
- [72] S. Venkatraman and J. Jr. Caffery, "Hybrid TOA/AOA techniques for mobile location in non-line-of-sight environments", *IEEE WCNC'04*, 21-25 Mar. 2004, Atlanta, Georgia USA.
- [73] A.Y. Olenko, K.T. Wong and E. Hui-On Ng, "Analytically derived TOA-DOA statistics of uplink/downlink wireless multipaths arisen from scatterers on a hollow-disc around the mobile", *IEEE Antennas and Wireless Propagation Letters*, vol. 2, pp. 345-348, 2003.
- [74] R. E. Kalman, "A New Approach to Linear Filtering and Prediction Problems," *Transactions of the ASME – Journal of Basic Engineering*, no. 82 (Series D), pp. 35-45, 1960.
- [75] R. S. Ornedo and K. A. Farnsworth, "GPS and radar aided inertial navigation system for missile system applications," in *Proc. IEEE 1998 Position Location*

and Navigation Symp., pp. 614–621, Apr. 1998, Palm Springs, CA, USA.

- [76] Y.C. Cao and J.A. Fang, “Constrained Kalman Filter for Localization and Tracking Based on TDOA and DOA Measurements”, *IEEE ICSPS’09*, pp. 28-33, 15-17 May. 2009, Singapore.
- [77] P. Tichavsk’y, C. Muravchik, and A. Nehorai, “Posterior Cramer–Rao bounds for discrete-time nonlinear filtering,” *IEEE Transactions on Signal Processing*, vol. 46, pp. 1386–1396, May. 1998.
- [78] L. Perea, J. How, L. Breger and P. Elosegui, “Nonlinearities in sensor fusion: Divergence issues in EKF, modified truncated SOF, and UKF”, *Proceedings of the AIAA Guidance Navigation and Control Conference and Exhibit*, edited by AIAA, August 2007.
- [79] B. Sklar, “Rayleigh fading channels in mobile digital communication systems .I. Characterization”, *Communications Magazine, IEEE*, vol. 35, no. 7, pp. 90-100, Jul. 1997.
- [80] B.W.M. Kuipers, M. Mackowiak and L.M. Correia, “Understanding Geometrically based Multiple Bounce Channel Models”, *Antennas and Propagation*, 2007. EuCAP 2007. The Second European Conference on, pp. 1-4, 11-16 Nov. 2007.
- [81] S. G. Ting, O. Abdelkhalik, and S. A. Zekavat, “Spacecraft Constellation Orbit

- Estimation via a Novel Wireless Positioning System,” proceedings AAS/AIAA Space Flight Mechanics Meeting, Savannah, GA, Feb. 8-12, 2009.
- [82] S. A. Zekavat, O. Abdelkhalek, and H. Tong, “Aircraft Navigation and Spacecraft Coordination via Wireless Local Positioning Systems,” proceedings 2008 Integrated Comm. Navigation and Surveillance (ICNS) Conference, Bethesda, MD, May 5 – 7, 2008.
- [83] S. A. Zekavat, O. Abdelkhalik, S. G. Ting, and D. Fuhrmann, “A Novel Space-Based Solar Power Collection via LEO Satellite Networks: Orbital via a Novel Wireless Local Positioning System,” to appear in proceedings of IEEE Aerospace Conference, 2010.
- [84] S. G. Ting, O. Abdelkhalik, and S. A. Zekavat, “Differential Geometric Estimation for Spacecraft Formations Orbits via a Novel Wireless Positioning,” to appear in proceedings of IEEE Aerospace Conference, 2010.